Surprises in Brownian Motion

Brownian Donkeys and Parrondo's Paradox

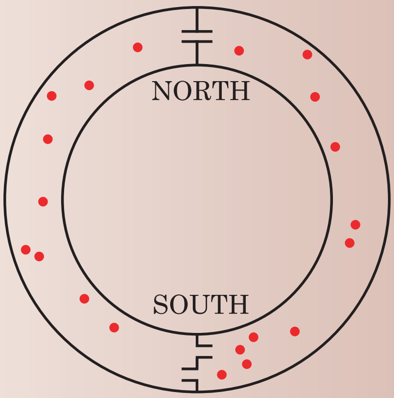

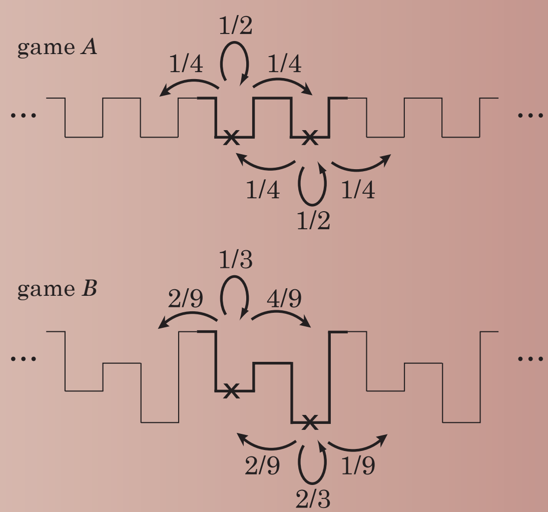

B. Cleuren

2004

CONTENTS

While the behavior of equilibrium systems is rather well documented and understood on the basis of general principles, the study of nonequilibrium systems appears to be much more intricate. The two topics presented in this thesis are dealing with nonequilibrium Brownian motion, leading to surprising and counterintuitive behavior.

The first part discusses *Brownian donkeys*. Such systems are characterised by a special response behavior, referred to as absolute negative mobility: when applying an external force, the particles always move in a direction opposite to that of the force. In other words, the particles climb up a potential gradient. The energy needed to do this is extracted by the Brownian particle from the nonequilibrium fluctuations. We present several explicit constructions involving either a single or a collection of Brownian particle(s).

The second part deals with the *Parrondo paradox*. In short, this paradox states that the random or periodic alternation between fair games need no longer be fair. After reviewing the original paradox we introduce the concept of strategy, in which the player(s) can now decide at each turn on the choice of the next game. We present a systematic study of several strategies, including the so-called greedy and optimal one. For the original games, the search for the optimal strategy turns out to be difficult, if not impossible. We introduce a new version of the paradox, the so-called primary Parrondo paradox, whose dynamics involves only superstable fixed points, and for which a full analytical solution for any strategy, together with the identification of the optimal strategy, becomes possible.

In tegenstelling tot evenwichtssystemen, die bestudeerd en verklaard kunnen worden op basis van algemene principes, is de studie van niet-evenwichtssystemen ingewikkelder, en leidt vaak tot verrassende resultaten. In deze thesis worden twee systemen beschreven die beide gebaseerd zijn op niet-evenwichts Brownse beweging.

Het eerste onderwerp gaat over *Brownse ezels*. Deze systemen hebben de verrassende eigenschap dat wanneer een externe kracht aangelegd wordt, de deeltjes gaan bewegen in de richting tegengesteld aan deze van de externe kracht. De energie die hiervoor nodig is wordt door de Brownse deeltjes uit de niet-evenwichtsfluctuaties bekomen. Voor deze Brownse ezels is dus de verhouding tussen de snelheid en de aangelegde kracht, de zogenaamde mobiliteit, negatief. Dat dit verschijnsel ook kan voorkomen in Brownse systemen, wordt hier aangetoond d.m.v. een aantal expliciete constructies. Hoofdstuk 1 geeft een korte inleiding over Brownse systemen, en voert de nodige begrippen en grootheden in die later gebruikt worden. Ook wordt een voorbeeld gegeven van zowel een één-deeltje als een meer-deeltjes systeem, waarvoor de negatieve mobiliteit op een intuitieve manier verklaard kan worden. Hoofdstukken 2 en 3 beschrijven een variant van het eerder genoemde collectief basis model. Een groep interagerende deeltjes bewegen langsheen een cirkel, met op de noord- en zuidpool een potentiaalberg. De niet-evenwichtssituatie wordt verkregen door de potentiaalberg op de zuidpool af te koelen. In Hoofdstuk 2 wordt de beweging van de deeltjes als een Ising model beschreven, wat toelaat om analytische berekeningen te doen. Uit de resultaten van deze berekeningen volgt dat negatieve mobiliteit voorkomt met minstens 4 deeltjes. In de Ising beschrijving is de positie van de Brownse deeltjes een discrete coördinaat, en dit heeft echter als nadeel dat er geen rekening gehouden wordt met de preciese vorm van het temperatuursprofiel, de potentële- en interactie-energie. In Hoofdstuk 3 wordt dit model daarom opnieuw bestudeerd, waarbij de positie van de deeltjes nu een continue vrijheidsgraad is. Deze beschrijving houdt wel rekening met de preciese vorm, maar heeft dan weer als nadeel dat analytische berekeningen veel omslachtiger worden. Daarom worden talrijke simulaties uitgevoerd, die aantonen dat het mogelijk is om met slechts 3 deeltjes negatieve mobiliteit te krijgen. Hoofdstukken 4 en 5 bespreken twee ééndeeltjes systemen. In Hoofdstuk 4 wordt aangetoond dat eenvoudige niet-Markoviaanse uitbreidingen van de standaard random walk kunnen leiden tot negatieve mobiliteit. Hoofdstuk 5 tenslotte is een variant op een basis model uit Hoofdstuk 1. Deze variant heeft als voordeel dat een experimentele realisatie mogelijk wordt.

Het tweede onderwerp van deze thesis gaat over de *Parrondo paradox*. Deze paradox, genoemd naar de Spaanse fysicus Juan Parrondo, luidt als volgt: afwisselend spelen van twee eerlijke spelen kan leiden tot een winnend resultaat. De afwisseling kan zowel willekeurig als periodisch zijn en gebeurt zonder inspraak van de speler. De inspiratie voor deze paradox is een bepaald type van Brownse motor, namelijk de ”flashing ratchet”. Hoofdstuk 6 geeft een gedetailleerde bespreking van de paradox en toont aan hoe de werking van de Brownse motor nagebootst kan worden door gebruik te maken van getrukeerde munten. In Hoofdstuk 7 wordt de paradox op twee manieren veralgemeend. Ten eerste beschouwen we nu een collectie van spelers en ten tweede krijgen deze spelers inspraak in de keuze van het spel. Ze kunnen na onderling overleg zelf beslissen welk spel ze tijdens de volgende beurt gaan spelen. Bij het maken van de spelkeuze laten de spelers zich leiden door een bepaalde strategie. De vraag die dan gesteld kan worden is de volgende: bij welke strategie is de winst maximaal? Het antwoord op deze vraag is niet vanzelfsprekend. Exacte resultaten worden gegeven voor $1, 2$ en 3 spelers en in de meanfield limiet (aantal spelers naar oneindig). Een verrassende conclusie is dat de zogenaamde "hebberige" strategie, waarbij de spelers het spel kiezen dat op dat ogenblik de meeste winst geeft, niet noodzakelijk optimaal is (enkel bij 1 en 2 speler(s) is deze hebberige strategie optimaal). In Hoofdstuk 8 wordt een nieuwe "primaire" variant op de originele Parrondo spelen ingevoerd. Deze nieuwe spelen zijn conceptueel en technisch eenvoudiger, en laten toe om de optimale strategie te bepalen voor een willekeurig aantal spelers.

ACKNOWLEDGEMENTS

This thesis would not have been possible without the continuous support and help from many persons, whom I hereby would like to thank.

Dank aan, thanks to,

Prof. dr. Chris van den Broeck, for giving me the opportunity to work in his group, and for creating a friendly and stimulating atmosphere by his never-ending enthusiasm.

Friends and colleagues at LUC, in particular prof. dr. Roger Serneels, prof. dr. Carlo Vanderzande, prof. dr. Herman Janssen, Pascal Meurs, dr. Peter Leoni, dr. Jef Hooyberghs, dr. Ioana Bena, René Liberloo, Michel De Roeve and Rik Lempens.

Prof. dr. Ryoichi Kawai, for his help and support with the numerous computer simulations.

Prof. dr. Peter Reimann and dr. Ralf Eichhorn for their interest in this work and careful proofreading of the manuscript. Also thanks for the many stimulating discussions and collaboration during (and in between) my visits at Bielefeld university.

Prof. dr. Juan Parrondo and Luis Dinis for fruitful cooperation and exchange of ideas on the paradoxical games.

De vrienden buiten het LUC, (ex-)medestudenten, Johan en Ilse, en niet te vergeten "de mannen" voor de vele levendige en dikwijls nachtelijke discussies.

Mijn ouders, voor alle mogelijkheden en kansen die ze mij gegeven hebben. Zonder hun hulp en steun was dit alles niet mogelijk.

Tine, mijn steun en toeverlaat gedurende de voorbije jaren. Ondanks de vele verstrooide en afwezige momenten is zij er altijd voor mij. Bedankt.

Part I

Brownian Donkeys

1

MOVING BACKWARDS NOISILY

1.1 Introduction

When a stone is dropped in a pool of water, it sinks to the bottom. A piece of wood rises to the surface. Likewise, a mixture of oil and water will spontaneously separate, with the lighter fluid (oil) on top. Even though these phenomena are considered to be common sense, their explanation required the famous "Eureka" insight of Archimedes. His principle states that a surrounding fluid exerts on an intruder body a force equal to the weight of the displaced fluid. The basic idea is that the force exerted by the fluid is the same whether a volume is occupied by fluid or by the intruder, hence the fluid will carry its own weight. This argument is simple and powerful, yet there are circumstances in which it is not valid and heavy particles can rise to the surface. An intreaguing and well documented example is the case of the *Brazil nut*. Its story goes back to the 1930's. During the long overseas transport from South America to Europe, boxes containing different kinds of nuts were heavily shaken. One expects that this would cause the mixture to homogenize. But surprisingly the opposite is true: when opening such a box, the large Brazil nuts were found located on the top, see Fig. 1.1 for an example. The same phenomenon is observed in the more general context of what is now called granular matter. This term refers to a collection of discrete macroscopic particles. Examples are sand and breakfast cereals. In the laboratory, one usually works with glass or metal beads. When a mixture of two such granular species of different size is shaken, a spontaneous separation takes place, with the larger particles on top. Even more surprising is the fact that this phenomenon can occur even if the larger particles are heavier, clearly in contrast to Archimedes' principle. Figure 1.2 shows a series of snapshots taken during an experiment in which a large metal disk, surrounded by glass beads, rises to the surface. The apparatus is mounted on a vibrating plate.

So what is wrong with the Archimedes principle in these cases? The detailed explanation of the Brazil nut phenomenon appears to be quite intricate, and many subtle and counteracting effects are present. For more details, we refer to the review [1]. We restrict ourselves here to the main observation that the system is not at rest, or more precisely not at equilibrium. Because of the shaking, there is a continuous input of energy. At second thought, this is clearly required because the upward motion of heavier particles replacing lighter particles in the gravitational field implies an increase of potential energy. In fact, the gravitational force plays an essential role: if the field would be switched off, there would be no distinction between up and down and no preferential direction to move in. Hence the gravitational force results in its own "demise", in a way similar to a stubborn donkey that starts to move in an opposite direction when being pulled. In physical parlance, the difference between the stone and nut lies in the response behavior: the stone moves in the direction of the force, whereas the nut moves in the opposite direction. Hence the proportionality factor between force and speed, the so-called mobility, which has usually a positive sign, is found to be negative for the Brazil nut.

FIG. 1.1. Photo of a mixture of nuts after shaking. The large Brazil nuts (marked by an "X") are found on top.

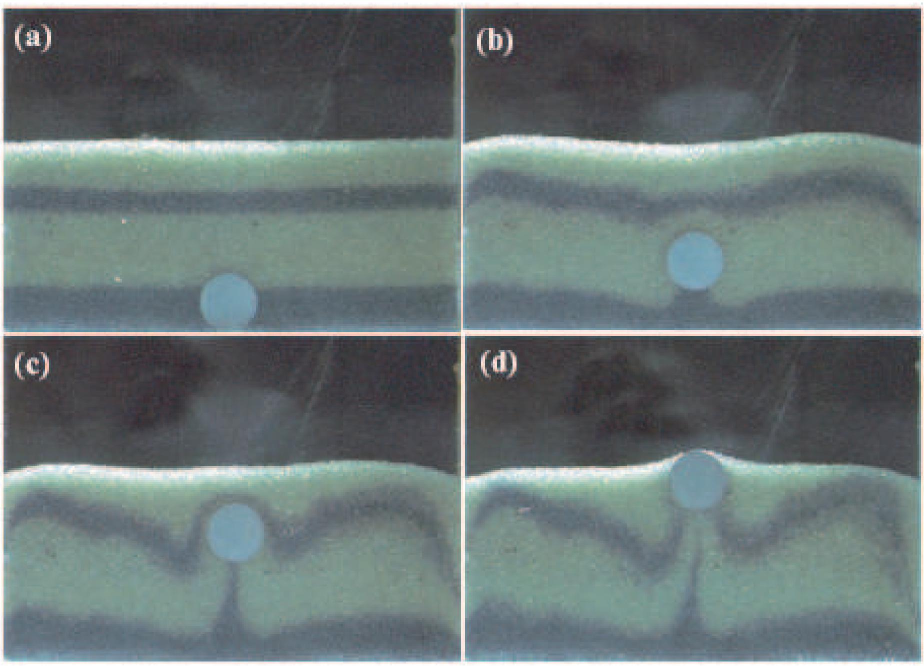

FIG. 1.2. Snapshots taken during an experimental verification of the Brazil nut effect, as reported by Liffman *et al* [2]. When the whole system is vibrated, the large metal disk, surrounded by glass beads, is rising to the surface.

The Brazil nut is an example of how the energy input of the seemingly random shaking can be converted into useful work and thereby lifting the heavy particle. Other examples of similar macroscopic *machines* are the windmill and the self-winding wrist-watch. These systems operate by the rectification of macroscopic fluctuations. The question then naturally arises whether a similar procedure can be used based on fluc-

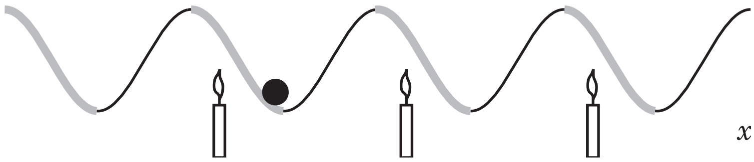

Fig. 1.3. Sketch of the Landauer ratchet, in which each potential barrier is heated on its right-hand side. With the help of this extra thermal energy, the Brownian particle can climb the heated side more easily. The result is an average motion to the left.

tuations arising due to the thermal motion of microscopic particles. Harnessing these fluctuations is becoming more and more important in view of the rise of nanotechnology and the ever decreasing size of technological applications. Whether it is possible to convert thermal fluctuations into useful work is a question touching on the foundations of statistical physics and thermodynamics. Indeed, it is impossible to extract work in a cyclic way from a system in thermodynamical equilibrium at a given temperature, as this would be in contradiction with the second law of thermodynamics. For nonequilibrium systems however, the situation is different. An important class of systems capable of delivering work from nonequilibrium fluctuations are *Brownian motors* [3]. These small-scale machines operating away from equilibrium make good use of the random motion of the microscopic particles, and convert that energy to deliver useful work. An example of such a Brownian motor is the kinesin protein, found in eucaryotic cells [4]. This protein is the transporter of the cell, moving various cargo around. The energy needed to perform this task is extracted from chemical reactions taking place inside the cell. Another example of a Brownian motor is the so-called *Landauer ratchet* [5, 6]. In this model, a Brownian particle is moving in a periodic, symmetric potential. When the temperature is modulated periodically along the horizontal axis, the particle starts moving in a certain direction, see Fig. 1.3. This motion can then be used to deliver work, for example by pulling a load.

In the Brazil nut example, the energy input from the shaking is used to perform work against the applied (gravitational) force. The question can be raised whether this is also possible when using the energy extracted from nonequilibrium fluctuations, i.e. by the intervention of a Brownian motor. In fact we wonder whether the Brownian motor itself can be the object that uses its energy to move against an applied force. As we will show in a number of explicit constructions, the answer is affirmative. However before turning to those physical examples, we introduce two toy models in which negative mobility driven by fluctuations can be understood on a intuitive basis and verified by a simple analytic calculation.

1.2 General framework

How can we describe the motion of the Brownian particles? What are the basic physical quantities involved? The answer to these questions is given in this section, together with a short description of the models that will appear in the following chapters.

The motion of Brownian particles is very irregular. The incessant thermal motion of the surrounding molecules causes rapid changes in the speed and position of the particle. In principle, the time evolution of the whole system can be obtained by writing down the equations of motion for every particle and molecule involved. But due to the large number of molecules, this is a hopeless task. Instead, we will describe such systems on a mesoscopic level. The basic idea is as follows. We first identify all possible configurations σ of the Brownian particles. Such a configuration includes information about the particle's position, its internal states,..., but discards any information about the surrounding molecules. Due to the many collisions between the Brownian particle and its surrounding, the system does not remain forever in a certain configuration, but evolves in time by making transitions between different configurations. Due to the random nature of the collisions, we can not predict when such a transition takes place. The time evolution is no longer deterministic, but is described as a stochastic process. Furthermore, by invoking the time separation between the fast molecular events and the slow time scale of observation, we assume that this process is Markovian. This means that the future state of the system only depends on the present state, and not on the history. The quantity of interest is the probability $P_\sigma(t)$ to find the system in configuration σ at time t. The time evolution of the probability distribution is described by the so-called master equation [7]:

$$\frac{\partial}{\partial t} P_\sigma(t) = \sum_{\sigma'} \left\{ k_{\sigma' \to \sigma} P_{\sigma'}(t) - k_{\sigma \to \sigma'} P_\sigma(t) \right\}, \tag{1.1}$$

where $k_{\sigma' \to \sigma}$ are called the transition rates (per unit time) to make a transition from configuration σ' to σ. The specific form of the master equation reflects the fact that the probability $P_\sigma(t)$, according to the first term, increases due to transitions from configurations σ' toward configuration σ, and decreases due to transitions away from configuration σ, as represented by the second term. Once the solution of the master equation is known, one can calculate the average position of the particle(s) as

$$\langle x(t) \rangle = \sum_\sigma x_\sigma P_\sigma(t), \tag{1.2}$$

where x_σ is the position of the Brownian particle in configuration σ. Of central interest to us will be the stationary average velocity v, defined as:

$$v = \lim_{t \to \infty} \frac{\langle x(t) \rangle}{t}. \tag{1.3}$$

This velocity will, upon application of an external force F, obviously depend on F. The *mobility* μ is then defined as the derivative of the velocity with respect to F:

$$\mu \equiv \frac{\partial v}{\partial F}. \tag{1.4}$$

It is this quantity that characterises the response behavior of the particles: if μ is positive (negative), the change in particle velocity when applying an external force is in the same (opposite) direction as that of the force. If the derivative is evaluated at $F = 0$ one speak of the *absolute* mobility, otherwise it is called the *differential* mobility. The calculation of this mobility for different models will be our main occupation in the following chapters.

We also mention here another important characteristic of the particle motion, namely the diffusion coefficient D, defined as:

$$D = \lim_{t \to \infty} \frac{\langle [x(t) - \langle x(t) \rangle]^2 \rangle}{2t} = \lim_{t \to \infty} \frac{\langle x(t)^2 \rangle - \langle x(t) \rangle^2}{2t}. \tag{1.5}$$

The diffusion coefficient is a measure of the spreading of the particles around the average position. At equilibrium, it is related to the mobility by the Einstein relation (see below).

1.3 Equilibrium versus nonequilibrium systems

A closed system in contact with a thermal heat bath evolves toward equilibrium, with the probability for a configuration given by a Boltzmann factor. If an energy E_σ is associated with each configuration σ, the equilibrium distribution P_σ^{eq} reads:

$$P_\sigma^{\mathrm{eq}} = \frac{1}{Z} e^{-\beta E_\sigma}, \tag{1.6}$$

with Z being the normalisation factor and $\beta = 1/k_B T$ with $k_B = 1.38 \times 10^{-23}$J/K the Boltzmann constant and T the temperature of the heat bath. Clearly, the master equation must reproduce this result. That is, starting from a given initial distribution, the system must evolve toward equilibrium, and the stationary solution of the master equation must be equal to the equilibrium distribution P_σ^{eq}. This requirement places a constraint on the transition rates. For closed systems in contact with a heat bath, one can proof that the following relation between the transition rates must hold [7]:

$$k_{\sigma \to \sigma'} P_\sigma^{\mathrm{eq}} = k_{\sigma' \to \sigma} P_{\sigma'}^{\mathrm{eq}}. \tag{1.7}$$

This relation is known as the detailed balance condition [8]. It is easy to check that the time independent solution to (1.1) is then given by the Boltzmann distribution. Equation 1.7 states that in equilibrium the (probability) flux between any two configurations vanishes. An important consequence is related to the response properties when applying an external force. For systems in equilibrium, the mobility can be expressed in terms of the diffusion coefficient:

$$\mu = \frac{D}{kT}. \tag{1.8}$$

This relation was first derived by Einstein in his 1905 paper on Brownian motion, nearly 100 years ago. By definition, the diffusion coefficient is positive, and so the particles move in the same direction as the applied external force.

The situation away from equilibrium is totally different. For such systems the detailed balance condition no longer applies, and this will give rise to surprising behavior.

1.4 Brownian donkeys I: single particle model

The first toy model we consider involves only a single Brownian particle. The original idea is due to Eichhorn *et al* [9]. We review their main results by means of a discretised version of the model, since this technique will be used for the main part of this thesis.

Consider a particle hopping in the periodic structure shown in Fig. 1.4. This structure consists of two lanes with periodically placed pockets. The pockets in the upper lane have an opening on the left, while those in the lower lane are open on the right. The particle can move around by jumping to nearest neighbor sites, separated by the dashed lines, but it cannot cross the solid lines. Clearly the presence of the pockets reduces the velocity of the particle. Not only must the particle zig-zag around them, but it can also get trapped in such a pocket. Suppose for example that we apply a force to the right. This force favoures a corresponding particle motion to the right, and so the particle is likely to get trapped in one of the pockets in the upper lane. Escape out of such a pocket is very rare, since it requires a jump of the particle against the external force. Furthermore, the mean escape time out of such a trap increases with increasing force, so

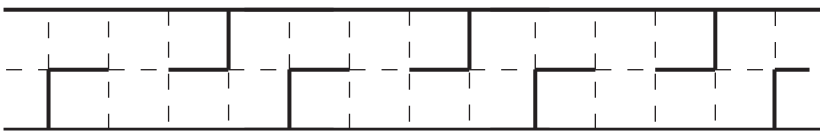

FIG. 1.4. The periodic structure with the pockets in the upper and lower lane.

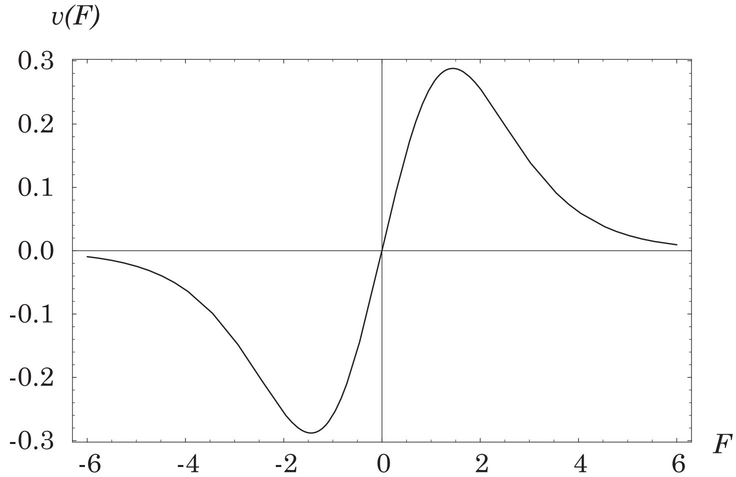

FIG. 1.5. Stationary velocity as a function of the external force F ($\gamma = \beta = 1$). Starting with $F = 0$, the velocity increases for increasing F, until it reaches a maximum (around $F \approx 1.4$). From then of, the velocity decreases for increasing F.

that the velocity-reducing effect of the pockets becomes more pronounced for stronger forces. Figure 1.5 shows the velocity of the particle as a function of the external force F. For small values the response is as expected, with the velocity increasing as the force becomes stronger. For larger values of F however, the influence of the pockets becomes visible: the increase in velocity becomes smaller until a maximum is reached. From then on, the velocity is largely determined by the escape out of the pockets. Eventually the velocity goes to zero as the force increases further, indicating that the particle getss trapped in a pocket for a long time. The phenomenon whereby the velocity decreases when the force is increased is also known as *differential negative mobility*.

The intuitive explanation given above can be confirmed by an explicit calculation of the particle velocity. We do this following the general framework given before. It turns out that, in order to calculate the velocity of a particle moving in a periodic structure such as the one shown in Fig. 1.4, it suffices to consider the particle motion in only one period of that structure, but with periodic boundary conditions [10, 11]. The configurations σ then correspond to the 8 sites per period, as shown in Fig. 1.6. The periodic boundary conditions imply that a particle leaving site 4 with a jump to the right, ends up in site 1. We define $P_\sigma(t)$, $\sigma \in \{1, 2, ..., 8\}$, as the probability for the particle to be in configuration σ at time t. The transition rates between the different configurations are shown in Fig. 1.6. Transition rates corresponding to a particle jump in the horizontal direction are defined as $k^{\pm}$ (the index $+/-$ refers to a jump to the right/left), while the transition rates corresponding to a particle jump in the vertical direction are defined as γ. The explicit form of the horizontal rates is given by the Arrhenius factor:

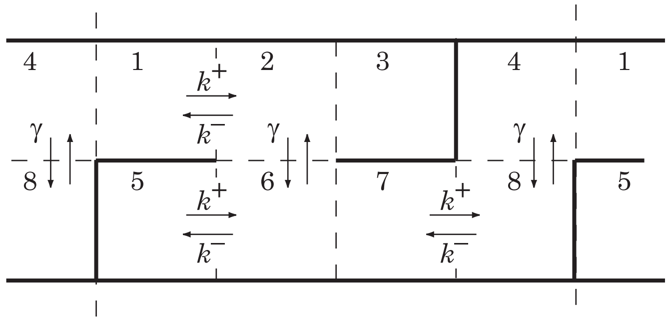

FIG. 1.6. Sketch of the lattice. The particle can jump to nearest neighbor sites.

$$k^+ = e^{\beta F/2};$$
$$k^- = e^{-\beta F/2},$$

where F is the energy difference between (horizontal) neighboring sites due the presence of the external force.

Collecting the $P_\sigma(t)$ in a vector $\mathbf{P}(t) = (P_1(t), P_2(t), ..., P_8(t))^T$, the master equation describing the time evolution of the probability distribution can be written compactly in matrixform as:

$$\frac{\partial}{\partial t}\mathbf{P}(t) = \mathbf{R}.\mathbf{P}(t), \tag{1.9}$$

where R is the transition matrix, which for this system is given as:

$$\mathbf{R} = \begin{pmatrix} -k^+-k^- & k^- & 0 & k^+ & 0 & 0 & 0 & 0 \\ k^+ & -k^+-k^--\gamma & k^- & 0 & 0 & \gamma & 0 & 0 \\ 0 & k^+ & -k^- & 0 & 0 & 0 & 0 & 0 \\ k^- & 0 & 0 & -k^+-\gamma & 0 & 0 & 0 & \gamma \\ 0 & 0 & 0 & 0 & -k^+ & k^- & 0 & 0 \\ 0 & \gamma & 0 & 0 & k^+ & -k^+-k^--\gamma & k^- & 0 \\ 0 & 0 & 0 & 0 & 0 & k^+ & -k^+-k^- & k^- \\ 0 & 0 & 0 & \gamma & 0 & 0 & k^+ & -k^--\gamma \end{pmatrix}. \tag{1.10}$$

The steady-state velocity is given as 4 times the stationary probability flux across the boundary between sites 4 and 1 [11]:

$$v(F) = 4\left(k^+P_4^{\rm st} - k^-P_1^{\rm st}\right), \tag{1.11}$$

where $P_\sigma^{\rm st} = \lim_{t\to\infty} P_\sigma(t)$ is the stationary solution of the master equation, which can be obtained by solving the eigenvalue problem $\mathbf{R}.\mathbf{P}^{\rm st} = 0$. The final expression reads:

$$v(F) = \frac{4\gamma e^{\beta F}\left(e^{\beta F} - 1\right)}{1 + e^{\beta F} + e^{2\beta F} + e^{3\beta F} + \gamma e^{\beta F/2} + 6\gamma e^{3\beta F/2} + \gamma e^{5\beta F/2}}. \tag{1.12}$$

A plot of $v(F)$ as a function of F is given in Fig. 1.5.

For such symmetrical systems with differential negative mobility, it is possible to obtain absolute negative mobility. The idea is to apply an additional time oscillatory external force, together with the already present (constant) force F [9]. For simplicity we assume that this additional force has a square wave form with amplitude A and period T. The total force applied to the system is then $A + F$ during one half period,

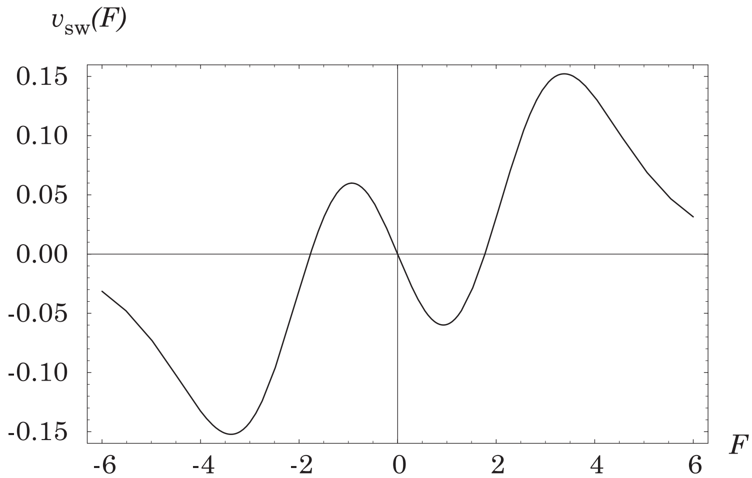

FIG. 1.7. Plot of $v_{\rm sw}(F)$ vs. F for $A = 2$.

and $-A+F$ during the other half period. We further assume that the time between the switching ($T/2$) is sufficiently long, compared to the time needed to reach the stationary state in each half period. In this case the time-averaged velocity over one period, defined as $v_{\rm sw}(F)$, is (approximately) given as the average of the two velocities attained in each half period:

$$v_{\rm sw}(F) = \frac{1}{2}\left[v(A+F) + v(-A+F)\right]. \tag{1.13}$$

Clearly, if A is chosen so that $v(A)$ (and also $v(-A)$ by symmetry) lies in the region with differential negative mobility, then $v_{\rm sw}(F)$ has absolute negative mobility. An example is shown in Fig. 1.7 for $A = 2$.

The role played by the time varying force is crucial: without this ingredient, the reference stat (with $F = 0$), is in equilibrium, and hence the mobility has to be positive. We will encounter a similar model in Chapter 5, in which a nonequilibrium reference state is obtained without the need for such a time varying additional forcing. We finally note that it is not necessary to have an asymptotically slow switching rate. As demonstrated in [9], absolute negative mobility is also present for faster switching rates. See also [12–14] for other approaches to absolute negative mobility in single particle models, and for a large variety of different geometrical set-ups.

1.5 Brownian donkeys II: collective behavior

Statistical mechanics typically tries to derive the global behavior of a large number of interacting units from their individual properties. This behavior can be dramatically different from what happens on the level of a single element. The occurrence of phase transitions are a prime example. In the last decades, the focus has shifted from the study of equilibrium systems, which is based on the known equilibrium distribution, to nonequilibrium models which are necessarily based on a dynamic formulation. These systems display a fortiori an even richer behavior than their equilibrium counterparts. As examples we cite models for traffic with the interaction between cars giving rise to jams [15], the panic behavior of people who are trying to get out of a burning building [16], neural networks that are able to learn from examples [17], optimization

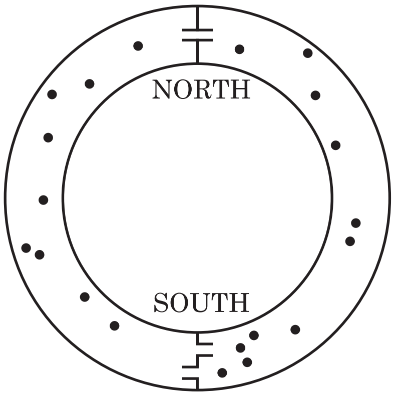

FIG. 1.8. Sketch of the basic collective model. A collection of N particles move along a circle, which is divided into two parts. The particles can move between the two parts by crossing the gates, located at the north and south pole.

[18], the immune system [19] and the stockmarket [20, 21]. The concepts and techniques of statistical physics have proven valuable in tackling such multi-variate problems in quite different fields of knowledge. Our intention here is to introduce a new collective effect, namely negative mobility arising due to the stochastic interaction between the different Brownian particles in a nonequilibrium system, and to study it using the techniques from nonequilibrium statistical mechanics. To do so we first present a toy model in which negative mobility can be understood on an intuitive basis and can be confirmed by a simple analytic theory.

Consider a circle divided in half by two gates, one located at the North pole, the other on the South pole, cf. Fig. 1.8 for a sketch of the model. In each separate half of the circle, particles can move freely about and pass one another without any disturbance. At the gates the situation is different: the latter form barriers which the particles can cross only one at a time and provided they have enough thermal energy. Furthermore, the two gates operate in different ways. The gate on the North pole has a fixed height and is always open. The operation of the South gate is essentially different, see also Fig. 1.9. If the particle density in one half of the circle is below a critical value ρ_c, the particles can by thermal excitation cross the gate coming from that side. Otherwise, the gate is closed. The essential nonequilibrium ingredient, which is in fact also the source of energy, is that this closure is uni-directional. Particles coming from the other half can still cross the gate, provided of course that the density on that side is below the critical value and that they have sufficient thermal energy. Note that such uni-directionality is not compatible with a system at equilibrium, since it would be in violation with the principle of detailed balance [8]. Note also that such uni-directionality is quite common in biological systems, e.g., the transport through a cell membrane can be mediated by uni-directional carriers [22].

Our purpose is now to study the mobility of the system, i.e. the motion of the particles in response to an applied driving force. Before presenting calculations, we give an intuitive explanation of the result, involving a collection of N particles. The particle density on either side is taken equal to the fraction of particles on that particular side. We will limit the discussion to values for $\rho_c < 1/2$. In absence of a driving force, the steady state is expected to be symmetric with respect to both halves, with on average an equal particle density. Also the gate on the South pole will be closed, in both directions,

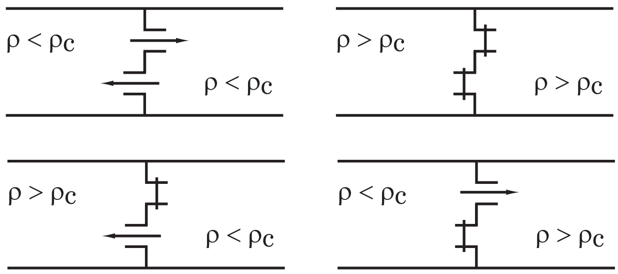

FIG. 1.9. Sketch of the four possible situation for the gate at the south pole. The gate is characterised by the critical density ρ_c. The particle density on a particular part of the circle is represented by the symbol ρ. Depending on the value of ρ, the gate is either open or closed for particles coming from that part.

most of the time. Occasionally it will open from one side when fluctuations drive the density below ρ_c in the corresponding half of the circle. But this will happen equally often on both sides, and will become quite unlikely if the number of particles is large. In any case, there is no systematic average drift of particles along the circle. Suppose now that a small driving force is applied, say in the clockwise direction. Initially, we expect the particles to start moving in this direction, crossing over the North gate, with the South gate remaining closed. As a result, the particle density will increase in the right hand side, and decrease in the left half. Since the force is small, we expect to reach a new steady state, with slightly more particles residing on the right hand side of the circle. However, this steady state will be accompanied by a small but continuous average flux of particles! Indeed, with the new distribution, the particle density on the left side is lower, i.e. closer to the critical value ρ_c, hence fluctuations are more likely to open the South gate for particles coming from the left. Hence we expect a flow of particles counterclockwise, moving in a direction opposite to that of the external driving force!

To quantify this negative mobility, we have to describe in more detail the motion of the Brownian particles. We make the following simplifying assumptions. First, we will not follow in detail the motion of the particle in each of the half circles, but identify their location by a binary value "left" or "right". At any time, the state of the system of N particles is thus completely specified by the number of particles i in the right half of the circle, $i \in \{0, 1, ..., N\}$. Second, we assume that the crossing of the particles through the gates can be described as a thermally activated barrier crossing. Note that for the South gate, this crossing is direction dependent, which in a thermal activation picture would translate in a different temperature of the barrier shoulder left and right (somewhat akin to the Landauer ratchet mentioned before).

With these assumptions, the stochastic dynamics of the system reduces to a discrete state Markov process. The probability $P_i(t)$ to find the system in configuration i at time t thus obeys the following master equation:

$$\begin{cases} \frac{\partial}{\partial t} P_0(t) = -k^+(0)P_0(t) + k^-(1)P_1(t), \\ \dots \\ \frac{\partial}{\partial t} P_i(t) = -[k^+(i) + k^-(i)]P_0(t) + k^+(i-1)P_{i-1}(t) + k^-(i+1)P_{i+1}(t), \\ \dots \\ \frac{\partial}{\partial t} P_N(t) = -k^-(N)P_N(t) + k^+(N-1)P_{N-1}(t), \end{cases} \tag{1.14}$$

where $k^+(i)$ and $k^-(i)$ are the transition rates per unit time from i to $i+1$ or $i-1$ respectively. Such a change in configuration can be realized by either a jump through the North gate *or* by a jump through the South gate, to which we will refer by subscripts n and s respectively. Then, each transition rate $k^\pm(i)$ is the sum of two contributions:

$$k^\pm(i) = k_n^\pm(i) + k_s^\pm(i). \tag{1.15}$$

The separate rates are given by an Arrhenius law:

$$k_n^+(i) = (N-i)e^{\beta F/2}; \tag{1.16}$$
$$k_n^-(i) = ie^{-\beta F/2}; \tag{1.17}$$
$$k_s^+(i) = (N-i)e^{-\beta F/2}\mathrm{H}(\rho_\mathrm{c} - \frac{N-i}{N}); \tag{1.18}$$
$$k_s^-(i) = ie^{\beta F/2}\mathrm{H}(\rho_\mathrm{c} - \frac{i}{N}). \tag{1.19}$$

In these expressions the factor $e^{\pm\beta F/2}$ takes into account the effect of the driving force F. If F is positive, a clockwise particle motion is promoted, and so the $+(-)$ sign is used, promoting transitions in a (counter) clockwise direction. The closing mechanism of the South gate is expressed by a Heavyside function $\mathrm{H}(x)$. An overall proportionality factor has been set equal to unity by a suitable choice of the time unit. Finally, the combinatorial prefactors express the fact that any particle can make a jump.

After these preliminaries, we can start the calculations. The stationary solution of the master equation reads:

$$P_i^{\mathrm{st}} = \frac{1}{Z}k^+(0)...k^+(i-1)k^-(i+1)...k^-(N), \tag{1.20}$$

with Z the normalization constant. The average particle velocity v can be expressed as the total probability flux across the North gate[1], divided by the total number of particles (the circumference of the circle has been set equal to unity):

$$\begin{aligned} v &= \frac{1}{N}\sum_{i=0}^{N}[k_n^+(i) - k_n^-(i)]P_i^{\mathrm{st}} \\ &= e^{\beta F/2} - \frac{1}{N}[e^{\beta F/2} + e^{-\beta F/2}]\langle i\rangle, \end{aligned} \tag{1.21}$$

with $\langle i\rangle = \sum_{i=0}^{N} iP_i^{\mathrm{st}}$ equal to the average number of particles on the right side. Taking the derivative of this expression with respect to F at $F=0$ gives the mobility:

$$\mu = \frac{\beta}{2} - \frac{2}{N}\frac{\partial\langle i\rangle}{\partial F}\bigg|_{F=0}. \tag{1.22}$$

The calculations can be performed explicitly for not too large values of N. Below, we reproduce the explicit analytic result of v and μ for N up to 3.

[1] We could also have taken the particle flux at the South pole since in the stationary regime the fluxes through the two gates must be equal.

$$
\begin{aligned}
v_1 &= \frac{2\sinh(\frac{F\beta}{2})\mathrm{H}(\rho_\mathrm{c}-1)}{1+\mathrm{H}(\rho_\mathrm{c}-1)};\\
v_2 &= \frac{\sinh(\frac{F\beta}{2})\left[(4\cosh(F\beta)+3)\mathrm{H}(\rho_\mathrm{c}-1)+\mathrm{H}(\rho_\mathrm{c}-\frac{1}{2})\right]}{1+\cosh(F\beta)+(3\cosh(F\beta)+2)\mathrm{H}(\rho_\mathrm{c}-1)+\mathrm{H}(\rho_\mathrm{c}-\frac{1}{2})};\\
v_3 &= \frac{2\sinh(\frac{F\beta}{2})\left[(8\cosh(F\beta)+5)\mathrm{H}(\rho_\mathrm{c}-1)+3\mathrm{H}(\rho_\mathrm{c}-\frac{2}{3})\right]}{2+2\cosh(F\beta)+2(7\cosh(F\beta)+4)\mathrm{H}(\rho_\mathrm{c}-1)+5\mathrm{H}(\rho_\mathrm{c}-\frac{2}{3})+\mathrm{H}(\rho_\mathrm{c}-\frac{1}{3})},
\end{aligned}
\tag{1.23}
$$

with corresponding mobilities:

$$
\begin{aligned}
\mu_1 &= \beta - \frac{\beta}{1+\mathrm{H}(\rho_\mathrm{c}-1)};\\
\mu_2 &= \frac{\beta}{2} - \frac{\beta(1-\mathrm{H}(\rho_\mathrm{c}-1))}{2+5\mathrm{H}(\rho_\mathrm{c}-1)+\mathrm{H}(\rho_\mathrm{c}-\frac{1}{2})};\\
\mu_3 &= \frac{\beta\left[13\mathrm{H}(\rho_\mathrm{c}-1)+3\mathrm{H}(\rho_\mathrm{c}-\frac{2}{3})\right]}{4+22\mathrm{H}(\rho_\mathrm{c}-1)+5\mathrm{H}(\rho_\mathrm{c}-\frac{2}{3})+\mathrm{H}(\rho_\mathrm{c}-\frac{1}{3})}.
\end{aligned}
$$

For larger values of N, the expressions become unwieldy, but (1.22) can be easily calculated numerically. A summary of results is reproduced in Figs. 1.10 and 1.11. In agreement with the intuitive discussion, we find that the mobility is always negative for $\rho_\mathrm{c} < 1/2$. For a given value of ρ, the maximum effect is realized for a specific finite value of N, which increases without bound as $\rho_\mathrm{c} \to 1/2$. This can be understood from the fact that the amplitude of the fluctuations in the density, which decrease as $1/\sqrt{N}$, have to be of optimal size, not too small but also not too large. Obviously $\rho_\mathrm{c} = 1/2$ is a special borderline case since any fluctuations will open or close the South gate. By suppressing these fluctuations in the limit $N \to \infty$, the naked effect of the external biasing force, lowering the density below the critical value on one side and raising it above on the other side, will prevail with an infinitely large negative mobility as a result. In the regime $\rho_\mathrm{c} > 1/2$, the South gate is usually open on both sides so that the application of a force will result in a normal mobility. Yet the same arguments concerning the fluctuations and their effect on the current apply as for $\rho_\mathrm{c} < 1/2$. Their effect is however reduced by the normal mobility, which is the only one prevailing in the limit $N \to \infty$.

1.6 Outline

In the following chapters we present a number of explicit constructions. They demonstrate the possibility for absolute negative mobility to occur in a wide variety of nonequilibrium systems, involving either a single Brownian particle, or a collection of them.

Chapter 2 and 3 present a collective model, similar to the collective toy model introduced above. This new model presents a physical realisation of the asymmetrically operating south gate of the toy model. A collection of attracting Brownian particles move on a circle, in the presence of two potential barriers. The nonequilibrium situation is realized by cooling one of these barriers, while the asymmetry of the gate is now taken over by the attractive interaction between the particles (it is easier for a particle to move toward the majority, than to escape from it). A discretized Ising-like version is studied analytically in Chapter 2. The results of these calculations show that absolute negative mobility occurs with a minimal of four particles [23]. In Chapter 3 this model is studied again, but now the particles move in a continuous space. Since it is no longer

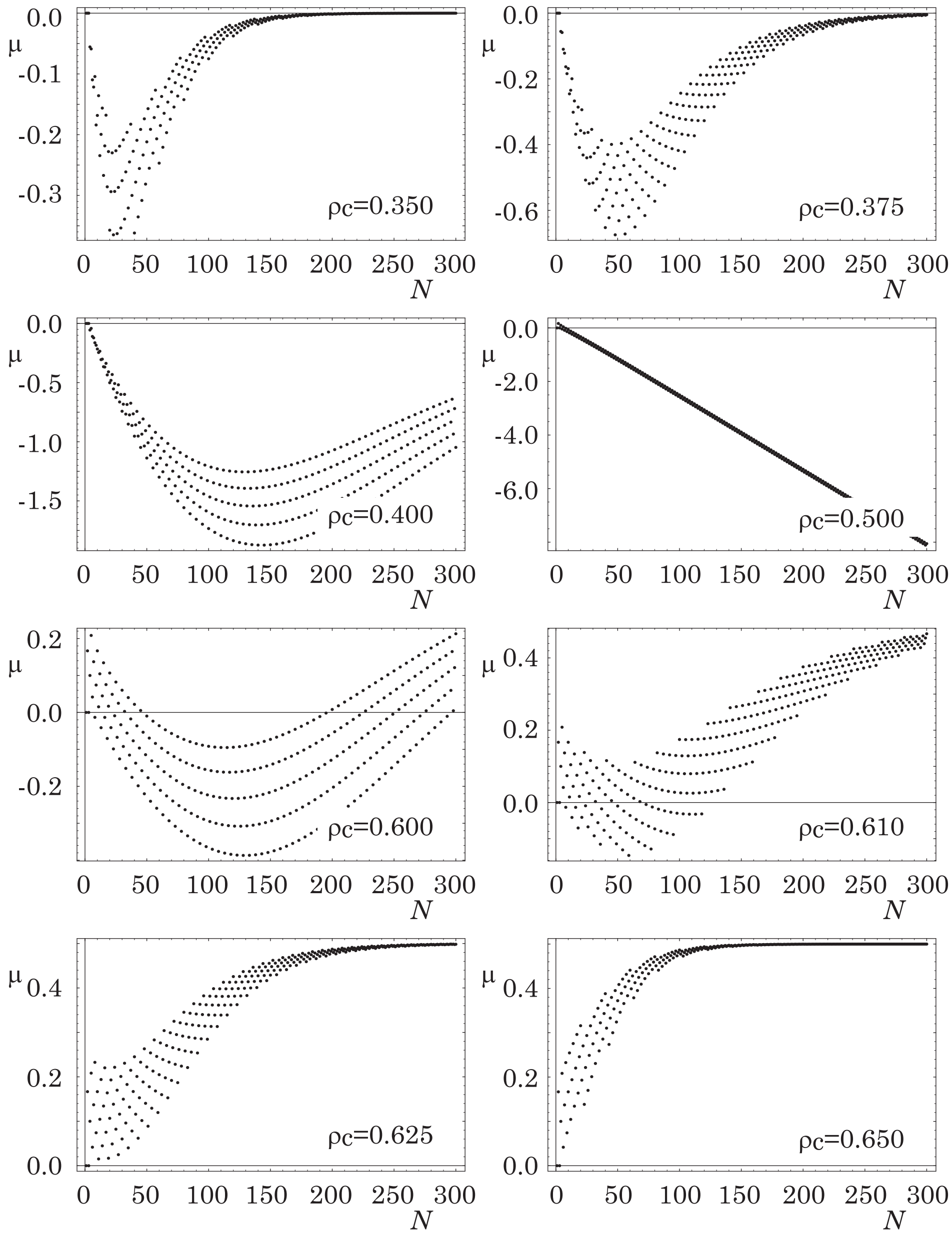

FIG. 1.10. The mobility μ as a function of N for different values of ρ_c ($\beta = 1$).

possible to perform analytical calculations, the results presented there are obtained from extensive computer simulations. The main conclusion is that for this model, absolute negative mobility occurs with a minimal possible number of three particles [24].

Chapter 4 and 5 deal with single-particle models. In Chapter 4 we move away from a detailed physical model, and show that simple non-Markovian extensions of the basic random walk can result in donkey like behavior [25]. Possible applications of this model are included.

Chapter 5 is an extension of the toy model presented in Section 1.4. The particle now performs a random walk in a three layer lattice, instead of the two layers considered before [26]. With this modification, there is no longer need for a time oscillatory forcing.

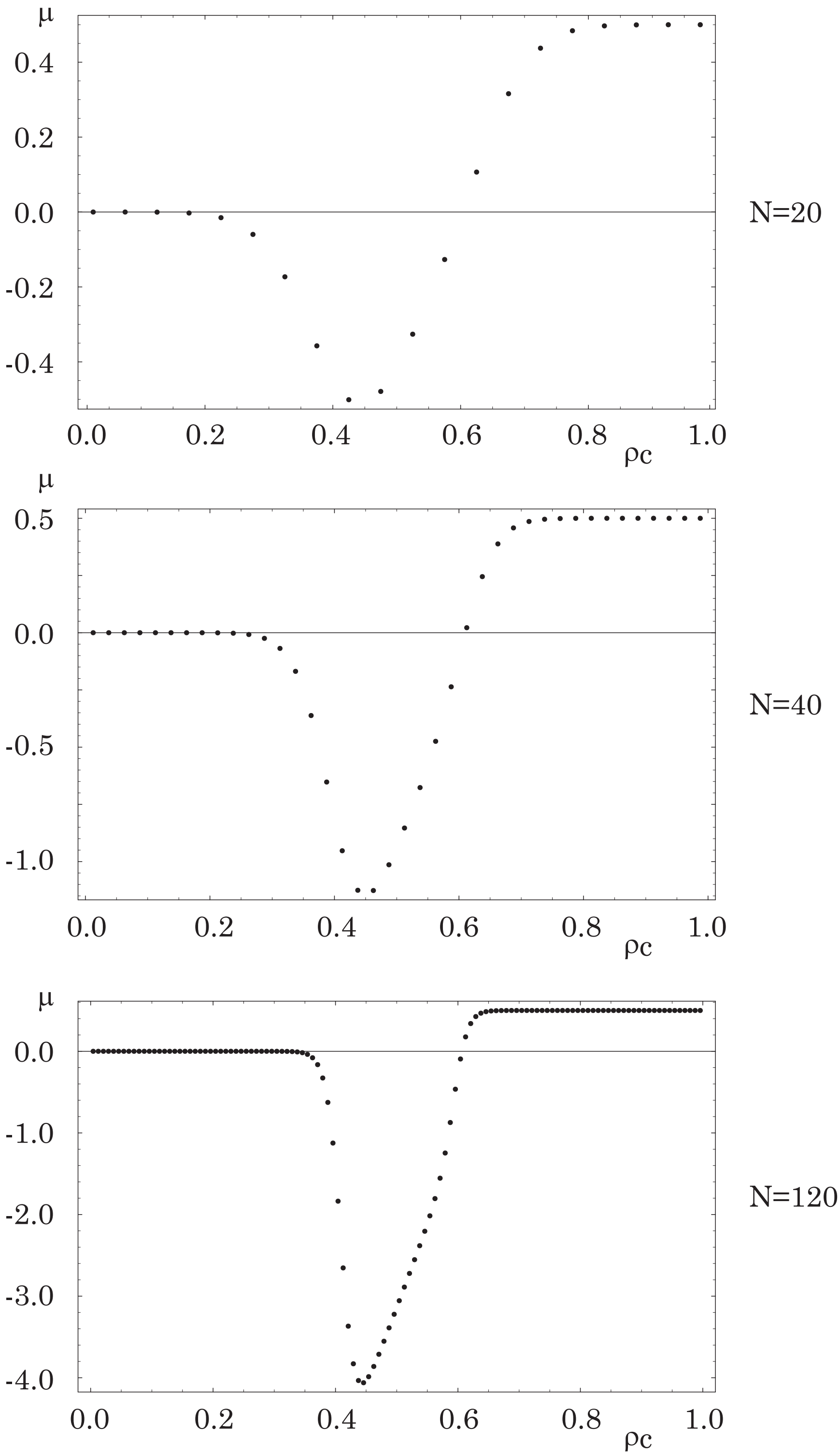

FIG. 1.11. The mobility μ as a function of ρ_c for different number of particles ($\beta = 1$).

The basic motivation for developing this model, is that it can be easily adopted for an experimental realisation of absolute negative mobility.

2

ISING MODEL FOR A BROWNIAN DONKEY

2.1 Introduction

Absolute negative mobility, defined as a motion induced by a small applied force but in a direction which is on average opposite to that of the force, is impossible for a thermodynamic system at equilibrium. As already mentioned before, such a motion would violate the second law since it implies that the (single) heat bath under consideration is performing work against the force. It would also contradict the stability of the equilibrium state since fluctuations generating a force would be amplified. Nothing however prevents the appearance of this phenomenon in nonequilibrium systems, as illustrated by the behavior of a donkey: this animal allegedly has the perverse habit of moving in a direction opposite to the one which is required of it. In this chapter we present a simple physical construction, involving a small number of particles subject to nonequilibrium thermal fluctuations, that displays absolute negative mobility. Since the phenomenon is closely related to the rectification of thermal noise in Brownian motors [27–30](for a recent review on Brownian motors, see [3]), we propose to call this type of system a Brownian donkey.

As a way to motivate the model introduced below and to explain its mode of operation, we first give an intuitive discussion of the basic idea, cf. Fig. 2.1. A set of Brownian particles move on a circle, in the presence of a hot symmetric barrier on the north pole and a cold one on the south pole. The particles are furthermore experiencing mutually attractive binary interactions. The perfect symmetry between clockwise and counter-clockwise motion implies that there is on the average no preferred rotational direction of the particles. However, upon application of a small external torque, say clockwise, acting on all the particles, this symmetry is broken and one expects that the configuration with most of the particles sitting on the right shoulder of the cold barrier is most likely to occur. In this configuration, a counter-clockwise rotation of a single particle is facilitated because it can first overcome the attractive interactions with its partners thanks to the high thermal activation present on the north pole, after which it can be pulled back into the pack over the cold barrier by the combined attractive interactions of the remaining particles. Another plausibility argument for the existence of this phenomenon, that refers directly to the literature on Brownian motors, can be given by noting that a single particle living in the above configuration, with the other particles at frozen positions, realizes a Landauer-Buttiker ratchet [6, 31]. Whether this process becomes the dominant transport mechanism with a net motion in a direction opposite to the applied torque has to be investigated in more detail.

2.2 Ising model

As a simple prototype for the above situation we turn to an Ising-type model, with the particles being in one of only two states, corresponding to being either on the left hand side of the circle (spin up) or right hand side (spin down). The motion over the poles is described as a thermally activated process, i.e. according to an Arrhenius law,

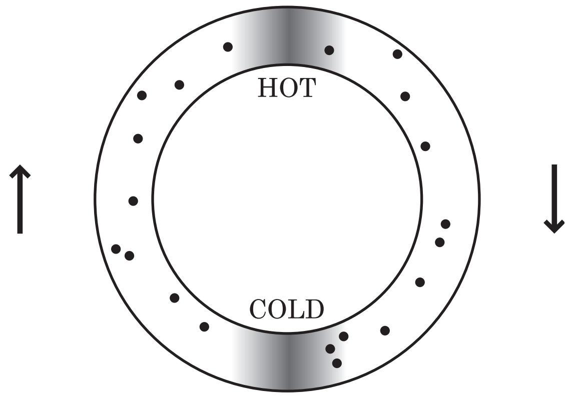

FIG. 2.1. A set of Brownian particles on a circle, in the presence of a hot symmetric barrier on the north pole and a cold one on the south pole.

taking place at the corresponding temperature over a potential barrier that reflects the combined effect of the barrier and the attractive interactions with the other particles. Note that our model differs from other nonequilibrium Ising models, where the spins are in contact with heat baths at different temperatures [32, 33], by the fact that one distinguishes in each spin-flip between rotation of the spin clockwise or counter-clockwise. The physical motivation for this distinction has been explained above.

Since all particles are supposed to be identical, the state of a system with N particles is fully described by the number i of particles in one of the states, say the spin down state ($\downarrow$), with $i = 0, ..., N$. Considering standard Markovian dynamics compatible with the assumed Arrhenius law, the configurational probability $P_i(t)$ obeys the same master equation as given in Section 1.5:

$$\begin{cases} \frac{\partial}{\partial t}P_0(t) &= -k^+(0)P_0(t) + k^-(1)P_1(t), \\ \dots & \\ \frac{\partial}{\partial t}P_i(t) &= -[k^+(i) + k^-(i)]P_0(t) + k^+(i-1)P_{i-1}(t) + k^-(i+1)P_{i+1}(t), \\ \dots & \\ \frac{\partial}{\partial t}P_N(t) &= -k^-(N)P_N(t) + k^+(N-1)P_{N-1}(t). \end{cases} \tag{2.1}$$

We use the same notation as before, with $k^\pm(i)$ the transition rate from configuration i to $i \pm 1$. Every change of configuration can be realized by a jump over either one of the two poles, each being at its respective temperature T_1 (north pole) and T_2 (south pole). The transition rates $k^\pm(i)$ are then given by the sum of the corresponding rates, $k^\pm(i) = k_1^\pm(i) + k_2^\pm(i)$. The latter are assumed to be of the Arrhenius type ($\beta_{1,2} = \frac{1}{k_B T_{1,2}}$):

$$\begin{cases} k_1^+(i) = (N-i)e^{-\beta_1[H+\Delta V_{\text{int}}(i)-F]}; \\ k_2^+(i) = (N-i)e^{-\beta_2[H+\Delta V_{\text{int}}(i)+F]}; \\ k_1^-(i) = ie^{-\beta_1[H-\Delta V_{\text{int}}(i-1)+F]}; \\ k_2^-(i) = ie^{-\beta_2[H-\Delta V_{\text{int}}(i-1)-F]}, \end{cases} \tag{2.2}$$

where an overall factor has been set equal to unity by a suitable choice of the time unit. The combinatorial prefactors expresses the fact that any particle can make the jump. H is the height of the potential barrier, for simplicity taken to be the same at both poles. $\Delta V_{\text{int}}(i) \equiv V_{\text{int}}(i+1) - V_{\text{int}}(i)$ is the change of interaction energy when going from i to $i+1$. This interaction energy is due to the pairwise interaction between any

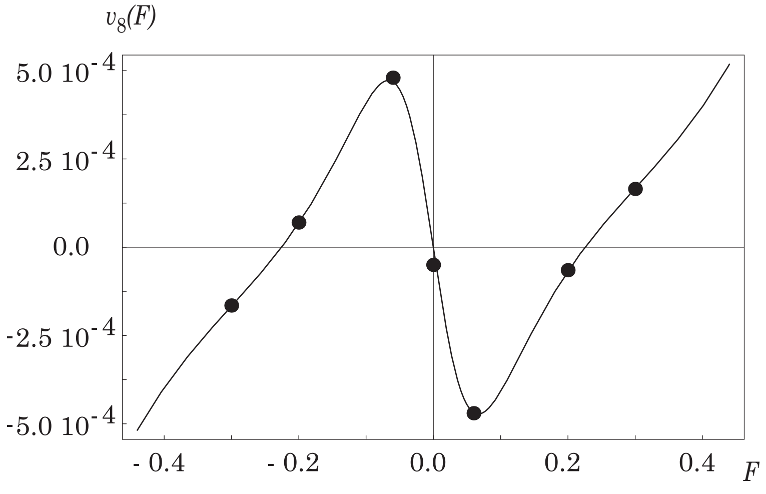

FIG. 2.2. Velocity as a function of the external force for $\beta_1 = 3$, $\beta_2 = 6$, $H = 1$ and $V = 0.8$. The solid line corresponds to the analytical result, while the circles correspond to numerical simulations.

two particles, and is calculated as follow: if the two particles are on the same side (both spin up or spin down), the contribution is 0. When they are located at different sides, the contribution is V/N. And so, the total interaction energy in state i is:

$$V_{\text{int}}(i) = \frac{V}{N} i(N-i). \tag{2.3}$$

In the following we set $V > 0$, so that the interaction is attractive. Finally, F is an external or applied torque, measured along a clockwise direction.

The calculation of the steady state properties of the Markovian dynamics described by (2.1) is essentially a problem in matrix algebra. For example, the steady state probability P_i^{st} is the (right) eigenvector corresponding to the zero eigenvalue of the transition matrix appearing on the r.h.s. of (2.1) [7]. Up to moderate values of N (≈ 10) its exact explicit evaluation can be handled by symbolic manipulators. The basic quantity of interest to us is the steady state velocity v_N, defined as the net average number of transitions from the spin up to the spin down state over the barrier at temperature T_1, divided by the number of particles N:

$$v_N = \frac{1}{N} \sum_{i=0}^{N} \left[k_1^+(i) - k_1^-(i) \right] P_i^{\text{st}}. \tag{2.4}$$

As before, we set the circumference of the circle equal to 1. As an example we quote the following result for $N = 1$, obtained by inserting the explicit expressions for the steady state probabilities P_0^{st} and P_1^{st}:

$$v_1 = \frac{(e^{2(\beta_1+\beta_2)F} - 1)e^{-(\beta_1+\beta_2)(F+H)}}{e^{\beta_1(F-H)} + e^{\beta_2(F-H)} + e^{-\beta_1(F+H)} + e^{-\beta_2(F+H)}} \,. \tag{2.5}$$

Similar but much more lengthy expressions are found for larger values of N. As required by the symmetry of the system, the current is exactly zero in the absence of an applied force $F = 0$. For an illustration of the force dependence, see the plot of $v_8(F)$ in Fig.

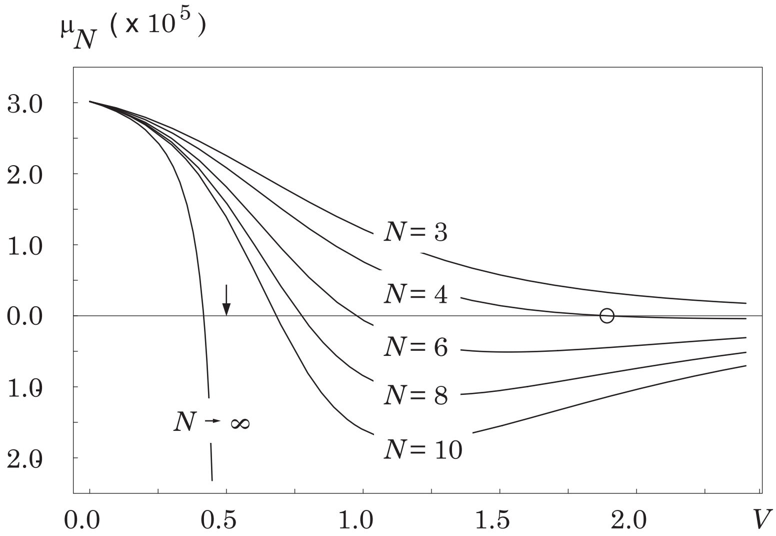

FIG. 2.3. The mobility μ_N as a function of the interaction energy V for different values of N ($\beta_1 = 2$, $\beta_2 = 3$ and $H = 4$). The open circle corresponds to a change of sign in μ_4, and the arrow indicates the location of the phase transition at $V = 0.5$ in the mean field limit.

2.2. The striking feature is the appearance of a regime of negative mobility, namely for $-0.22 < F < 0.22$, confirming the possibility for absolute negative mobility suggested by the intuitive arguments given before. To investigate in more detail the behavior for F small, we introduce the mobility μ_N, defined by $\mu_N = \partial v_N / \partial F|_{F=0}$. We again quote following explicit results:

$$
\begin{aligned}
\mu_1 &= \tfrac{\beta_1+\beta_2}{e^{\beta_1 H}+e^{\beta_2 H}}; \\
\mu_2 &= \big[\beta_1 e^{\beta_1(H+(3/2)V)} + \beta_2 e^{\beta_2(H+(3/2)V)} + (2\beta_1+\beta_2)e^{\beta_2(H+V/2)+\beta_1 V} \\
&\quad +(\beta_1+2\beta_2)e^{\beta_1(H+V/2)+\beta_2 V}\big] \big/ \big[(e^{\beta_1(H+V/2)} + e^{\beta_2(H+V/2)} \\
&\quad +e^{\beta_2(H+V/2)+\beta_1 V} + e^{\beta_1(H+V/2)+\beta_2 V})(e^{\beta_1(H+V/2)} + e^{\beta_2(H+V/2)})\big] .
\end{aligned}
\tag{2.6}
$$

We also give a result, valid $\forall N$, regarding the mobility μ_N to first order in V:

$$\mu_N = \frac{\beta_1+\beta_2}{e^{\beta_1 H}+e^{\beta_2 H}} + \left(\frac{N-1}{N}\right) \frac{(\beta_1-\beta_2)\left(\beta_1 e^{\beta_2 H} - \beta_2 e^{\beta_1 H}\right)}{\left[e^{\beta_1 H}+e^{\beta_2 H}\right]^2} V + O(V^2) . \tag{2.7}$$

In Fig. 2.3 we represent μ_N as a function of the interaction strength for several values of N. One observes negative absolute mobility for $N \geq 4$ when the interaction is sufficiently high. Furthermore the effect becomes more pronounced, all in complete agreement with the intuitive arguments given above, as the number N of particles increases.

2.3 Mean field analysis

While the above calculations become more and more involved as N gets larger, the limit $N \to \infty$ can be solved exactly using simple algebra. In this limit, the mean field approximation becomes (supposedly) exact with any particle interacting with the mean field of the other particles. The latter can then be calculated self-consistently. We introduce the probabilities $P_\uparrow(t)$ and $P_\downarrow(t)$ for a particle to be in the $\uparrow$ and $\downarrow$-states respectively. Since the total probability is normalized, the single relevant quantity is the variable $2p(t) = P_\uparrow(t) - P_\downarrow(t)$, which obeys the following master equation:

$$\frac{dp}{dt} = -k(\uparrow\rightarrow\downarrow)\left(\frac{1}{2}+p\right) + k(\downarrow\rightarrow\uparrow)\left(\frac{1}{2}-p\right), \tag{2.8}$$

with transition rates

$$\begin{aligned} k(\uparrow\rightarrow\downarrow) &= k_1(\uparrow\rightarrow\downarrow) + k_2(\uparrow\rightarrow\downarrow) \\ &= \exp\left\{-\beta_1\left[H + 2Vp - F\right]\right\} + \exp\left\{-\beta_2\left[H + 2Vp + F\right]\right\}, \end{aligned} \tag{2.9}$$

and

$$\begin{aligned} k(\downarrow\rightarrow\uparrow) &= k_1(\downarrow\rightarrow\uparrow) + k_2(\downarrow\rightarrow\uparrow) \\ &= \exp\left\{-\beta_1\left[H - 2Vp + F\right]\right\} + \exp\left\{-\beta_2\left[H - 2Vp - F\right]\right\}. \end{aligned} \tag{2.10}$$

Note that the resulting master equation is nonlinear: the effective barrier produced by the mutual interactions is calculated in a self-consistent manner by assuming that, in the limit $N \to \infty$, the numbers of particles in the $\uparrow$ and $\downarrow$-states are self-averaging and equal to $NP_\uparrow$ and $NP_\downarrow$ respectively. The nonlinearity gives rise to the possibility of multiple steady state solutions of (2.8). The appearance of such solutions is due to symmetry breaking phase transitions that disrupt the ergodicity of the system. In particular, for $\beta_1 = \beta_2 = \beta$, the mean field equation for the steady state reduces to that for the Ising model, namely $2p^{\mathrm{st}} = \tanh(2\beta V p^{\mathrm{st}})$. In the nonequilibrium situation, $\beta_1 \neq \beta_2$, a more complicated bifurcation diagram is obtained. As an example we reproduce the region of multiple solutions in Fig. 2.4 for some typical values of the parameters. The steady state velocity $v_\infty = k_1(\uparrow\rightarrow\downarrow)P_\uparrow^{\mathrm{st}} - k_1(\downarrow\rightarrow\uparrow)P_\downarrow^{\mathrm{st}}$ can again be obtained directly from the steady state probability. For simplicity we restrict ourselves to the analysis of the region where the symmetric solution $p^{\mathrm{st}} = 0$ is stable, namely for $V < V_{cr} \equiv (e^{\beta_1 H} + e^{\beta_2 H})/(\beta_1 e^{\beta_2 H} + \beta_2 e^{\beta_1 H})$. Note that the symmetric solution is not necessarily unique since the system can undergo first order phase transitions with coexisting stable steady state solutions of (2.8), see also Fig. 2.4. With reference to the symmetric solution $p^{\mathrm{st}} = 0$, the following exact result for the mobility μ_∞ is easily derived:

$$\mu_\infty = \frac{\beta_1 + \beta_2 - 2\beta_1\beta_2 V}{e^{\beta_1 H} + e^{\beta_2 H} - \beta_1 V e^{\beta_2 H} - \beta_2 V e^{\beta_1 H}}, \tag{2.11}$$

showing negative mobility for $(\beta_1 + \beta_2)/(2\beta_1\beta_2) < V < V_{cr}$. The series expansion of μ_∞ for small V reproduces as expected the $N \to \infty$ limit of (2.7). More importantly one finds that μ_∞ diverges to $-\infty$ for $V \to V_{cr}$, see also Fig. 2.3. The explanation for the diverging absolute negative mobility is to be found in the diverging susceptibility which is a trademark of second order phase transitions: a small applied force results in a strong symmetry breaking which produces, again following the intuitive mechanism explained before, a flux of particles in the opposite direction.

So far we have formulated our model for particles moving on a circle. Equivalently, one could assume that the particles move in one dimension on a periodic potential with alternating hot and cold peaks and with pairwise interactions that have exactly the same periodicity. In particular this implies that the interactions are of infinite range, which is not a very realistic feature. To investigate whether the phenomenon of absolute negative mobility survives when one considers finite-range interactions, we

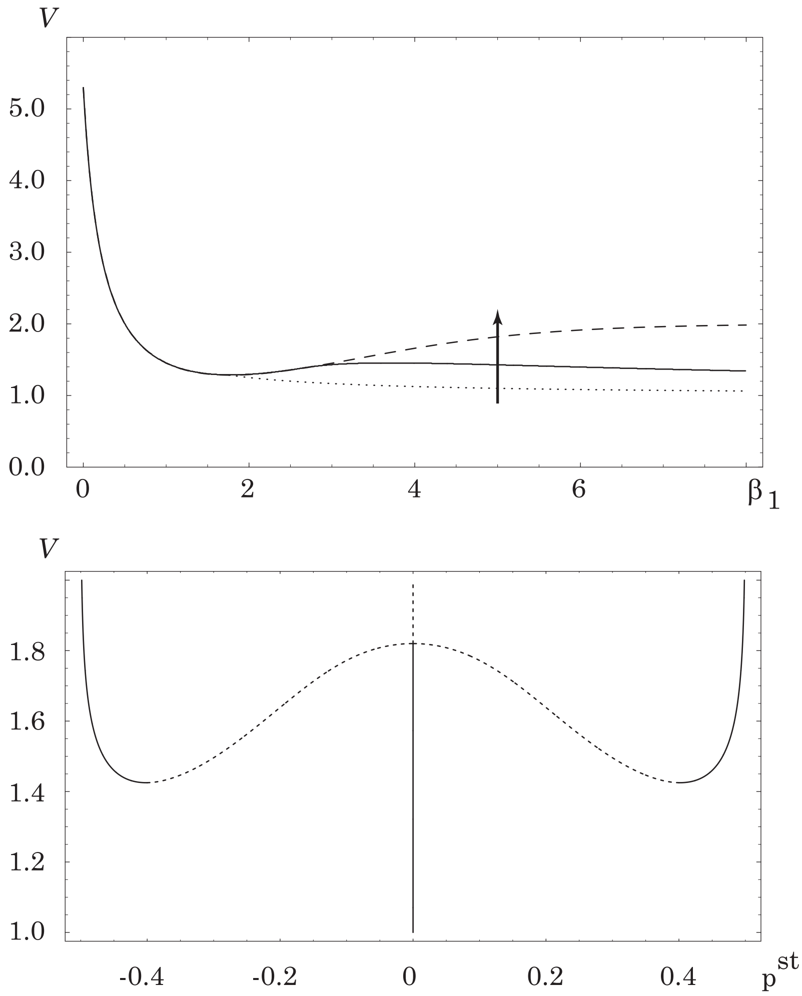

FIG. 2.4. Phase diagram for $\beta_2 = 1/2$ and $H = 1$. Equation (2.8) possesses multiple steady state solutions in the parameter region above the solid line, while the symmetric solution $p^{\mathrm{st}} = 0$ loses its stability above the dashed line corresponding to the critical value $V = V_{cr}$. Note that both lines coincide exactly below a critical value of $\beta_1 \approx 2.8$. The dotted line represents the zero mobility boundary, with absolute negative mobility appearing between the dotted and the dashed lines. The inset shows the bifurcation diagram along the path indicated by the arrow. Stable steady state solutions of (2.8) are shown as solid lines, while unstable solutions are represented by dashed lines.

have performed numerical simulations for the situation where the particles are subject to an additional attractive harmonic pairwise interaction, which effectively cuts off the interaction described above beyond a finite range. The results are collected in Fig. 2.5, from which one concludes that the phenomenon indeed remains present as long as the range of the harmonic force is at least comparable to the wavelength of the periodic potential.

2.4 Conclusion

The phenomenon of a Brownian donkey is not new. It has been documented in several mean field models [34–37]. The present model, however, drastically reduces the com-

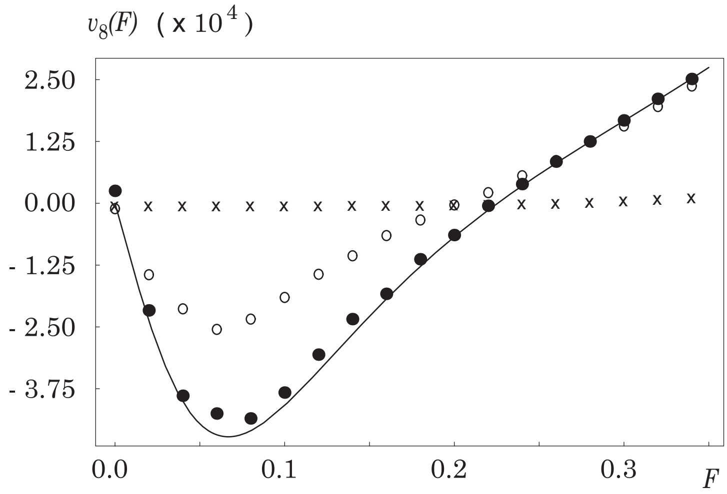

FIG. 2.5. The current as a function of the external force for $\beta_1 = 3$, $\beta_2 = 6$, $H = 1$, $V = 0.8$ and $N = 8$. The solid line corresponds to the analytical result without harmonic interaction, while the other results are in the presence of an additional pairwise attractive harmonic force with force constant $10^{-3}(\bullet)$, $10^{-2}(\circ)$ and $10^{-1}(\times)$ respectively.

plexity of the analysis by formulating the problem as a nonequilibrium Ising model. In particular this allows us, for the first time, to investigate analytically the case of a finite N, and to conclude that the phenomenon of absolute negative mobility occurs for $N \geq 4$. In fact one expects from the heuristic analysis, with one particle attracted over the cold barrier by the majority of the other particles, that $N = 3$ would be the smallest number of particles for which this specific scenario can be realized. This will be confirmed by the numerical study of the continuous model carried out in the next chapter. Furthermore, Brownian donkeys based on other rectification effects are of course not ruled out, as demonstrated by various single-particle models.

3

A TRIO OF BROWNIAN DONKEYS

3.1 Introduction

In the previous chapter, the particle motion is described as a hopping process over the barriers. This description is valid as long as the energy needed to cross the barriers is significantly larger than the thermal energy. The resulting Ising-like description has the advantage that one can study in detail a system with interacting particles, something that is impossible in continuous space. The disadvantages are that the model does not capture in detail the effect of a specific temperature profile, potential landscape and interaction potential.

In this chapter we turn to a continuous description of the model, as shown in Fig. 3.1. Since it is now no longer possible to obtain analytical results, we present a systematic numerical study of the system, and show that for specific parameter values, absolute negative mobility occurs for a minimum of three particles.

3.2 Continuous description

As before, we consider a collection of N particles moving on a circle. The position of the particles along this circle is denoted by x_i, $i \in \{1, ..., N\}$. The particles move in a background potential $V(x) = V\cos(2x)$, see also Fig. 3.2. A numerical study of the system is based upon integration of the following set of N coupled Langevin equations, describing the overdamped motion of the particles:

$$\dot{x}_i = F + 2V\sin(2x_i) - \frac{K}{N}\sum_{j=1}^{N}\sin(x_i - x_j) + \sqrt{2T(x_i)}\xi_i(t), \tag{3.1}$$

with F the external force and K specifying the coupling strength between the particles. The simple specific form $-\frac{K}{N}\sin(x_i - x_j)$ for the interaction force between two particles is justified as follow. First, the interaction depends only on the distance between the particles measured along the circle, and must be periodic since the particles move on a circle. Second, the force has to be an odd function with respect to the distance, as a result of Newton's third law. Our ansatz can therefore be seen as the first order term in a Fourier expansion of the interaction force. The thermal noise is represented here by the random force (the so-called Langevin force) $\sqrt{2T(x_i)}\xi_i(t)$. ξ_i is a Gaussian white noise with zero mean $\langle\xi_i(t)\rangle = 0$ and delta correlated $\langle\xi_i(t)\xi_j(t')\rangle = \delta_{ij}\delta(t - t')$. This term is to be interpreted in the Stratonovich sense [7]. The strength of the noise is determined by the position dependent temperature $T(x_i)$, which is taken of the following form:

$$T(x) = (T_H - T_L)\cos^2(x/2) + T_L, \tag{3.2}$$

with T_L and T_H respectively the minimum and maximum temperature. Figure 3.2 shows both the potential and temperature profile. Note that a similar model in the absence of a potential $V = 0$, was treated in [35] in the mean field limit $N \to \infty$.

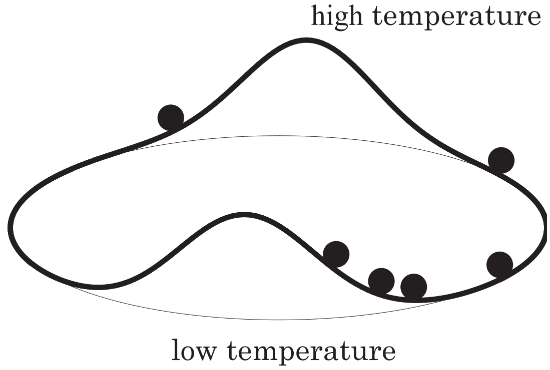

FIG. 3.1. Sketch of the system. In the presence of a clockwise applied force, the particles are more likely to be found on the right side of the cold barrier.

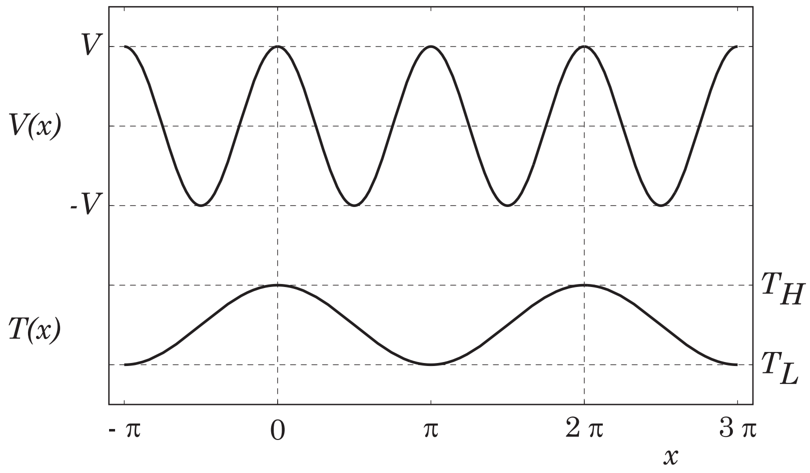

FIG. 3.2. The potential and temperature profile.

The results presented in the following section are obtained by numerical integration of the set of N coupled differential equations given by (3.1). As integration scheme, the *improved Euler* or *Heun* method is used [38].

3.3 Numerical results

The main results are reproduced in the Figs. 3.3-3.5. The first observation is that by optimizing the parameters one can amplify the negative mobility significantly. In Fig. 3.3, an optimal value of the potential barrier height is identified, keeping the other parameter values fixed. The values of the latter parameters were actually determined by subsequent optimization with respect to each of them. The plot is for $N = 20$ particles and a negative mobility of about -4.0×10^{-3} is reached in this way. By repeating this procedure of sequential optimization with reducing the number of particles, one actually finds that negative mobility persists including for the case of the minimum of three interacting walkers. Note however that the mobility becomes very small, of the order of -6.0×10^{-5}, while the diffusion is large. In Fig. 3.5 the average position and the dispersion are plotted as a function of time and it becomes clear that the negative mobility will only become the dominant process for very large times.

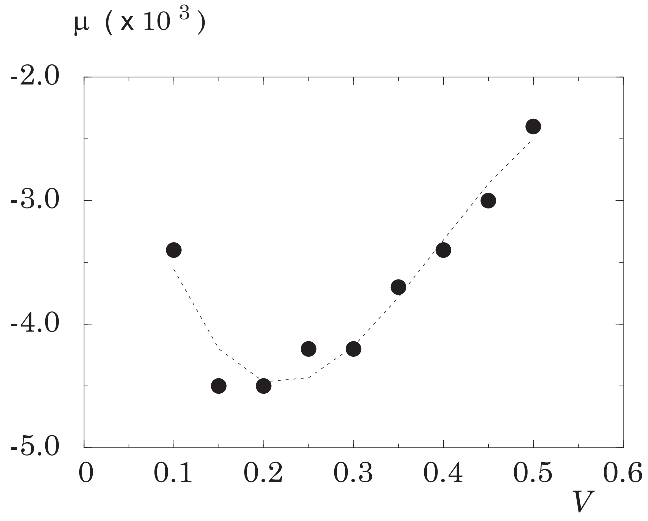

FIG. 3.3. Mobility as a function of the potential barrier height V. The dotted line indicates the trend ($K = 1.29$, $F = 0.06$, $T_H = 1.0$, $T_L = 0.1$, and $N = 20$).

3.4 Discussion

The main purpose of this chapter was to give numerical evidence for the existence of negative mobility in a model of interacting Brownian particles. It was found that the phenomenon exists for the minimum of three interacting walkers, even though the mobility was found to be very small. The latter observation suggests that the experimental detection of the phenomenon will require a lot of fine tuning. However we have not performed a systematic optimization search with respect to the parameters available in the model defined above (since we worked sequentially mostly for reasons of available computer time). More importantly we expect that the negative mobility will be further amplified by optimizing the analytic form of substrate potential, temperature profile and interaction potential. Another modification that may be of relevance in an experimental context is the addition of short range repulsive interaction between the particles. In conclusion, there seems to be no basic limitation for the amplitude of negative mobility. As a general argument supporting this conclusion we refer to the theory of linear irreversible thermodynamics (see for example [39]) with the observation that temperature gradients can generate particle fluxes and that the corresponding Onsager coefficient, being an off-diagonal element of the linear response matrix, is not restricted to have a particular sign or amplitude.

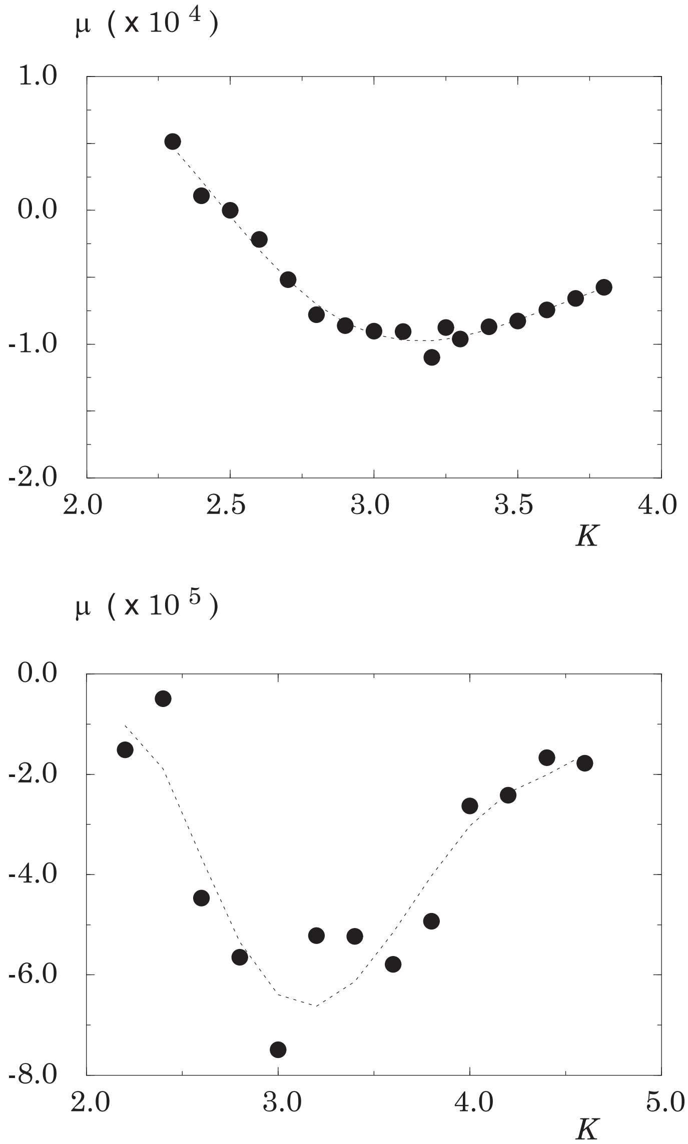

FIG. 3.4. Mobility as a function of the coupling strength K for $N = 4$ (upper part) and $N = 3$ (lower part). The dotted lines indicate the trend ($T_H = 1.0$, $T_L = 0.1$, and $V = 0.3$).

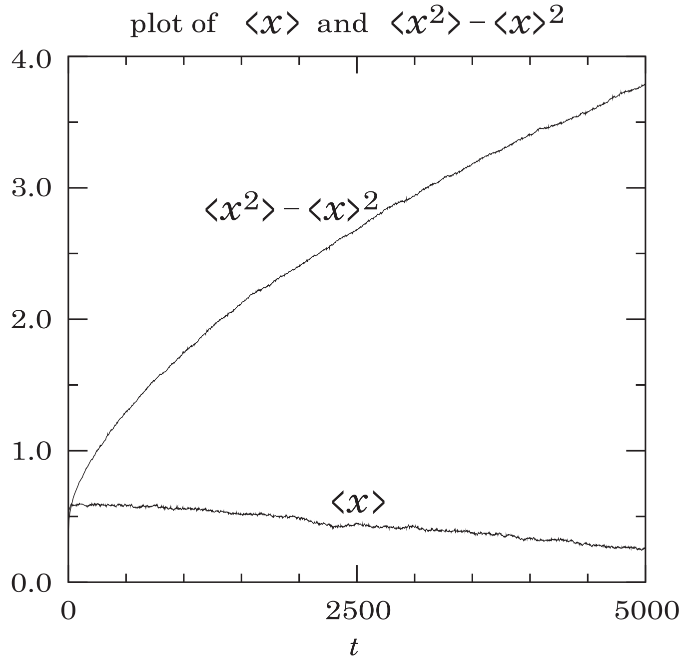

FIG. 3.5. Plot of the average position $<x>$ of the center of mass and variance Δx for $N = 3$ ($F = 0.06$, $T_H = 1.0$,$T_L = 0.0$, $V = 0.3$, and $K = 3.0$). The variance measures the spreading of the particles with respect to the center of mass.

4

RANDOM WALKS WITH ABSOLUTE NEGATIVE MOBILITY

The random walker is a basic paradigm in science that has been applied to a wide range of problems in many different fields, from the microscopic world of chemical kinetics over stock exchange models, to the outer regions of space. In statistical mechanics and the theory of stochastic processes, it has been studied in great detail and provides a technically simple and conceptually transparent discretized version of the Wiener process. When referring to the erratic motion of thermally agitated particles, the latter is also known as Brownian motion. For excellent reviews on random walks and applications we refer to the following works [40–45].

In this chapter, we show how very simple non-Markovian modifications of the standard random walk can result in absolute negative mobility. In contrast to the previous chapters, we now move away from a detailed physical model, thereby putting this phenomenon in a much broader context.

4.1 Introduction: the standard random walk

Before presenting the modifications, we first review the main results of the standard random walk in one dimension, and introduce the necessary tools for analysing these random walks. In the basic model, a particle moves around in a one dimensional lattice by making jumps to nearest neighbor sites. For simplicity, the time between two jumps is taken to be constant. With probability p the particle jumps to the right, and with probability $q = 1 - p$ it jumps to the left. Defining $n \in \mathbb{N}$ as the number of steps taken by the particle, we write $x(n)$ as the position of the particle after n steps. Setting the distance between two adjacent sites equal to 1, we have $x(n) \in \mathbb{Z}$. For this random walk, we now want to calculate the drift velocity v and diffusion coefficient D, defined as:

$$v \equiv \lim_{n\to\infty} \frac{\langle x(n)\rangle}{n}; \tag{4.1}$$

$$D \equiv \lim_{n\to\infty} \frac{\langle x^2(n)\rangle - \langle x(n)\rangle^2}{2n}. \tag{4.2}$$

The brackets $\langle . \rangle$ denote an average over a large number of realisations. The quantities $\langle x(n)\rangle$ and $\langle x^2(n)\rangle$ denote respectively the first and second moment, defined in general as:

$$\langle x^m(n)\rangle = \sum_{x=-\infty}^{\infty} x^m(n) P(x, n). \tag{4.3}$$

$P(x, n)$ is the (conditional) probability to be at position x after n steps, given the initial condition $x(0) = 0$, i.e. the particle starts at the origin. The time evolution of $P(x, n)$ is given by the following master equation:

$$P(x, n + 1) = pP(x - 1, n) + qP(x + 1, n), \tag{4.4}$$

with initial condition $P(x, 0) = \delta_{x,0}$ (since we are interested in the asymptotic behavior, the final results do not depend on the initial conditions).

A possible solution to the problem consists in solving (4.4) by using combinatorial arguments (see for example [45]) and then substituting the expression for $P(x,n)$ in (4.1) and (4.2). There is however a more diligent method [44, 45], which uses the so-called generating function. In this method, the key quantity is no longer the probability distribution $P(x,n)$, but rather its Fourier-Laplace transform $F(k,z)$ defined as:

$$F(k,z) = \sum_{x=-\infty}^{\infty} e^{ikx} \sum_{n=0}^{\infty} z^n P(x,n). \tag{4.5}$$

The calculation of $F(k,z)$ is usually simpler, and contains the same information as $P(x,n)$. For the basic random walk model, the calculation of $F(k,z)$ is straightforward, and is reproduced here. We start from the definition (4.5), and replace $P(x,0)$ with the initial conditions given above:

$$\begin{aligned} F(k,z) &= \sum_{x=-\infty}^{\infty} e^{ikx} \left[\delta_{x,0} + \sum_{n=1}^{\infty} z^n P(x,n) \right] \\ &= 1 + \sum_{x=-\infty}^{\infty} e^{ikx} \sum_{n=0}^{\infty} z^{n+1} P(x,n+1). \end{aligned} \tag{4.6}$$

$P(x,n+1)$ can be replaced by using the master equation (4.4), and this leads to an equation involving only the unknown function $F(k,z)$:

$$\begin{aligned} F(k,z) &= 1 + \sum_{x=-\infty}^{\infty} e^{ikx} \sum_{n=0}^{\infty} z^{n+1} \left[pP(x-1,n) + qP(x+1,n) \right] \\ &= 1 + z \left(pe^{ik} + qe^{-ik} \right) F(k,z). \end{aligned} \tag{4.7}$$

The solution of this equation reads:

$$F(k,z) = \frac{1}{1 - z\left(pe^{ik} + qe^{-ik}\right).} \tag{4.8}$$

From this final expression, one can determine v and D as follows. First, expand $F(k,z)$ around $k=0$. Using $e^{ikx} = \sum (ikx)^m/m!$, (4.5) becomes:

$$F(k,z) = \sum_{m=0}^{\infty} \frac{(ik)^m}{m!} \sum_{n=0}^{\infty} z^n \sum_{x=-\infty}^{\infty} x^m P(x,n) = \sum_{m=0}^{\infty} \frac{(ik)^m}{m!} \langle x^m(z) \rangle, \tag{4.9}$$

with

$$\langle x^m(z) \rangle = \sum_{n=0}^{\infty} z^n \langle x^m(n) \rangle. \tag{4.10}$$

Knowledge of $\langle x^m(z) \rangle$ allows the calculation the moments (see Appendix A) and hence of v and D. For the basic random walk, the final results read:

$$v = 2p - 1; \tag{4.11}$$

$$D = 2p(1-p). \tag{4.12}$$

On average, the particle will acquire a drift velocity equal to $2p-1$. The diffusion coefficient D, which is a measure of the spreading around the average position, is maximal for $p = 1/2$, and goes to zero in the limit $p \to 0$ or $p \to 1$.

4.2 Random walk with absolute negative mobility

A well known non-Markovian modification is the so-called random walk with persistence [46], in which the step directions taken by the walker are correlated with previous ones. In the random walk modification presented below, it is the step sizes that are correlated, rather than their direction. The rule is the following. A particle performs the above described biased random walk. We introduce a new parameter, denoted by $N-1$, which gives the maximal allowed number of consecutive steps in the same direction. Hence, whenever the particle hops in the same direction for N successive time steps, this excursion is canceled, i.e., the particle is transferred back to the original position of N-steps ago, and its memory is cleared. Our main purpose now is to study how this limitation of large excursions impacts the resulting drift velocity. To do so, we note that the state of the particle is fully described by the knowledge of its position x, together with the length l of the last sequence of successive steps in the same direction ($l \in \{\pm 1, \ldots, \pm N\}$). Note that it is no longer possible to describe the particle motion by merely specifying the position, and hence x alone is no longer Markovian. The problem can be solved by including the length l, so that (x, l) defines again a Markov process. The situation here is reminiscent of classical mechanics in which one needs both position and velocity to describe the motion. The probability $P(x, l, n)$ to find the system in state (x, l) after n steps obeys the following master equation:

$$\begin{aligned} P(x, N, n) &= pP(x + N - 1, N - 1, n - 1) \\ P(x, j, n) &= pP(x - 1, j - 1, n - 1) \\ P(x, 1, n) &= pP(x - 1, N, n - 1) + p \sum_{m=-1}^{-N} P(x - 1, m, n - 1) \ , \end{aligned} \tag{4.13}$$

with initial conditions $P(x, l, 0) = \frac{1}{2}\delta_{x,0}\ \delta_{l,\pm N}$. A similar set of equations applies for the steps to the left (probability $q = 1 - p$). From (4.13) and using (4.5) with $P(x, n) = \sum_{l=\pm 1}^{\pm N} P(x, l, n)$, one obtains the following exact result for the Fourier transform of the generating function:

$$F(k, z) = \frac{1}{f(p, k) + f(1 - p, -k) - 1}, \tag{4.14}$$

with

$$f(p, k) = (1 - zpe^{ik})\frac{1 - (zp)^N}{1 - (zpe^{ik})^N} \ . \tag{4.15}$$

In the long time limit $n \to \infty$, the distribution becomes Gaussian and is characterized by the following drift velocity v and diffusion coefficient D (see Appendix A):

$$v = 2p - 1 + \frac{N\,(1-p)^N\,p}{1 - (1-p)^N} - \frac{N\ (1-p)\ p^N}{1 - p^N} \ , \tag{4.16}$$

and

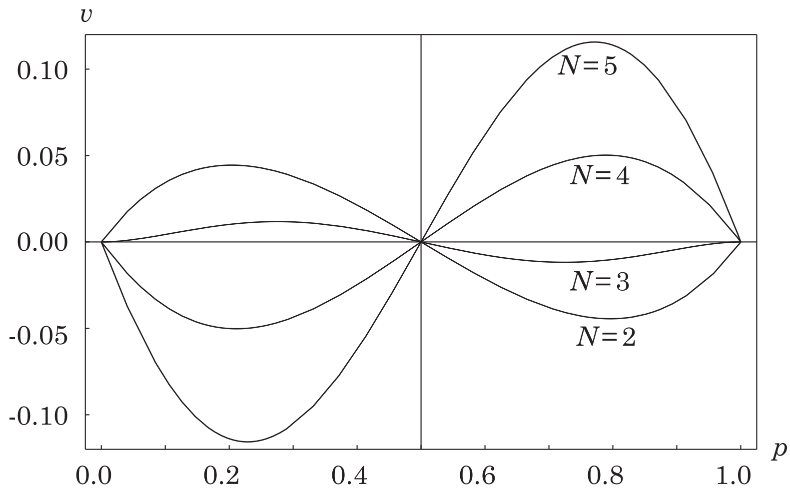

FIG. 4.1. The average speed v as a function of the bias p for different values of N. For $N = 2$ and 3 one observes negative mobility.

$$D = \frac{N^3}{(1-q^N)^3(1-p^N)^3}\left[\begin{array}{l}\Big\{p^{2N+1}q^N - p^N q - 2p^N(p-q)q^N + pq^N \\ -p^N q^{2N+1}\Big\}\Big\{p^N q + p^N(p-q)q^N - pq^N\Big\}\end{array}\right]$$
$$+\frac{N^2}{2(1-q^N)^2(1-p^N)^2}\left[\begin{array}{l}p^N q^N\Big\{p^N(2q-p) + q^N(2p-q) - 14pq \\ +4 - 2p^N q^N(p^2+q^2)\Big\} + pq(p^{2N}+q^{2N}) \\ +p^N q(4p-3) + pq^N(4q-3)\end{array}\right]$$
$$+\frac{N}{(1-p^N)(1-q^N)}\left[2pq\Big\{p^N - 2p^N q^N + q^N\Big\}\right] + 2pq\ . \tag{4.17}$$

Equation (4.16) is the central result of this chapter. In Fig. 4.1 the dependence of v on the bias p is plotted for different values of N. The key observation is that the particle moves in a direction opposite to the bias for $N = 2$ and 3. The intuitive reason is that the penalization of large excursions is strongest in the direction of the bias.

For the sake of completeness, we also represent the diffusion coefficient as a function of p in Fig. 4.2, for various values of N. Note the development of two symmetric peaks of increasing height as N becomes larger. This increased dispersion is due to the large steps corresponding to canceled excursions of size N. To have enough probability weight, such excursions however require a stronger bias when N becomes large.

4.3 Applications

We mention three examples that can be mapped on this type of random walk. The first one comes from chemistry. A linear polymer is growing in a mixture of A and B molecules, with concentrations c_A and c_B respectively. They attach to the polymer with a probability proportional to their relative concentration, i.e. , the probability that an A particle is chosen reads $p = [c_A/(c_A + c_B)]_{\text{mixture}}$. When two identical molecules

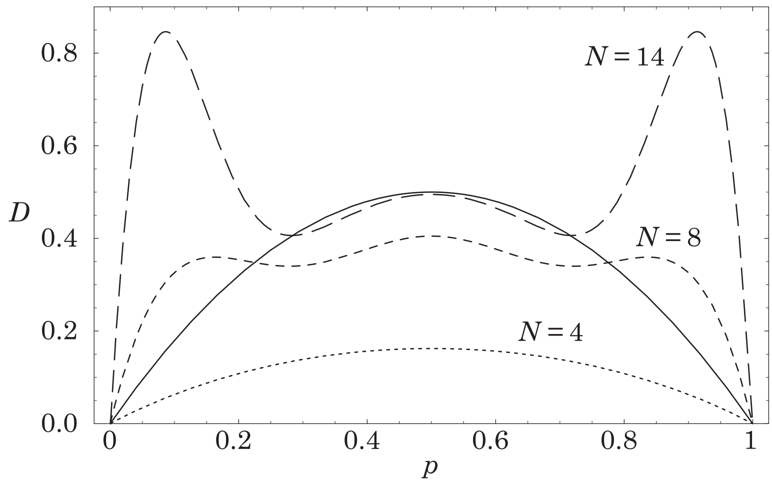

FIG. 4.2. The diffusion coefficient D as a function of the bias p for different values of N. The solid line represents the diffusion coefficient for the normal random walk.

attach *successively*, they dimerize and disconnect from the polymer. If we represent the succession of A and B molecules along the polymer as steps to right and left respectively of a random walk, we have a realization of our model with $N = 2$. The long time relative concentrations of A versus B *in the polymer* is given by the drift velocity $v = 2[c_A/(c_A + c_B)]_{\text{polymer}} - 1$. Hence negative mobility implies that the polymer will be rich in the species that is poor in the mixture.

Second, we turn to an example from physics. A charged particle is performing a cycloid motion in the (x, y) plane orthogonal to a magnetic field along the z direction, with an electric field parallel to the y-axis [47]. At each multiple of half the cyclotron period, one chooses the sign of the magnetic field to be either positive or negative with probabilities p and $q = 1 - p$ respectively. The sign of the electric field is switched if that of the magnetic field has not changed, otherwise it is taken to be positive. Clearly, when the magnetic field is switched to a positive value, the particle will rotate to a new position in the positive x direction. As long as the sign of this field does not change, the particle will rotate back and forth between this new position and its original position. A similar dynamics takes place for negative magnetic field, but taking place now in the negative x direction. The position of the particle at half multiples of the period thus undergoes the above described random walk, again with $N = 2$. Negative mobility implies that the drift motion along the x-axis will be opposite to what is expected from the dominant direction of the magnetic field.

As a last example, we construct a new paradoxical game (see also part 2 of this work for other paradoxical games). A banker offers an investment with, on average, a positive yearly return. In our random walk model, the probability for winning a unit of capital is $p > 1/2$. A nervous investor wants more protection against losses. The banker proposes to cancel the losses in N successive years. But he argues that, in all fairness, he then also has to cancel the wins in N successive years. The capital of the investor now undergoes the above described random walk with the paradoxical result that the investment will have on average a negative return if $N = 2$ and 3. Figure 4.3 visualizes the sad story of the nervous investor.

Fig. 4.3. Cartoon of the new paradoxical game.

4.4 Collective effects

The random walk model introduced above is a prototype. Many variations and modifications can be envisaged. We discuss next, in some detail, possible cooperative versions. We cite two prominent mechanisms that may appear quite naturally when the walkers interact: crowding and greediness. As an example of crowding, consider a set of Brownian particles in a channel with a periodic array of gates. Note that such a set-up can be easily realized experimentally using, for example, latex particles suspended in a flow through fabricated micro-pores in silicon wafers [48]. The gates should be such that a single particle can easily pass through while the passage is hampered when several particles are present on the same side of the gate. Upon application of an external bias, such a crowding will appear more frequently on the side of the gates which is upstream of the force, with negative mobility as a *possible* outcome. We stress that this intuitive argument can be misleading. Indeed, as already mentioned in the introduction, negative mobility is ruled out near equilibrium by the fluctuation dissipation theorem. One thus either has to work in the regime of nonlinear response, or linear response around a nonequilibrium state. An explicit example of the latter case is given by the model introduced in [23] (see also Chapter 2), where the narrow gate (represented by a barrier) is also cooled. A biochemical alternative corresponds to a gate that operates unbiased active transport, which is deactivated when more then one particle attaches to the same site [22].

The second mechanism, greediness, is more intricate and possibly more surprising: it involves informed walkers that modify their jump statistics in a greedy way in response to the motion of the other walkers. A deterministic analogue is the so-called Braess paradox [49, 50], in which it is found that the addition of a new route to go from one point to another actually slows down the traffic in that direction. The opening of the new route makes the original flow pattern unstable against greedy defectors, who, by choosing a trajectory that is faster for them with respect to the original flow pattern, produce a cascade of modifications leading to a stable but sub-optimal equilibrium. The paradox is also well known in macro- economics where these type of sub-optimal states are referred to as Nash equilibria. In short, just like in the traffic problem, the pursue of individual interests can be the demise of a collective goal. In the context of random walkers, one can imagine negative mobility to appear when, as a result of the installation of a bias, walkers greedily choose routes that appear, with respect to the existing flow patterns, favorable to themselves, but effectively result in an overall delay of the motion in the direction of the bias.

4.5 Discussion

We close with a discussion of the distinctive features of walks with negative mobility and a tour d'horizon of related results from the literature. First, such walkers are reservoirs of energy that become available *upon request*. Rather then dissipating energy supplied by an external force, the walker, which moves in a direction opposite to the force, actually performs work. Usual Brownian motors also have this capability, but in the present case energy is only released when loading takes place. Concomitantly, the direction of the loading is irrelevant. Second, whereas usual walkers get trapped in the minima of an external potential, the ones with negative mobility move toward the maxima. The roles of stability and instability are thus interchanged. This property might conceivably play a role in triggering a chemical reaction with the walker as catalyst. Third, other related results from the literature include linear response around nonequilibrium steady states, reconsidered in the light of anomalous response properties in [51], and differential negative mobility in networks with dead ends [9]. Finally, negative mobility can also appear when the force acts, not only on the walkers, but also, directly or indirectly, on the substrate, see for example the well known anomalous transport of electrons [52].

5

BROWNIAN MOTION WITH ABSOLUTE NEGATIVE MOBILITY

5.1 Introduction

In this chapter we present another single particle model with absolute negative mobility. The purpose is to introduce a new model for Brownian negative mobility which has the advantage that it could be easily realized experimentally. Note that the construction from [9] is presently the subject of an experimental verification, but in this model the reference nonequilibrium state is, in contrast to ours, not a steady state since it requires the application of time oscillatory forcing (cf. Section 1.5).

We start by explaining the intuitive idea behind the mode of operation of our system by focusing on a discrete random walk model. A Brownian particle is performing a random walk on the three layer lattice represented in Fig. 5.1, which is aligned along the x-axis. In the upper and lower layer, the motion of the particle is biased along x, but in opposite directions ($+x$ and $-x$ direction for upper and lower layer respectively) and with equal amplitude. Transitions between these layers are possible by hopping across the intermediate layer. The latter consists of pockets of three states with access to the upper and lower layer located at the left and right hand side of these pockets respectively. All the corresponding transitions are unbiased. The overall symmetry thus dictates that the random walker will not acquire a systematic speed along the x-axis. Upon application of an external force however, say along the $+x$ direction, the walker will preferentially reside in the right hand side of the pockets, facilitating the entry into the lower layer where the motion however is biased into the $-x$ direction. One can expect that when this bias is sufficiently large, a net motion against the direction of the force, hence negative mobility, is observed. We will show below that this is indeed the case. It should also be clear that the above described mechanism is rather general and can be realized by many other similar constructions. One such example will be analyzed in full analytic detail in Section 5.3, see Fig. 5.3.

5.2 Random walk model

The three layer lattice represented in Fig. 5.1 is a periodic repetition of a 3×3 unit cell. The position of a particle in this lattice is thus specified by the following coordinates: the site number $i \in \{1,2,3\}$, the horizontal layer $\alpha \in \{-,0,+\}$ and the cell number $I \in \mathbb{Z}$. Assuming that the sites have a linear dimension equal to 1, the corresponding position along the horizontal x-axis is $x_{[i,\alpha,I]} = i+3I$. The probability to find the particle at position $[i,\alpha,I]$ at time t will be denoted by $P_{[i,\alpha,I]}(t)$. A particle can jump between nearest neighbor sites, as indicated by the arrows. The transition rates are chosen as follow: in the vertical direction, *i.e.* for allowed transitions between different layers, the rates are equal to γ. In the horizontal direction, the rates are given as:

$$\begin{array}{llll} k^{+}_{\leftarrow} = e^{-\beta(B+F)/2} & ; \; k^{+}_{\rightarrow} = e^{\beta(B+F)/2} & ; \\ k^{0}_{\leftarrow} = e^{-\beta F/2} & ; \; k^{0}_{\rightarrow} = e^{\beta F/2} & ; \\ k^{-}_{\leftarrow} = e^{-\beta(-B+F)/2} & ; \; k^{-}_{\rightarrow} = e^{\beta(-B+F)/2} & . \end{array} \tag{5.1}$$

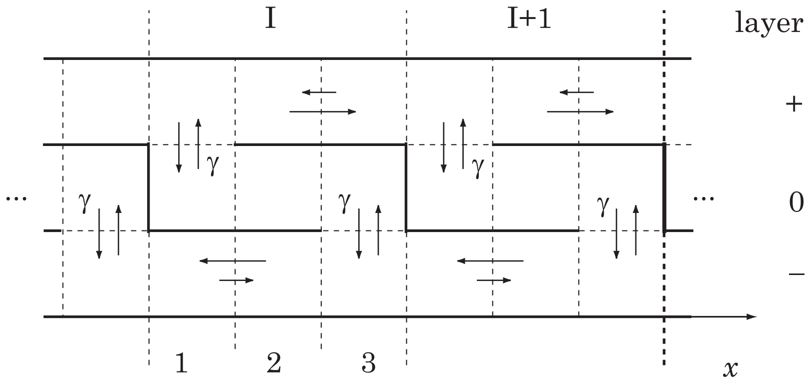

FIG. 5.1. Representation of the three layer lattice. Particles can jump between nearest neighbor sites across the dotted lines.

The arrows in the subscripts $\leftarrow$ and $\rightarrow$ denote transitions to the left and to the right respectively. The factors B and F are the energy differences between neighboring sites along the x-axis as a result of the applied bias ($+B$, 0 and $-B$ in upper, middle and lower layer respectively) and the external force (applied in all layers) respectively. The resulting master equation describing the time evolution of $P_{[i,\alpha,I]}(t)$ is reproduced in Appendix B.

Our focus here is on the asymptotic transport properties, and more specifically, on the asymptotic average horizontal velocity v:

$$v = \lim_{t\to\infty} \frac{\langle x(t)\rangle}{t}, \tag{5.2}$$

with $\langle x(t)\rangle = \sum_{i,\alpha,I} x_{[i,\alpha,I]} P_{[i,\alpha,I]}(t)$. Rewriting this as $v = \lim_{t\to\infty} \frac{\partial}{\partial t}\langle x(t)\rangle$ and using the master equation, cf. (B.1), we obtain:

$$v = 3(k^{+}_{\rightarrow} P_{[3,+]} - k^{+}_{\leftarrow} P_{[1,+]}) + 3(k^{-}_{\rightarrow} P_{[3,-]} - k^{-}_{\leftarrow} P_{[1,-]}), \tag{5.3}$$

where

$$P_{[i,\alpha]} = \lim_{t\to\infty} \sum_{I} P_{[i,\alpha,I]}(t), \tag{5.4}$$

is the steady state probability for a particle to be at any of the sites i in layer α. Calculation of the $P_{[i,\alpha]}$ can be reduced to an algebraic problem (see Appendix B), and gives the following result:

$$\begin{aligned} P_{[1,0]} &= \frac{P_0 e^{-\beta F}}{1+e^{-\beta F}+e^{\beta F}} \;;\; P_{[2,0]} = \frac{P_0}{1+e^{-\beta F}+e^{\beta F}} \;; \\ P_{[3,0]} &= \frac{P_0 e^{\beta F}}{1+e^{-\beta F}+e^{\beta F}} \;;\; P_{[i,\pm]} = \frac{1}{3} P_{\pm}. \end{aligned} \tag{5.5}$$

P_α is the reduced probability to be in state α:

$$P_{\pm} = \frac{3e^{\mp\beta F}}{1+4e^{-\beta F}+4e^{\beta F}} \;;\; P_0 = \frac{1+e^{-\beta F}+e^{\beta F}}{1+4e^{-\beta F}+4e^{\beta F}}. \tag{5.6}$$

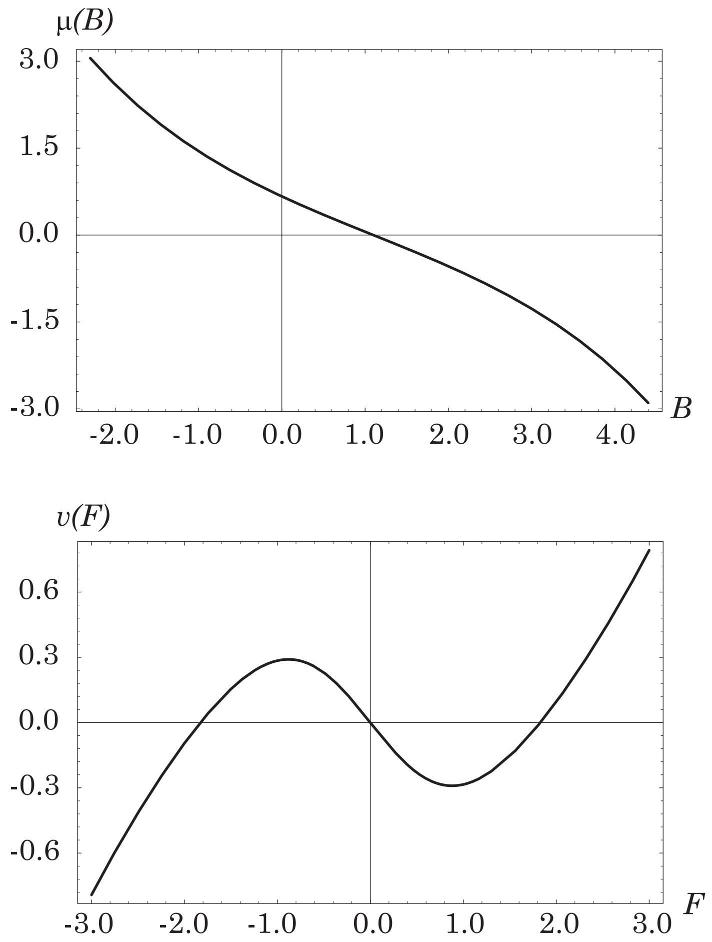

FIG. 5.2. Upper part: plot of the mobility μ as a function of the bias B. The lower part shows $v(F)$ for $B = 2$ ($\beta = 1$).

Combined with Eq. (5.3) we obtain the final result:

$$v = \frac{3e^{-\beta(B+F)/2}(e^{3\beta F} + e^{\beta(B+F)} - e^{\beta(B+2F)} - 1)}{4 + e^{\beta F} + 4e^{2\beta F}}. \tag{5.7}$$

The corresponding (absolute) mobility μ is:

$$\mu = \left.\frac{\partial v(F)}{\partial F}\right|_{F=0} = \frac{1}{3}\beta e^{-\beta B/2}(3 - e^{\beta B}). \tag{5.8}$$

Fig. 5.2 shows a plot of μ as a function of the bias B. For values of B larger then $\ln(3)/\beta$, μ becomes negative. Close to equilibrium, *i.e.* for small values of B, the mobility is positive, as required by the fluctuation dissipation theorem.

5.3 Diffusion model

To formulate a spatially continuous analogue, we consider an overdamped Brownian particle, possessing a discrete degree of freedom $\alpha = -1, 0$ or $+1$, and moving along the x-axis in a one-dimensional potential $V_\alpha(x) = V(x) - \alpha x B$, with $V(x)$ spatially

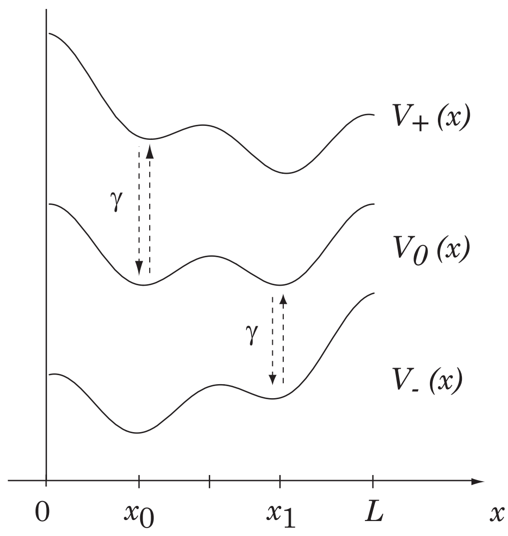

FIG. 5.3. Schematic representation of the different states and their transitions in the diffusion model. The potential is $V(x) = \cos(x) + \cos(2x)$.

periodic with period L, $V(x+L) = V(x)$. Unbiased transitions can take place between the discrete states, but only at specific positions, namely x_0 modulo L between $\alpha = 0$ and $\alpha = +1$ and x_1 modulo L between $\alpha = 0$ and $\alpha = -1$ respectively, cf. Fig. 5.3. We proceed to find the average velocity along the x-axis upon application of an additional force F which is independent of the discrete state. As in the discrete model, the position of a particle is completely determined by the coordinates $x \in [0, L[$, the state variable α, and the cell number I. The probability to find the particle in state α at position $x + IL$ is $P_{[x,\alpha,I]}(t)$. As before, we define:

$$\begin{aligned} \langle x(t) \rangle &= \textstyle\sum_{\alpha,I} \int_0^L dx(x + IL) P_{[x,\alpha,I]}(t) \ , \\ v &= \lim_{t\to\infty} \tfrac{\partial}{\partial t} \langle x(t) \rangle \ , \end{aligned} \tag{5.9}$$

and find (see Appendix B, and compare with (5.3)) that:

$$v = L \sum_\alpha J_\alpha \ , \tag{5.10}$$

with $J_\alpha = \lim_{t\to\infty} \sum_I J_{[x,\alpha,I]}(t)$ the steady state probability current in layer α, given as:

$$\begin{aligned} J_\alpha &= P_\alpha \frac{k_B T [1 - e^{-(F+\alpha B)L/k_B T}]}{\int_0^L \Phi_\alpha(y) dy} ; \\ \Phi_\alpha(x) &= \int_x^{x+L} dy \ e^{[V_\alpha(y) - V_\alpha(x) - F(y-x)]/k_B T} . \end{aligned} \tag{5.11}$$

P_α are the probabilities to be in state α and follow from (B.6) and normalization $P_- + P_0 + P_+ = 1$:

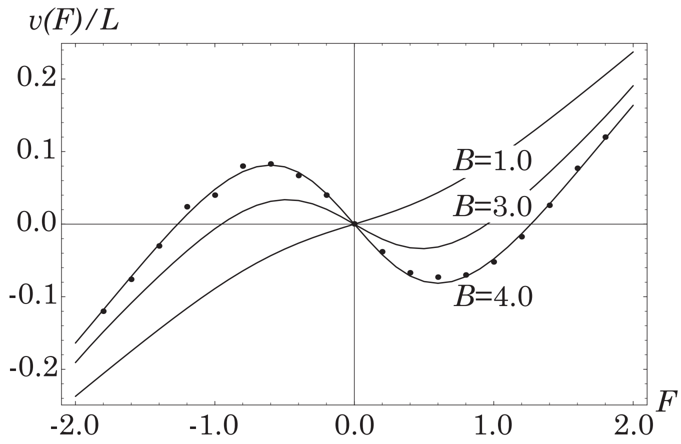

FIG. 5.4. The average speed $v(F)$ as a function of the applied force F for different values of the bias B ($V(x) = \cos(x) + \cos(2x)$). The circles for $B = 4$ were obtained by numerical simulations.

$$
\begin{aligned}
P_- &= \tfrac{1}{Z}\left[\int_0^L \Phi_-(y)dy\right]\Phi_0(x_1)\Phi_+(x_0) \ ; \\
P_0 &= \tfrac{1}{Z}\Phi_-(x_1)\left[\int_0^L \Phi_0(y)dy\right]\Phi_+(x_0) \ ; \\
P_+ &= \tfrac{1}{Z}\Phi_-(x_1)\Phi_0(x_0)\left[\int_0^L \Phi_+(y)dy\right] \ .
\end{aligned}
\tag{5.12}
$$

The above results are valid for any choice of the potential and transition points. To reproduce a situation leading to negative mobility similar in spirit to that of the discrete model, we choose a symmetric potential $V(x)$ with two minima, playing a role akin to the left and right states in the pockets of layer 0 in the discrete model. They are separated from each other by on one side a high maximum, mimicking the absence of transitions from $[1, 0, I]$ and $[3, 0, I]$ to $[3, 0, I-1]$ and $[1, 0, I+1]$ respectively in the discrete model, and a low maximum analogous to the states $[2, 0, I]$. It is now also clear how to choose the points of transition x_0 and x_1, namely at the location of the two minima. For the purpose of illustration, we will use $V(x) = \cos(x) + \cos(2x)$, and the resulting construction is schematically represented in Fig. 5.3. The appearance of negative mobility for sufficiently large bias B is illustrated in Fig. 5.4, showing v as a function of the external force F for different values of the bias B.

5.4 Discussion

While there are undoubtedly several direct physical realizations of the basic idea presented here, the most straightforward being particles suspended in the hydrodynamic flow represented in Fig. 5.5, we conclude with a more surprising concoction. Consider ellipsoidal particles with a permanent dipole and mass m, sedimenting under influence of a gravitational force in the presence of an electric force acting in the vertical but upward direction. The internal degree of freedom analogous to α is here the angle $\theta \in [-\pi, \pi]$ of the particle's dipole axis with the vertical direction (measured clockwise). For a given value of θ, particles acquire an average velocity whose horizontal x-component is $v(\theta) = (mg/2)(\mu_\perp - \mu_\parallel)\sin(2\theta)$, where $\mu_\perp$ and $\mu_\parallel$ are the orthogonal ($\theta = \pm\pi/2$) and parallel ($\theta = 0$ or $\pm\pi$) mobilities respectively. The motion is biased to the left and right respectively depending on whether $\theta > 0$ or $\theta < 0$, see Fig. 5.6.

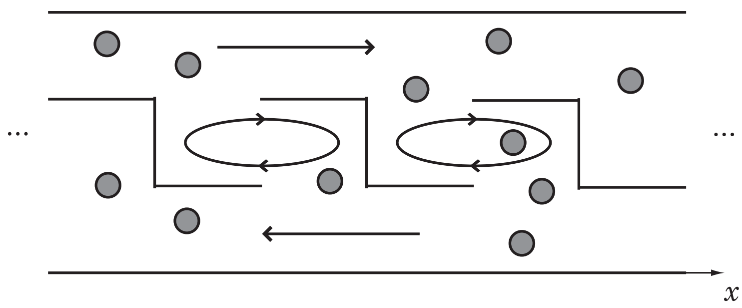

Fig. 5.5. The arrows represent the hydrodynamic flow in which the suspended particles, represented by the dots, move. Upon application of an external force on these particles, for example in the $+x$ direction, transitions to the lower layer are more likely, resulting in negative mobility if the flow is suffiently strong.

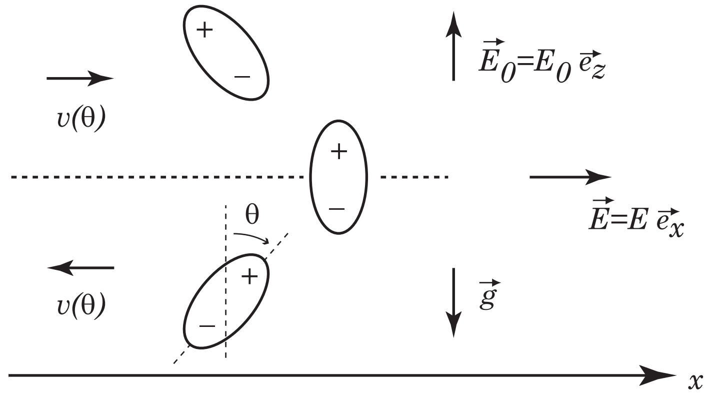

Fig. 5.6. The application of an additional electric field $\vec{E}$ induces preferential transitions to the configurations that move in the opposite direction.

These θ values are the analogue of the two oppositely biased states in the basic model. Transitions between different angles occur as a result of rotational diffusion. Because of symmetry, positive and negative θ-values are equally likely and the resulting average drift is zero. The crucial observation is now that the application of an additional electric field along the x-axis will favor the internal state θ that is characterized by a motion induced by the gravitational field in the opposite direction, hence negative mobility is expected if this effect is larger than the direct response to the electric force.

Part II

Parrondo Games

6

INTRODUCTION

Random or periodic alternation between fair games need no longer be a fair game. This surprising observation is known as the Parrondo paradox, named after its inventor Juan Parrondo. The origin of the paradox can be traced back to a particular type of Brownian motor, namely the flashing ratchet (see below). Parrondo formulated this Brownian motor in terms of coin tossing games, and this in turn stimulated research in various disciplines, see [53–56] and further references therein.

This part of the thesis focuses on a multi-player version of the Parrondo games, in which the players can decide which game to play. The interest in this problem is first that one observes counter-intuitive phenomena reminiscent of those found in economy and game theory, like the fact that Nash equilibria need not be Pareto optimal [57], or that greedy algorithms can lead to sub-optimal solutions [49]. Second, those phenomena are now observed in models that have a physical realization (a continuous realization corresponds to a set of N Brownian particles moving in a periodic asymmetric potential that can be flashed on and off at will [58]). Third and more importantly, the origin of this behavior is of a dynamic and more precisely stochastic nature, in contrast to the static equations in economy and game theory.

The outline of this part is as follow: this chapter presents the original single-player games. The presentation follows closely the historical way: we start with explaining the working principles of the flashing ratchet, which then serve as the starting point in the derivation of corresponding games. A basic analysis of the games is given, which explains the paradoxical behavior, together with a short overview of possible variations and modifications found in the literature. In Chapter 7 a multi-player version is introduced, together with the important concept of a strategy. This multi-player version with strategy is played as follow: at each turn, the players collectively decide which game they will play next. They make their decision after mutual consultation, and according to a given strategy. After the decision is made, all players individually play the chosen game. The important question to answer is: what is the optimal strategy, leading to a maximal gain? It turns out that for the original Parrondo games, this problem is very difficult and possibly of the NP-complete class [59]. In Chapter 8, we turn to a new formulation of the Parrondo paradox, which is both conceptually and technically simpler than the original games, and for which it is possible to determine the optimal strategy in the multi-player version.

6.1 From flashing ratchets...

The flashing ratchet is one of the prototypes of a Brownian motor [3]. In this model, a Brownian particle is subject to an asymmetric periodic potential which is flashed on and off in a random or periodic way in the course of time. Surprisingly, a net motion of the particle results, even when the potential is on average unbiased. A typical example of such a potential is the untilted sawtooth potential, depicted in Fig. 6.1.

How such an asymmetric potential can give rise to a directed particle motion is illustrated as follow. First, consider an initial situation with the potential switched on, and all particles located inside one period. We further assume that the temperature is small, so that the potential energy difference between maxima and minima is much larger than the thermal energy k_BT. Under this assumption, the particles are mostly found near the minimum of the potential, as shown by a sharply peaked particle density in Fig. 6.1(a). Now, the potential is switched off, and the particles can freely diffuse. This diffusion is caused by the thermal fluctuations of the environment, and is symmetric: some particles move to the left, some particles move to the right, while the average position does not change. In Fig. 6.1(b) the diffusion is visualised by a spreading of the particle density. If the potential is switched on again, the particles will slide down the potential toward a minimum (Fig. 6.1(c)). Which minimum a particle reaches depends on its position just before the potential is switched on: particles in the gray region move to the minimum on the left, while particles in the black region move toward the minimum on the right. The remaining particles in the white region return to the starting minimum. Due to the asymmetry of the potential, the fraction of particles in the black region is larger than those in the gray region, and the net result is a particle motion to the right. The flashing ratchet acts as a rectifier of thermal noise: the asymmetric potential promotes a particle motion to the right, while it suppresses motion to the left.

The necessary ingredients for directed motion in an unbiased system are (i) a spatial asymmetry, (ii) thermal fluctuations, and (iii) a mechanism to drive the system out of equilibrium [3]. In the example of the flashing ratchet these ingredients correspond to the asymmetric potential, the thermal environment and the on/off switching of the potential respectively. While for the flashing ratchet time and position of the particles is taken as a continuous parameter, Parrondo [60] realized that this mechanism also works when both time and spatial degree of freedom of the Brownian particle are discrete. In other words, he translated the phenomenon in the context of discrete state Markovian processes, which can propitiously be represented as Markovian games of chance.

6.2 ...to gambling games

The kind of games we envisage are simple coin tossing games: the player wins or loses one unit of capital, say 1€, depending on the outcome (head or tails) of a coin toss. The rules of the games will be chosen in such a way that the behavior of the player's capital, mimics the motion of the Brownian particle in the flashing ratchet. To this end, we associate each state of the potential (on/off) with a game:

- Game A corresponds to the off-state of the potential. In this state, the Brownian particle undergoes free diffusion, and it's average position does not change. It is well known (see for example [44]) that this motion is adequately described in discrete space by a jump process, taking steps to the left or to the right with equal probability. So, we define the rules for game A as follow: the player throws a fair (unbiased) coin having equal probability to land on either side: with probability $p_1 = 1/2$ the player wins 1€ and with probability $1 - p_1 = 1/2$ the player loses 1€. The capital of the player undergoes an unbiased random walk when playing game A. The role of the position of the particle is now taken over by the amount of money, i.e. the capital, the player has (see Fig. 6.2).
- The on-state of the potential is described by game B. One period of the potential is characterised by a short interval with a positive slope, and a longer interval with a

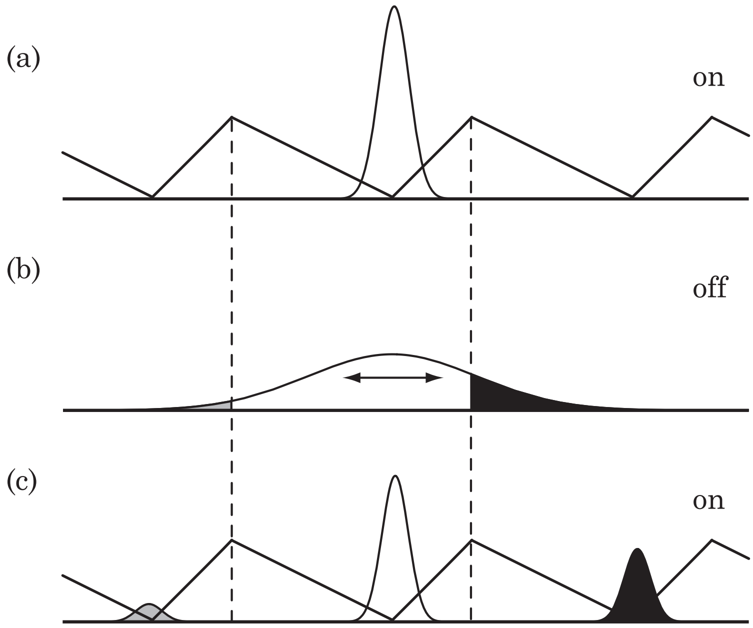

Fig. 6.1. Illustration of a flashing ratchet. (a) Initially, the potential is on, and the particles are all located near a minimum of the potential. Then, (b) the potential is switched off, and the particles can freely diffuse. When the potential is switched on again (c), the particles in the black region move toward the minimum on their right, while those particles in the gray region move toward the minimum on their left.

negative slope (see Fig. 6.1). Game B will therefore make use of two different coins, one for each slope of the potential. A *good* coin mimics the behavior of the particle in the interval where the potential has a negative slope, i.e. where the Brownian particle on average moves to the right. This coin has a probability of winning equal to $p_2 = 3/4$, versus $1 - p_2 = 1/4$ for the probability to lose. When the player uses this coin, his capital will increase on average. The *bad* coin mimics the behavior of the particle in the interval where the potential has a positive slope, and has a probability $p_3 = 1/10$ to win, and probability $1-p_3 = 9/10$ to lose. Which coin the player must use depends on his capital: when the capital is a multiple of 3, use the bad coin, otherwise use the good coin. With this modulo 3 rule, the rules of game B are periodic, and inside one period the good coin is used in a larger interval then the bad coin, as was required by the asymmetric sawtooth potential. The specific choice of winning and losing probabilities of the coins ensure that game B is fair (see later).

Figure 6.2 shows the correspondence between the games and the potential. In the next section we will analyse these games in more detail. In particular, we will show that the two games are fair when being played separately (either game A or game B). However, if the player randomly, or periodically, switches between the games, his capital increases.

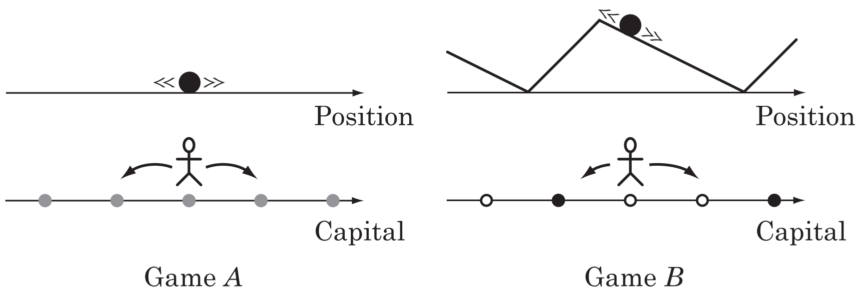

FIG. 6.2. Comparison between the games and the two states of the flashing ratchet. In game A the player uses the unbiased coin (•), while in game B the bad coin (●) is used when the player's capital is a multiple of 3. The good coin (○) is used otherwise.

6.3 Analysis of the Parrondo games

In this section we present the necessary mathematical tools to analyse the games. In particular we answer the question how to calculate the expected gain when playing a game. Since game A is a special case of game B, we'll develop the formalism with game B as an example. The results for game A can then easily be obtained afterward.

In order to calculate the average gain of game B we need information about the player's capital, since we must know which coin the player will use. More specifically, we only need to know the value of the player's capital modulo 3. We say that the player *is in state* i whenever his capital modulo 3 is equal to $i \in \{0, 1, 2\}$. Then, in state 0, the player uses the bad coin, and so with probability 9/10 he loses 1€, and with probability 1/10 he wins 1€. The average amount of money the player receives is (from here on we drop the currency indication):

$$(-1)\frac{9}{10} + (+1)\frac{1}{10} = -\frac{4}{5}. \tag{6.1}$$

Similar, for the states 1 and 2, this amount is:

$$(-1)\frac{1}{4} + (+1)\frac{3}{4} = \frac{1}{2}. \tag{6.2}$$

Now, defining $P_i(n)$ as the probability for the player to be in state i after having played n games, the expected gain of game B, labeled G_B, becomes:

$$\begin{aligned} G_B(n) &= -\frac{4}{5}P_0(n) + \frac{1}{2}\left[P_1(n) + P_2(n)\right] \\ &= -\frac{4}{5}P_0(n) + \frac{1}{2}\left[1 - P_0(n)\right] = \frac{1}{2} - \frac{13}{10}P_0(n). \end{aligned} \tag{6.3}$$

The number $G_B(n)$ expresses the average gain received by the player in the $(n+1)$-th turn.

We now can check if game B is fair. A game is said to be fair if, on average, the total amount of money the player has, does not increase/decrease indefinitely after playing that game a large number of times. Quantitatively this definition of fairness implies that the long time behavior of $G_B(n)$ goes to zero:

$$G_B^{\mathrm{st}} \equiv \lim_{n\to\infty} G_B(n) = 0. \tag{6.4}$$

After having played a large number of games, in the limit $n \to \infty$, the probabilities $P_i(n)$ reach a stationary value, defined as:

$$P_i^{\mathrm{st}} \equiv \lim_{n\to\infty} P_i(n). \tag{6.5}$$

In order to calculate these stationary values P_i^{st}, we must write down the evolution equations for the $P_i(n)$. These are obtained as follow. If the player is in state 0 after $n+1$ games, he must be, after having played n games, either in state 1 and losing, or in state 2 and winning. This leads to:

$$P_0(n+1) = \frac{1}{4}P_1(n) + \frac{3}{4}P_2(n). \tag{6.6}$$

With the same reasoning, the following equations for $P_1(n)$ and $P_2(n)$ are obtained:

$$P_1(n+1) = \frac{1}{10}P_0(n) + \frac{1}{4}P_2(n), \tag{6.7}$$
$$P_2(n+1) = \frac{9}{10}P_0(n) + \frac{3}{4}P_1(n). \tag{6.8}$$

These three equations can be compactly written in matrix notation:

$$\mathbf{P}(n+1) = \mathbf{R}_B\mathbf{P}(n), \tag{6.9}$$

with

$$\mathbf{P}(n) = (P_0(n), P_1(n), P_2(n))^T, \tag{6.10}$$

and $\mathbf{R}_B$ being the *transition matrix* of game B:

$$\mathbf{R}_B = \begin{pmatrix} 0 & 1/4 & 3/4 \\ 1/10 & 0 & 1/4 \\ 9/10 & 3/4 & 0 \end{pmatrix}. \tag{6.11}$$

Equation (6.9) describes the evolution of the probability distribution $\mathbf{P}(n)$ under the action of game B. Playing game B for a large number of games $n \gg 1$, the distribution attains a stationary value, meaning that $\mathbf{P}(n+1) = \mathbf{R}_B\mathbf{P}(n) \approx \mathbf{P}(n)$. Taking the limit $n \to \infty$, the stationary distribution $\mathbf{P}^{\mathrm{st}} = (P_0^{\mathrm{st}}, P_1^{\mathrm{st}}, P_2^{\mathrm{st}})$ is obtained by solving the linear equations $\mathbf{P}^{\mathrm{st}} = \mathbf{R}_B\mathbf{P}^{\mathrm{st}}$. $\mathbf{P}^{\mathrm{st}}$ is the right eigenvector with eigenvalue 1 of the $\mathbf{R}_B$-matrix. Matrices like $\mathbf{R}_B$, whose elements are nonnegative and for which each column adds up to unity, are called *stochastic matrices*, and appear in the theory of Markov chains [7]. Such matrices always have an eigenvector with eigenvalue 1. The normalized solution reads:

$$P_0^{\mathrm{st}} = \frac{5}{13}\ ;\ P_1^{\mathrm{st}} = \frac{2}{13}\ ;\ P_2^{\mathrm{st}} = \frac{6}{13}. \tag{6.12}$$

Substituting the value of P_0^{st} into (6.3) gives the stationary average gain of game B:

$$G_B^{\mathrm{st}} = 0. \tag{6.13}$$

We conclude that game B is fair.

The same conclusion can be made for game A. For this game the transition matrix $\mathbf{R}_A$ is:

$$\mathbf{R}_A = \begin{pmatrix} 0 & 1/2 & 1/2 \\ 1/2 & 0 & 1/2 \\ 1/2 & 1/2 & 0 \end{pmatrix}, \tag{6.14}$$

and the stationary solution of $\mathbf{P}^{\text{st}} = \mathbf{R}_A \mathbf{P}^{\text{st}}$ reads:

$$P_0^{\text{st}} = \frac{1}{3} \; ; \; P_1^{\text{st}} = \frac{1}{3} \; ; \; P_2^{\text{st}} = \frac{1}{3}. \tag{6.15}$$

The stationary gain of game A is 0:

$$G_A^{\text{st}} = \lim_{n \to \infty} G_A(n) = 0. \tag{6.16}$$

This is of course expected, since the expected gain is identically 0 for every state i.

6.4 Random switching between the two games

After these preliminaries, we now turn to the case of interest, namely the situation in which the player *randomly* plays either game A or game B. By randomly we mean that there is a probability 1/2 to play a particular game. Which game will be played can be determined for example by tossing a fair coin at each turn. Note that we do not allow the player to have control about this process: the choice of the game is determined by some external intervention. The opposite situation, in which the player can decide which game will be played, is considered in Chapter 7.

For this random game, the probabilities of winning and losing in a given state i are obtained from the probabilities of game A and B in the following way. The probability to win has two contributions: either the player wins by playing game A, or he wins by playing game B. Quantitatively, this statement can be written as:

$$\text{Prob.}_{\text{win,random}} = \frac{1}{2}\text{Prob.}_{\text{win,A}} + \frac{1}{2}\text{Prob.}_{\text{win,B}}. \tag{6.17}$$

The same rule applies for the probabilities of losing, so that the transition matrix describing this new game is also a linear combination of $\mathbf{R}_A$ and $\mathbf{R}_B$. The evolutions equation for the random game is then:

$$\mathbf{P}(n+1) = \left[\frac{\mathbf{R}_A + \mathbf{R}_B}{2}\right] \mathbf{P}(n), \tag{6.18}$$

with a normalised solution equal to:

$$P_0^{\text{st}} = \frac{245}{709} \; ; \; P_1^{\text{st}} = \frac{180}{709} \; ; \; P_2^{\text{st}} = \frac{284}{709}. \tag{6.19}$$

With this result we can now write down the expression for the average gain G:

$$G^{\text{st}} = \frac{1}{2}\left[G_A^{\text{st}} + G_B^{\text{st}}\right] = \frac{1}{2} G_B^{\text{st}} = \frac{1}{2}\left[\frac{1}{2} - \frac{13}{10} P_0^{\text{st}}\right] = \frac{18}{709}. \tag{6.20}$$

So we conclude that randomly switching between the two fair games A and B leads to a winning game. This is the so-called *Parrondo paradox*, which states that random (or periodic, see the following section) switching between fair games need no longer be fair.

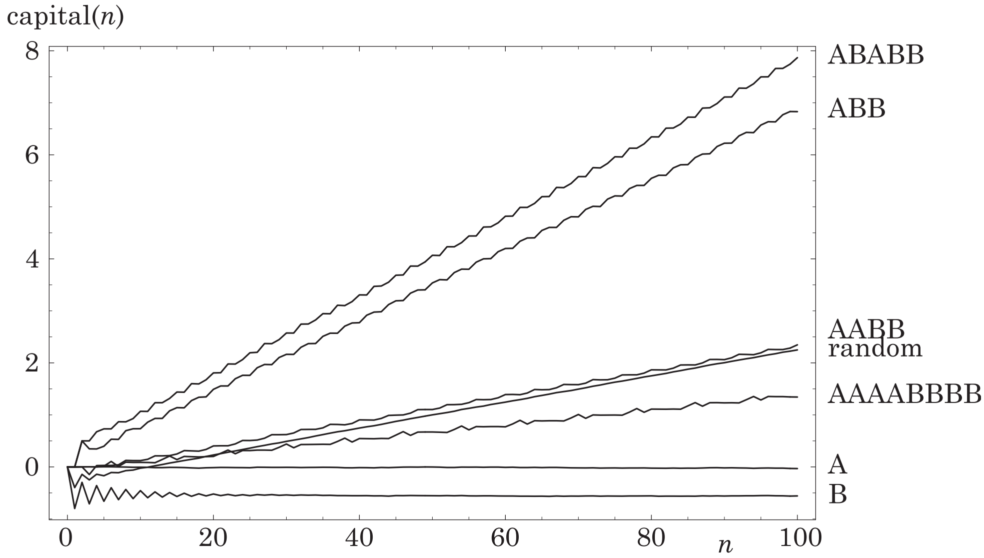

FIG. 6.3. Average capital of the player as a function of the number of games played, for the random and periodic alternations. For the periodic alternations, the game sequence is shown next to the corresponding curve. This sequence is constantly repeated. Each curve is obtained after averaging over 100000 realisations, with the starting capital of the player in each realisation always equal to zero.

How can we understand the nonzero result for the random games? It is clear that since the average gain for game A is always zero, independent of the player's state, the positive gain must be attributed to game B. Looking at the value for P_0^{st}, which is $5/13 \approx 0.3846$ when exclusively playing game B and $245/709 \approx 0.3456$ for the random games, we can conclude that by occasionally playing game A, the probability that the capital is a multiple of three, is decreased. As a result, the bad coin is used less frequently when playing game B. The net result is an overall positive gain. By playing game A the player can avoid the bad coin of game B. The reason for this decrease of P_0^{st} is that game A tends to *smear out* the probabilities equally over the three states. This is similar to the behavior of the flashing ratchet in which the Brownian particle spreads out during the off-state of the potential. Figure 6.3 shows the average capital of the player as a function of the number of games played. It is clear that both games A and B are fair, and that the random alternation is a winning game.

6.5 Periodic switching between the two games

For later reference, we now investigate the periodic switching between the two games. The games A and B are now played in a well defined order: a sequence of games, such as for example AB, ABB, $AABB$, etc., is chosen and is then repeated over and over again. From Fig. 6.3 it follows that such periodic games are also winning, but the average gain (slope of the curve) depends largely on the chosen periodicity. We now proceed with the calculation of the stationary gain for such periodic games, and we do this with the sequence ABB as an example. The gain for more complicated sequences can be calculated in the same way.

For the sequence ABB, the player starts first with game A, followed by two games of B, and so on. Starting from the initial distribution $\mathbf{P}(0)$, the evolution of the probability distribution is then:

$$\begin{aligned}
&\mathbf{P}(1) = \mathbf{R}_A\mathbf{P}(0),\\
&\mathbf{P}(2) = \mathbf{R}_B\mathbf{P}(1) = \mathbf{R}_B\mathbf{R}_A\mathbf{P}(0),\\
&\mathbf{P}(3) = \mathbf{R}_B\mathbf{P}(2) = \mathbf{R}_B\mathbf{R}_B\mathbf{R}_A\mathbf{P}(0),\\
&\quad \ldots
\end{aligned}$$

Defining $\mathbf{R}_{ABB} = \mathbf{R}_B\mathbf{R}_B\mathbf{R}_A$, these evolution equations can be written in general as follow:

$$\begin{aligned}
\mathbf{P}(3n) \quad\;\; &= (\mathbf{R}_{ABB})^n\mathbf{P}(0),\\
\mathbf{P}(3n+1) &= \mathbf{R}_A(\mathbf{R}_{ABB})^n\mathbf{P}(0),\\
\mathbf{P}(3n+2) &= \mathbf{R}_B\mathbf{R}_A(\mathbf{R}_{ABB})^n\mathbf{P}(0).
\end{aligned}$$

In order to calculate the long time behavior $n \to \infty$, we note that the matrix $\mathbf{R}_{ABB}$, being a product of stochastic matrices, is also a stochastic matrix. And therefore, it has a right eigenvector with eigenvalue 1. For the sequence ABB this eigenvector is:

$$\lim_{n\to\infty} \mathbf{P}(3n) = \left(\frac{15871}{35601}, \frac{6173}{35601}, \frac{13557}{35601}\right)^T. \tag{6.21}$$

The long time behavior of $\mathbf{P}(3n+1)$ and $\mathbf{P}(3n+2)$ is then obtained by applying respectively R_A and R_BR_A on the eigenvector:

$$\lim_{n\to\infty} \mathbf{P}(3n+1) = \left(\frac{9865}{35601}, \frac{14714}{35601}, \frac{11022}{35601}\right)^T, \tag{6.22}$$

$$\lim_{n\to\infty} \mathbf{P}(3n+2) = \left(\frac{11945}{35601}, \frac{3742}{35601}, \frac{19914}{35601}\right)^T. \tag{6.23}$$

Applying R_B on (6.23) must of course lead to (6.21), as is required by consistency. Unlike the situation with a random switching between the games, there is no longer a unique stationary distribution. Instead, the distribution changes periodically in time. The average gain received by the player will then also change periodically. We can then define the stationary gain as the total average gain obtained during one complete period, divided by the number of games per period. For the ABB sequence this gives:

$$\begin{aligned}
G^{\text{st}}_{ABB} &= \lim_{n\to\infty} \frac{1}{3}\left(G_A(3n) + G_B(3n+1) + G_B(3n+2)\right)\\
&= \frac{1}{3}\left(0 + \frac{4976}{35601} + \frac{2272}{35601}\right) = \frac{2416}{35601} \approx 0.06786.
\end{aligned} \tag{6.24}$$

This number coincides with the (average) slope of the ABB sequence in Fig. 6.3. We mention here the following results for other sequences:

$$\begin{aligned}
G^{\text{st}}_{AABB} &= \frac{4}{163} \approx 0.02454,\\
G^{\text{st}}_{ABABB} &= \frac{514608}{47747645} \approx 0.07568,\\
G^{\text{st}}_{AAAABBBB} &= \frac{288}{21769} \approx 0.01323.
\end{aligned} \tag{6.25}$$

A systematic calculation of the gain for different sequences is performed in [61], using a symbolic manipulator. For sequences with a period length up to 12(!), the period-5 sequence $ABABB$ comes out the best (see also Fig 6.3). Whether this sequence is the absolute best one remains an open question. In the following chapter, such periodic sequences will appear again, albeit in a different context.

6.6 Variations and conclusions

The Parrondo paradox has received considerable attention, both in the physics community and outside (see for example [56, 62] and further references therein). Possible applications include biology [63], biological evolution [64], and finance [65]. Even the rise of Bill Clinton's popularity after the Lewinksy affair has been linked to the paradox [66].

The two games A and B as introduced here were the original games as derived by Parrondo. Afterward, many variations/extensions were created, such as for example:

- chaotic [67] alternation between games: instead of a random/periodic switching, the selection of the games is now based on the numeric sequence generated by a chaotic system (note that the player still has no control about the selection mechanism)
- a general modulo n rule, instead of the modulo 3 rule
- switching between more then two games [67]

These variations do not introduce any new ideas, and the same conclusions can be made as for the original games presented here, i.e. starting from fair games, the resulting game is no longer fair.

The games mentioned so far have a capital dependent set of rules: the probabilities of winning/losing depend on the player's capital. However, in view of the possible applications in biology, economics, etc., it would be desirable to have a set of rules based on other principles. An example is given in [68], in which game B now has *history* dependent rules. The probabilities of winning/losing now depend on the two last outcomes in the following way:

before last $n-2$	last $n-1$	prob. to win at n	prob. to lose at n
loss	loss	p_1	$1-p_1$
loss	win	p_2	$1-p_2$
win	loss	p_3	$1-p_3$
win	win	p_4	$1-p_4$

Game A is the same as introduced here. With the parameter values equal to $p_1 = 9/10, p_2 = p_3 = 1/4$ and $p_4 = 7/10$ for example, the new game B is fair. The case with two history dependent games was considered in [69].

Apart from the modifications for the single-player games, the concept of multi-player Parrondo games was introduced by R. Toral in [70]. One now considers an ensemble of players, each with a capital. At every time step, a player i is randomly chosen, together with a game (A or B). Game A is as before, while the rules for game B were inspired by the history games, and depend on the last obtained result (winner or loser) of the two neighbors (located at $i+1$ and $i-1$). The rules for player i are then:

player at $i-1$	player at $i+1$	prob. to win	prob. to lose
loser	loser	p_1	$1-p_1$
loser	winner	p_2	$1-p_2$
winner	loser	p_3	$1-p_3$
winner	winner	p_4	$1-p_4$

Another multi-player version using a variation of game A was presented in [71]. Game B is as before, with the original capital dependent rules. Game A is now based on a redistribution of capital: the selected player i chooses randomly another player, and donates one unit of his capital to that player. Surprisingly, the Parrondo paradox occurs also for this type of games. Even more surprisingly is the fact that the Parrondo paradox also works when the redistribution mechanism makes the rich players donate their money to the poor players.

So far, the player(s) had no control about the game he (they) would play. Recently Parrondo introduced the concept of strategy [72, 73], by which the player(s) were allowed to choose in each turn which game they would play. In the remaining chapters of this part, the concept of a strategy in both the single- and multi-player Parrondo games will be discussed in detail.

7

PARRONDO GAMES WITH STRATEGY

7.1 Introduction

The Parrondo paradox, which states that random or periodic switching between fair games may no longer be fair, derives from a deeper and less surprising statement in statistical mechanics: a system that undergoes random or periodic switching between two equilibrium dynamics is no longer at equilibrium. More specifically, equilibrium dynamics is characterized by detailed balance, implicating that any transition between two states of the system and the reverse transition are equally probable. This very strong probabilistic symmetry implies in particular the absence of fluxes -the analogue of fairness in the games- but is in no ways guaranteed by it. Switching between two dynamics with detailed balance can and typically will break detailed balance and produce fluxes. This phenomenon has been particularly well studied recently in the context of Brownian motors, with the flashing ratchet as one of the prototypes for rectification of thermal fluctuations [3]. Another type of equilibrium was introduced by von Neumann and Morgenstern in their groundbreaking formulation of game theory [74]. Players are allowed to choose a probabilistic (so-called mixed) strategy in relation to a pre-specified pay-off table between competing partners. The equilibrium strategy is optimal in the sense that no player can change his strategy without risking to be worse of. More recently, more complicated dynamical and iterated versions of this set-up have been investigated. We cite the open entry competition for algorithms fighting on the basis of the iterated prisoner's dilemma [75] (with the surprising feature of the simple tit-for-tat strategy comes out as a winner), and the theoretical activity with respect to the minority game, in which participants vote between two alternatives with the aim of belonging to the minority [76]. Finally, we mention the huge engineering field of plant control, with as main issue the optimization of the output usually in the presence of conflicting requirements or constraints (cf. the related issue of finding free energy minima in frustrated systems).

As mentioned in the previous chapter, a variation of the Parrondo paradox can be introduced, which provides a toy model in which all these issues appear [72]. The Parrondo game is now played by a group of players with the collective aim of maximizing their total gain. The players have, for each new game, the freedom to choose -after mutual consultation- which one is played next. They can make this choice using a mixed strategy (i.e. according to some probability distribution). In engineering parlor the various games can be compared to different operational states of a plant. Fairness in this context implies that the factory does not function properly -the output is zero- when only one mode of operation is followed. In the context of Brownian motors, this question would correspond to a collection of Brownian particles, each performing its own independent Brownian motion, but in a common potential that is switched on or off depending on the observed location of the particles [58]. The switching scenario should be optimized to achieve a particular goal, for instance, that of maximizing transport in a given direction. In the context of games, the question will be posed about how to

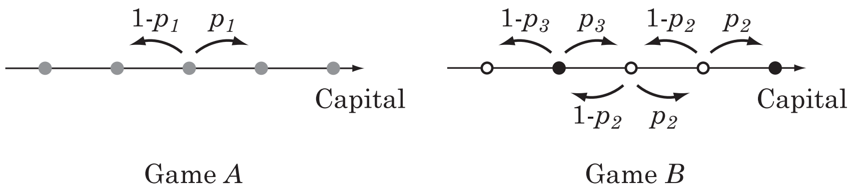

FIG. 7.1. Sketch of the two games, together with the corresponding transition rates between the different states.

optimize the overall gain of a community of players, by developing a strategy prescribing which game is to be played next, given the actual state of the players.

The question of identifying the optimal strategy turns out to be surprisingly difficult, even when we restrict ourselves, as we will do here, to the case of Markovian games. Then, the actual state of the players completely determines the probabilities for the events in the next game. At first, one might think that in this case the "greedy" strategy, which chooses at each turn the game that will generate the maximum total gain, will be optimal. It turns out that this is not the case [72]. The reason is that the choice of the game will also influence the state of the players, which may compromise the potential gain in the following game. To illustrate and clarify this issue, we present an exhaustive calculation of the gain for all possible strategies. This can be done either in the limit of a small number of players -we present results for up to 4 players- or in the limit of an infinite number of players using a mean field approach. In the latter limit, our analysis reveals a very rich behavior including the possibility of bifurcations, including bistability and abrupt transitions, in the gain of the players.

7.2 Strategy in the Parrondo game with a single player

For simplicity we will use the original Parrondo games introduced in the previous chapter [54, 62]. For reference, these games are shown in Fig. 7.1, together with the transition rates. Before turning to the discussion of strategies involving N players, we first illustrate the idea and results for the case of a single player. In the original Parrondo game, the type of game (A or B) is chosen at random or periodically. The main difference for the Parrondo game with strategy is that the player is allowed to choose which game he wants to play. After the game is played, the capital of the player is updated according to the outcome, and one moves to the next game. The main issue for the player is to come up with a good strategy: when selecting a game, he should make optimal use of all the relevant information, which for a single player (and Markovian games) is his actual capital modulo 3, a value which we will refer to as the (internal or reduced) state. In anticipation of the multi-player case, we will represent this state by a vector, namely $[1, 0, 0]$, $[0, 1, 0]$ or $[0, 0, 1]$, depending on whether the capital modulo 3 is equal to 0, 1 and 2 respectively. The most general (mixed) strategy is then defined by the probability distribution $s_{[1,0,0]}$, $s_{[0,1,0]}$ and $s_{[0,0,1]}$ to choose game A, when being in the respective states $[1, 0, 0]$, $[0, 1, 0]$ and $[0, 0, 1]$. Game B is then selected with probability $1 - s$. The efficiency of a strategy will reflect itself in the long-time average gain per game, denoted as G_1^{st}. The sub-index refers to the number of players which is one in the present case. To calculate the latter quantity, we need to study the statistics of the state of the player as it is induced by his strategy [62]. The probabilities $P_{[1,0,0]}(n), P_{[0,1,0]}(n)$ and $P_{[0,0,1]}(n)$ to observe the state $[1,0,0]$, $[0,1,0]$ or $[0,0,1]$ after playing the n-th game, obey the following master equation (using an obvious vector notation):

$$\mathbf{P}(n+1) = \mathbf{R}.\mathbf{P}(n)\,. \tag{7.1}$$

The elements of $\mathbf{R}$ are the transition probabilities between the states, see Table 7.1 for details. When playing game A and B separately $\mathbf{R}$ reduces to either $\mathbf{R}_A$ or $\mathbf{R}_B$ respectively, given by:

$$\mathbf{R}_A = \begin{pmatrix} 0 & 1-p_1 & p_1 \\ p_1 & 0 & 1-p_1 \\ 1-p_1 & p_1 & 0 \end{pmatrix}, \tag{7.2}$$

and

$$\mathbf{R}_B = \begin{pmatrix} 0 & 1-p_2 & p_2 \\ p_3 & 0 & 1-p_2 \\ 1-p_3 & p_2 & 0 \end{pmatrix}. \tag{7.3}$$

The transition matrix describing the (mixed) strategy game is then given by:

$$\mathbf{R} = \mathbf{R}_A.\mathbf{S} + \mathbf{R}_B.(\mathbb{1} - \mathbf{S}), \tag{7.4}$$

where $\mathbb{1}$ is the 3×3 identity matrix and $\mathbf{S}$ is the (diagonal) strategy matrix:

$$\mathbf{S} = \begin{pmatrix} s_{[1,0,0]} & 0 & 0 \\ 0 & s_{[0,1,0]} & 0 \\ 0 & 0 & s_{[0,0,1]} \end{pmatrix}. \tag{7.5}$$

The average gain upon playing the n-th game is given by:

$$\begin{aligned} G_1(n) = {} & P_{[1,0,0]}(n)\left[s_{[1,0,0]}(2p_1-1) + (1-s_{[1,0,0]})(2p_3-1)\right] \\ & + P_{[0,1,0]}(n)\left[s_{[0,1,0]}(2p_1-1) + (1-s_{[0,1,0]})(2p_2-1)\right] \\ & + P_{[0,0,1]}(n)\left[s_{[0,0,1]}(2p_1-1) + (1-s_{[0,0,1]})(2p_2-1)\right]. \end{aligned} \tag{7.6}$$

In the following we will focus entirely on the long-time steady state results. Hence, we only require the steady state solution $\lim_{n\to\infty}\mathbf{P}(n) = \mathbf{P}^{st}$, being the normalized eigenvector with eigenvalue 1 of the transition matrix $\mathbf{R}$:

$$\mathbf{R}.\mathbf{P}^{st} = \mathbf{P}^{st}. \tag{7.7}$$

Lengthy calculations, that are most easily performed using symbolic manipulators, lead to the following result, where we used the abbreviations
$s_0 = s_{[1,0,0]}$, $s_1 = s_{[0,1,0]}$ and $s_2 = s_{[0,0,1]}$:

$$\begin{aligned} G_1^{\mathrm{st}} = {} & 3\left[(1 + p_3(s_0-1) - p_1 s_0)\,(p_1 s_1 - 1) - {p_2}^2(1 + 2p_3(s_0-1)\right. \\ & -2p_1 s_0)\,(s_1-1)(s_2-1) + p_1\,(1 + p_3(s_0-1) + 2p_1\,(p_3 + p_1 s_0 \\ & -p_3 s_0)\,s_1 - p_1(s_0+s_1))\,s_2 + p_2\,(2 - s_1 - s_2 + p_3(s_0-1)\,(2 - s_2 \\ & -2p_1 s_2 + s_1(4p_1 s_2 - 2p_1 - 1)) + p_1\,(2s_1 s_2 - s_1 \\ & \left. -s_2 + s_0\,(s_1 + 2p_1 s_1 - 2 + s_2 + 2p_1 s_2 - 4p_1 s_1 s_2)))\right]/ \\ & \left[3 - p_1\,(s_0+s_1) + {p_2}^2(s_1-1)(s_2-1) + p_1\,(p_1 s_0 s_1 - s_2 + p_1(s_0+s_1)s_2)\right. \\ & -p_3(s_0-1)(p_1 s_1 + p_1 s_2 - 1) + p_2\,(s_1 + s_2 - 2 + p_3(s_0-1)(s_1+s_2-2) \\ & \left. +p_1\,(s_1 + s_2 - s_0(s_1+s_2-2) - 2s_1 s_2))\right]. \end{aligned} \tag{7.8}$$

Table 7.1 *List of all possible transitions between the configurations for one player, the corresponding change in capital and the transition probability.*

Transition	Capital	Transition probability game A	game B
$[1,0,0] \to [0,1,0]$	$+1$	p_1	p_3
$[0,0,1]$	-1	$1-p_1$	$1-p_3$
$[0,1,0] \to [0,0,1]$	$+1$	p_1	p_2
$[1,0,0]$	-1	$1-p_1$	$1-p_2$
$[0,0,1] \to [1,0,0]$	$+1$	p_1	p_2
$[0,1,0]$	-1	$1-p_1$	$1-p_2$

Replacing $p_1 = 1/2, p_2 = 3/4$ and $p_3 = 1/10$, the final result reads:

$$G_1^{\rm st} = \frac{6\,[10s_0 - 3(s_1+s_2) - 2s_1s_2 - 2s_0(s_1+s_2) + 2s_0s_1s_2]}{169 + 16s_0 + 3s_1 + 3s_2 + 5s_1s_2 - 8s_0(s_1+s_2)}. \tag{7.9}$$

The optimal strategy, giving the highest value of $G_1^{\rm st}$, is found to be a pure strategy, namely:

$$s_{[1,0,0]} = 1 \;\text{ and }\; s_{[0,1,0]} = s_{[0,0,1]} = 0. \tag{7.10}$$

The corresponding average gain per game is $G_1^{\rm st} = 60/185 \approx 0.3243$. Not surprisingly, this strategy has a very simple interpretation: whenever the player is in configuration $[1,0,0]$, i.e. when B is a losing game, the player chooses game A (with probability 1). Otherwise, that is in the states $[0,1,0]$ or $[0,0,1]$, the winning game B is chosen. Hence, the optimal strategy is in this case identical to the greedy strategy discussed in the introduction. For comparison, note that the original Parrondo game corresponds to the strategy

$$\{s_{[1,0,0]}, s_{[0,1,0]}, s_{[0,0,1]}\} = \{1/2, 1/2, 1/2\}, \tag{7.11}$$

in which the player chooses at random between the two games. For this strategy the average gain is $G_1^{\rm st} = 18/709 \approx 0.0254$, roughly a factor 13 smaller than for the optimal strategy!

7.3 Parrondo game with strategy for N players

The generalization to N players is now straightforward. At each time step, a game is chosen and is then played by all players. The strategy that is used to select a game will now depend on the capitals modulo 3 of all players. The collective state can now be represented by $[N_0, N_1, N_2]$ where N_i is the number of players who's capital modulo 3 is equal to $i = 0, 1, 2$ respectively ($N_0 + N_1 + N_2 = N$). The probability for the players to be in configuration $[N_0, N_1, N_2]$ after the n-th game is played, will be denoted by $P_{[N_0,N_1,N_2]}(n)$. A strategy is defined by the probabilities $s_{[N_0,N_1,N_2]}$ to choose game A when being in the corresponding state. The (steady state) analogue of (7.6) for N players is then:

$$G_N^{\rm st} = \frac{1}{N} \sum_{N_0,N_1,N_2} P^{st}_{[N_0,N_1,N_2]} \Bigg[s_{[N_0,N_1,N_2]}[2Np_1 - N] + (1 - s_{[N_0,N_1,N_2]})[2N_0p_3 + 2(N_1+N_2)p_2 - N] \Bigg], \tag{7.12}$$

where $G_N^{\rm st}$ is the average gain per player and per game. Note that the summation over N_0, N_1 and N_2 runs over all $(N+1)(N+2)/2$ different configurations. The stationary distribution $P^{st}_{[N_0,N_1,N_2]}$ is found as the normalized eigenvector of eigenvalue one of the transition matrix $\mathbf{R}$, which is now an $(N+1)(N+2)/2 \times (N+1)(N+2)/2$ matrix.

To illustrate the procedure, consider the $N = 2$ player game. In this case, there are a total of 6 different configurations, namely:

$$[2,0,0]\ ,\ [1,1,0]\ ,\ [1,0,1]\ ,\ [0,2,0]\ ,\ [0,1,1]\ ,\ [0,0,2]. \tag{7.13}$$

Table 7.2 summarizes all possible transitions between the configurations, the corresponding change in capital, and the transition probability. The matrix $\mathbf{R}_B$ is then:

$$\mathbf{R}_B = \begin{pmatrix} 0 & 0 & 0 & (1\text{-}p_2)^2 & p_2(1\text{-}p_2) & p_2p_2 \\ 0 & p_3(1\text{-}p_2) & p_2p_3 & 0 & (1\text{-}p_2)^2 & 2p_2(1\text{-}p_2) \\ 0 & (1\text{-}p_2)(1\text{-}p_3) & p_2(1\text{-}p_3) & 2p_2(1\text{-}p_2) & p_2p_2 & 0 \\ p_3p_3 & p_2p_3 & p_3(1\text{-}p_2) & 0 & 0 & (1\text{-}p_2)^2 \\ 2p_3(1\text{-}p_3) & 0 & (1\text{-}p_2)(1\text{-}p_3) & 0 & p_2(1\text{-}p_2) & 0 \\ (1\text{-}p_3)^2 & p_2(1\text{-}p_3) & 0 & p_2p_2 & 0 & p_2p_2 \end{pmatrix}. \tag{7.14}$$

$\mathbf{R}_A$ is found by replacing p_2 and p_3 in $\mathbf{R}_B$ with p_1. The calculation of the stationary distribution

$$\mathbf{P^{st}} = (P^{st}_{[2,0,0]}, P^{st}_{[1,1,0]}, P^{st}_{[1,0,1]}, P^{st}_{[0,2,0]}, P^{st}_{[0,1,1]}, P^{st}_{[0,0,2]})^T, \tag{7.15}$$

can be handled by a symbolic manipulator. The final result for G_2^{st} is rather lengthy and not reproduced here. An exhaustive search over all pure strategies allows to identify the following optimal strategy:

$$\{s_{[2,0,0]}, s_{[1,1,0]}, s_{[1,0,1]}, s_{[0,2,0]}, s_{[0,1,1]}, s_{[0,0,2]}\} = \{1,1,1,0,0,0\}, \tag{7.16}$$

and the corresponding value for $G_2^{\mathrm{st}} = 1312/5913 \approx 0,2219$. Furthermore this strategy is again identical to the greedy strategy: whenever the average gain for playing game B is negative, game A is chosen. This is the case for the configurations $[2,0,0]$, $[1,1,0]$ and $[1,0,1]$, with an expected gain in game B equal to $-8/5$,$-3/10$ and $-3/10$ respectively. Note also that the average optimal gain is only about 2/3 of that of a single player. This is obviously due to the fact that the same game has to be chosen for all players leading to a conflict of interest and reduced pay-off. Note finally that for the original Parrondo game, $s = 1/2$, collective effects are immaterial and one recovers the well known average gain $G_1^{\mathrm{st}} = 18/709$.

So far we found that the greedy strategy is optimal for $N = 1$ and $N = 2$. This is, as we proceed to show next, no longer the case for $N \geq 3$. We first focus on the case $N = 3$. It is straightforward to repeat the above calculations (involving now 10×10 matrices) but the procedure and final expressions are very lengthy so we just review the salient results. The different configurations are now:

$$\begin{gathered}[3,0,0]\ ,\ [2,1,0]\ ,\ [2,0,1]\ ,\ [1,2,0]\ ,\ [1,1,1]\ , \\ [1,0,2]\ ,\ [0,3,0]\ ,\ [0,2,1]\ ,\ [0,1,2]\ ,\ [0,0,3]\ .\end{gathered} \tag{7.17}$$

Referring to the ordering of the states in (7.17), the greedy strategy corresponds to $\{1,1,1,0,0,0,0,0,0,0\}$ for which we find an average steady state gain per game and per player equal to:

Table 7.2 *List of all possible transitions between the configurations for two players, the corresponding change in capital and the transition probability.*

Transition	Capital	Transition probability game A	Transition probability game B
$[2,0,0] \to [0,2,0]$	$+2$	p_1p_1	p_3p_3
$[0,0,2]$	-2	$(1-p_1)^2$	$(1-p_3)^2$
$[0,1,1]$	0	$2p_1(1-p_1)$	$2p_3(1-p_3)$
$[1,1,0] \to [0,1,1]$	$+2$	p_1p_1	p_2p_3
$[1,0,1]$	-2	$(1-p_1)^2$	$(1-p_2)(1-p_3)$
$[1,1,0]$	0	$p_1(1-p_1)$	$p_3(1-p_2)$
$[0,0,2]$	0	$p_1(1-p_1)$	$p_2(1-p_3)$
$[1,0,1] \to [1,1,0]$	$+2$	p_1p_1	p_2p_3
$[0,1,1]$	-2	$(1-p_1)^2$	$(1-p_2)(1-p_3)$
$[0,2,0]$	0	$p_1(1-p_1)$	$p_3(1-p_2)$
$[1,0,1]$	0	$p_1(1-p_1)$	$p_2(1-p_3)$
$[0,2,0] \to [0,0,2]$	$+2$	p_1p_1	p_2p_2
$[2,0,0]$	-2	$(1-p_1)^2$	$(1-p_2)^2$
$[1,0,1]$	0	$2p_1(1-p_1)$	$2p_2(1-p_2)$
$[0,1,1] \to [1,0,1]$	$+2$	p_1p_1	p_2p_2
$[1,1,0]$	-2	$(1-p_1)^2$	$(1-p_2)^2$
$[2,0,0]$	0	$p_1(1-p_1)$	$p_2(1-p_2)$
$[0,1,1]$	0	$p_1(1-p_1)$	$p_2(1-p_2)$
$[0,0,2] \to [2,0,0]$	$+2$	p_1p_1	p_2p_2
$[0,2,0]$	-2	$(1-p_1)^2$	$(1-p_2)^2$
$[1,1,0]$	0	$2p_1(1-p_1)$	$2p_2(1-p_2)$

$$G_3^{\mathrm{st}} = \frac{2317431670848}{4664732583395} \approx 0.1656. \tag{7.18}$$

However, the strategy $\{1,1,1,0,0,1,0,0,0,0\}$, which differs from the greedy strategy in choosing the neutral game A rather then the winning game B in configuration $[1,0,2]$, has a larger gain, namely:

$$G_3^{\mathrm{st}} = \frac{45185912531}{86483373591} \approx 0.1742. \tag{7.19}$$

In fact, the greedy strategy is only the third best one. The second best strategy is $\{1,1,1,0,1,1,0,0,0,0\}$, with average gain

$$G_3^{\mathrm{st}} = \frac{5984181363}{11678660585} \approx 0.1708, \tag{7.20}$$

differs in two configurations from the greedy one. The fourth best strategy, with average gain

$$G_3^{\mathrm{st}} = \frac{284867630136}{578009589745} \approx 0.1643, \tag{7.21}$$

is $\{1,1,1,0,1,0,0,0,0,0\}$. As a useful check of our calculations, we also note that we find three different strategies that give an average gain of 0, namely $\{0,0,0,0,0,0,0,0,0,0\}$, $\{0,0,0,0,1,0,0,0,0,0\}$ and $\{1,1,1,1,1,1,1,1,1,1\}$. The first and the last strategy correspond to a choice of uniquely playing game B and game A respectively, and the zero gain reflects that these games are fair. The second strategy corresponds to playing game B all the time except in configuration $[1,1,1]$, where game A is chosen. The explanation why this does not affect the average gain is that game A will, when the players

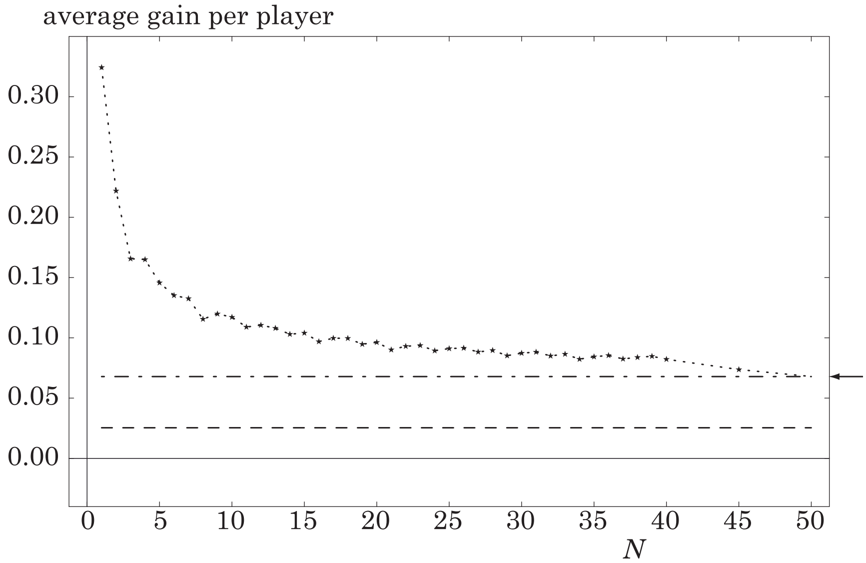

FIG. 7.2. Comparison between the greedy strategy ($\star$), the periodic sequence ABB (dashed-dotted line), and the random strategy (dashed line) for a different number of players N. The data for $N \leq 3$ is obtained from analytical calculations, those for $N \geq 4$ are obtained from simulations. As the number of players increases, the performance of the greedy strategy decreases, and coincides with the result for the ABB sequence, namely $G^{\mathrm{st}}_{ABB} = 2416/35601 \approx 0.06786$, in the limit $N \to \infty$. The observation that the greedy strategy leads to the period-3 limit cycle in this limit will be confirmed by doing a mean field calculation.

are evenly spread over the three states, maintain -statistically speaking- the uniform distribution over these states. The analytic results for $N \geq 4$ are unwieldy, so we have resorted to numerical simulations to further investigate the performance of the greedy algorithm as N becomes larger, cf. Fig. 7.2. As expected G^{st}_N decreases further with increasing N and appears to converge for $N \to \infty$ to an asymptotic value larger than that of the random game. This suspicion will be confirmed by the analytic evaluation of $\lim_{N\to\infty} G^{\mathrm{st}}_N$ for the greedy strategy, presented in the next section.

7.4 Mean field Parrondo strategy

The calculations made above become more and more involved as N becomes larger, but a significant simplification takes place in the limit $N \to \infty$. In this limit we introduce the fractions $x_0 = N_0/N$, $x_1 = N_1/N$, and $x_2 = N_2/N$, of players that have a capital equal to 0, 1, and 2, modulo 3 respectively. Note that $x_0 + x_1 + x_2 = 1$. Once the next game to be played has been selected, the law of large number stipulates that these quantities obey a deterministic equation of evolution identical to the equation for the probability of a single player. Hence for game A one has :

$$\mathbf{x}(n+1) = \mathbf{R}_A.\mathbf{x}(n), \tag{7.22}$$

with $\mathbf{R}_A$ given by (7.2). This mapping has a unique and stable fixed point $x_0^A = x_1^A = x_2^A = 1/3$. The dynamics when game B is chosen, is as follows

$$\mathbf{x}(n+1) = \mathbf{R}_B.\mathbf{x}(n), \tag{7.23}$$

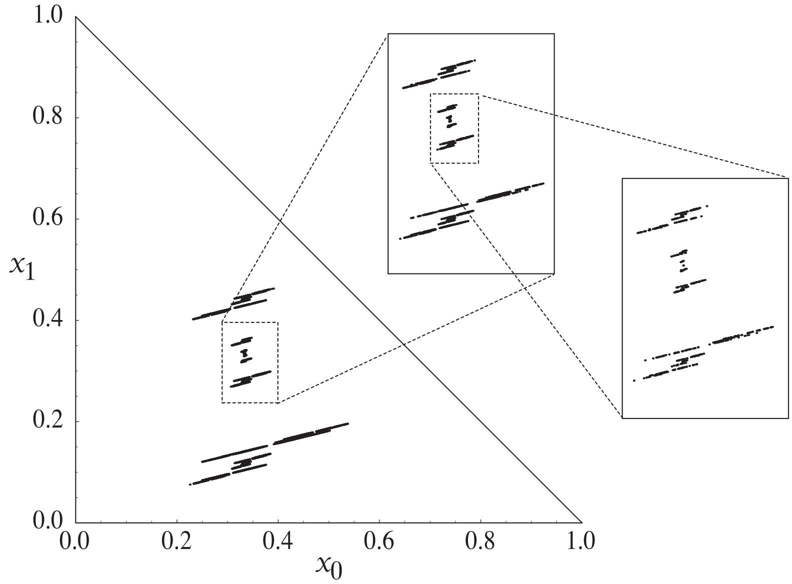

FIG. 7.3. Two dimensional fractal support of the steady state probability distribution in the case $s_{[x_0,x_1]} = 1/2$. The blown up insets illustrate the self-similarity of the fractal.

with $\mathbf{R}_B$ given by (7.3). The unique and stable fixed point of this map is: $x_0^B = 5/13$, $x_1^B = 2/13$, $x_2^B = 8/13$. The separate dynamics are thus linear maps converging exponentially fast to their respective unique fixed point. Non-trivial results arise when we introduce a strategy. In full analogy to the previous discussion, such a strategy is defined by the state dependent probability $s_{[x_0,x_1]}$ to select game A (when being in state $[x_0, x_1, x_2 = 1 - x_0 - x_1]$). $1 - s_{[x_0,x_1]}$ is the probability for game B. The dynamics for the strategy game is then as follow:

$$\mathbf{x}(n+1) = [\sigma(n)\mathbf{R}_A + (1-\sigma(n))\mathbf{R}_B]\,.\mathbf{x}(n), \tag{7.24}$$

where $\sigma(n)$ is a random variable equal to 1 with probability $s_{[x_0,x_1]}$ and 0 otherwise. We conclude that the resulting dynamics is in general a random and nonlinear map. Two limiting cases are worth mentioning. In the special case that $s[x_0, x_1]$ is a constant independent of $[x_0, x_1]$, (7.24) represents a random linear map, a case which has received considerable attention in the literature on fractals, since the invariant distribution is typically fractal or multi-fractal [77]. As an illustration we reproduce in Fig. 7.3 the numerically obtained support of the two-dimensional steady state probability in the case $s_{[x_0,x_1]} = 1/2$.

To make further progress, we turn to the other case which is of more interest to us here, namely we restrict ourselves to the case of pure strategies. A strategy is now defined by a boundary in the (x_0, x_1)-plane, separating the region where game A is played, $s_{[x_0,x_1]} = 1$, from the region where B is played, $s_{[x_0,x_1]} = 0$. The mapping (7.24) is then no longer random but becomes piece-wise linear. To fix the ideas and for comparison with previous results, we first focus on the greedy strategy in which game A is played when the expected gain in B is zero or negative, i.e., when $x_0(2p_3 - 1) + x_1(2p_2 - 1) + x_2(2p_2 - 1) \leq 0$. The boundary separating game A from game B is thus a straight line $x_0 = (1/2 - p_2)/(p_3 - p_2)$ or $x_0 = 5/13$ for the fair game choice $p_2 = 3/4$ and

$p_3 = 1/10$. Game A is selected for $x_0 \geq 5/13$. To find the invariant state that is reached in the long time dynamics, we make the following observations. First, both pieces of the map are contracting. Hence the long-time dynamics has to take place on a subset of measure zero, possibly a fixed point, a periodic orbit or a chaotic trajectory. The second observation is that the fixed point of the A dynamics, $x_0^A = 1/3$, lies outside the region in which game A is played, while the fixed point of the B dynamics, $x_0^B = 5/13$, lies exactly on the boundary. We conclude that neither of them can be a stable fixed point of the greedy dynamics. The third observation is that any point belonging to the A region, $x_0 > 5/13$, is, upon playing game A, mapped onto the B region, implying that game A is directly followed by game B. A fourth similar observation can be made if we divide the B region, $x_0 < 5/13$, into subregions B' and B'', indicated by the dashed line in Fig. 7.4: B' is mapped onto B'', and B'' onto the A region. We conclude that the greedy strategy leads to a game sequence built out of AB and/or ABB subsequences. One can now proceed to study the existence and stability of the fixed points corresponding to limit cycles of increasing complexity, e.g., $\ldots ABABAB \ldots$, $\ldots ABBABBABB \ldots$, etc. For example, the limit cycle $\ldots ABABAB \ldots$ would correspond to an alternation between the fixed points of the matrix $\mathbf{R}_A.\mathbf{R}_B$ and $\mathbf{R}_B.\mathbf{R}_A$. These fixed points are unique and stable, namely $(3/13, 1/13)$ going over by the map A into $(5/13, 6/13)$, and back by the map B. Both points lie however in the region where the "wrong" game is played, and therefore this cycle is not compatible with the greedy algorithm. The only stable limit cycle compatible with the greedy dynamics that we could identify, is the following one of period three:

$$\begin{tikzcd}
\left\{\frac{15871}{35601}, \frac{6173}{35601}\right\} \arrow[rr, "A"] & & \left\{\frac{9865}{35601}, \frac{14714}{35601}\right\} \arrow[dl, "B"] \\
& \left\{\frac{11945}{35601}, \frac{3742}{35601}\right\} \arrow[ul, "B"] &
\end{tikzcd}$$

This cycle corresponds to a game sequence $\ldots ABBABBABB \ldots$. The corresponding average gains at each of these steps are:

$$\ldots 0 \longrightarrow \frac{4976}{35601} \longrightarrow \frac{2272}{35601} \longrightarrow 0 \ldots,$$

with overall average gain

$$G_\infty^{\mathrm{st}} = \frac{1}{3}\left(\frac{4976}{35601} + \frac{2272}{35601}\right) = 2416/35601 \approx 0.06786, \tag{7.25}$$

in perfect agreement with the numerical results, cf. Fig. 7.2.

We turn to a last question of interest, namely whether there exists a strategy that beats the performance of the greedy strategy when $N \to \infty$. Building on our experience with the previous analysis, where the asymptotic dynamics are characterized by a limit cycle, we investigate this matter by proceeding in the reverse manner: we first identify a limit cycle with an average gain larger than the greedy strategy, and proceed to construct a strategy by choosing the boundary with the various points of the limit cycle sitting in the appropriate region of the (x_0, x_1) plane. The first problem was already solved in [61], with the period-5 sequence $ABABB$ coming out as the best. The five points of this limit cycle are:

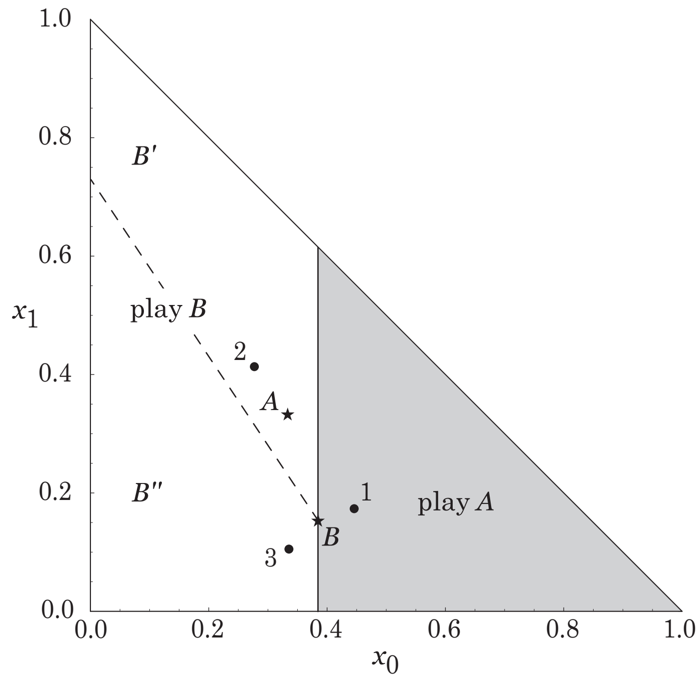

FIG. 7.4. Sketch of the (x_0, x_1)-plane. Game A is played in the gray region, game B in the white region. The fixed points of the A and B dynamics are shown by a $\star$. The full vertical line at $x_0 = 5/13$ shows the boundary line for the greedy strategy. The period-3 limit cycle is indicated by the $\bullet$ symbol (the index refers to the order in which they follow each other).

$$\begin{tikzcd}
\left\{\frac{4684919}{9549529}, \frac{1762493}{9549529}\right\} \arrow[rr, "A"] & & \left\{\frac{2432305}{9549529}, \frac{3893518}{9549529}\right\} \arrow[d, "B"] \\
\left\{\frac{2727665}{9549529}, \frac{862958}{9549529}\right\} \arrow[u, "B"] & & \left\{\frac{3391159}{9549529}, \frac{1049157}{9549529}\right\} \arrow[dl, "A"] \\
& \left\{\frac{3079185}{9549529}, \frac{4250186}{9549529}\right\} \arrow[ul, "B"] &
\end{tikzcd}$$

with corresponding average gains at each of these steps:

$$\ldots 0 \longrightarrow \frac{1612768}{9549529} \longrightarrow 0 \longrightarrow \frac{771824}{9549529} \longrightarrow \frac{2272}{9549529} \longrightarrow 0 \ldots,$$

and the overall average gain given by $G^{\mathrm{st}}_{\infty} = 3613392/47747645 \approx 0.07568$. By plotting the points of the limit cycle in the (x_0, x_1) plane, see Fig. 7.5, it becomes immediately apparent that this period-5 limit cycle is realized when the boundary line of the greedy strategy is shifted to the left, i.e., to a value $x_0 \in]1/3, 11945/35601[$. The lower boundary $x_0 > 1/3$ is needed to ensure that the fixed point of A is still in the region where B is played, while the condition $x_0 < 11945/35601$ destroys the period-3 limit cycle of the greedy algorithm. That this cycle is indeed realized, is confirmed in the simulations, cf. Fig. 7.6. With the boundary at x_0, the interpretation of the new strategy is straightforward: it is a more intelligent greedy strategy, in which game A is now played whenever the expected gain of B is below $1/2 - (13/10)x_0$ (this result is obtained from (7.6) with $\{s_{[0,1,0]}, s_{[0,1,0]}, s_{[0,1,0]}\} \to \{0, 0, 0\}$ (since game B is played) and $P_{[1,0,0]}(n) \to x_0$).

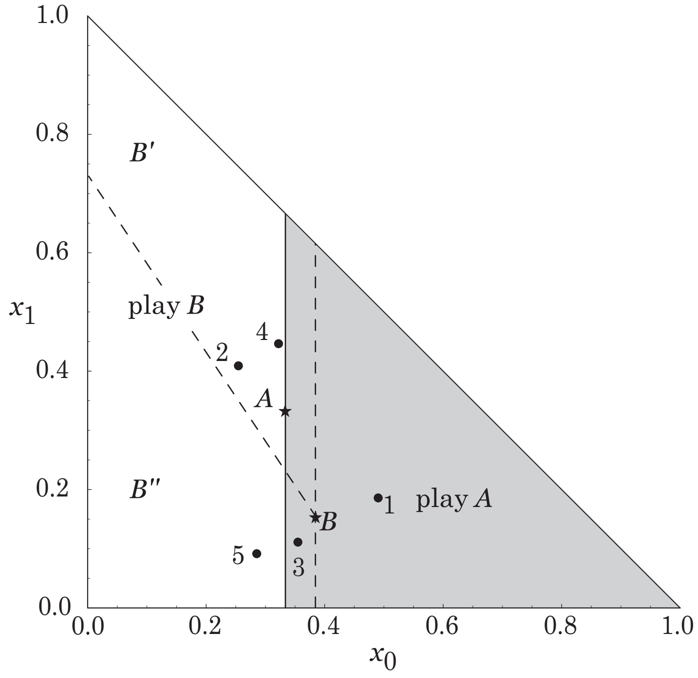

FIG. 7.5. Sketch of the (x_0, x_1)-plane. Game A is played in the gray region, game B in the white region. The fixed points of the A and B dynamics are shown by a $\star$. The full vertical line at $x_0 = 0.334$ shows the boundary for the better strategy, while the dashed vertical line at $x_0 = 5/13$ shows the boundary line for the greedy strategy. The period-5 limit cycle is indicated by the $\bullet$ symbol (the index refers to the order in which they follow each other).

7.5 Discussion

We close with some final remarks. First it should be clear from the mean field analysis that the gain is usually changing in function of an adopted pure strategy in a abrupt way, since cycles appear or disappear when the constituting points move into or out of the appropriate region. For example, upon moving the decision boundary starting from the greedy strategy at $x_0 = 5/13$ to smaller values, the performance of the plain greedy algorithm will persist until the increased gain of the intelligent version is abruptly reached when x_0 becomes smaller than 11945/35601. Second, we note that non-periodic sequences, generated by various chaotic time series, were considered in Reference [67]. We have not discussed these sequences here because they do not seem to have a simple strategic interpretation, and require for their generation, as far as we can see, fractal boundaries between the A and B regions. Third, there is the possibility for coexisting attractors. In this case, the gain will depend on the initial condition. Such a situation occurs for example when the boundary line of the greedy strategy is shifted to the left to a value $x_0 \in]11945/35601, 3391159/9549529[$. In this case, both the period-3 and period-5 limit cycle can occur. Fourth, we were only able to answer the question of the optimal strategy for $N = 1, 2$ and 3. The identification of the optimal strategy for $N \to \infty$ is an open problem, including the question of whether or not it has a fractal nature. This difficult question may be answered by introducing further simplifications in the Parrondo game. In the next chapter we introduce a primary model involving two rather than three states, for which such an analysis may indeed be performed.

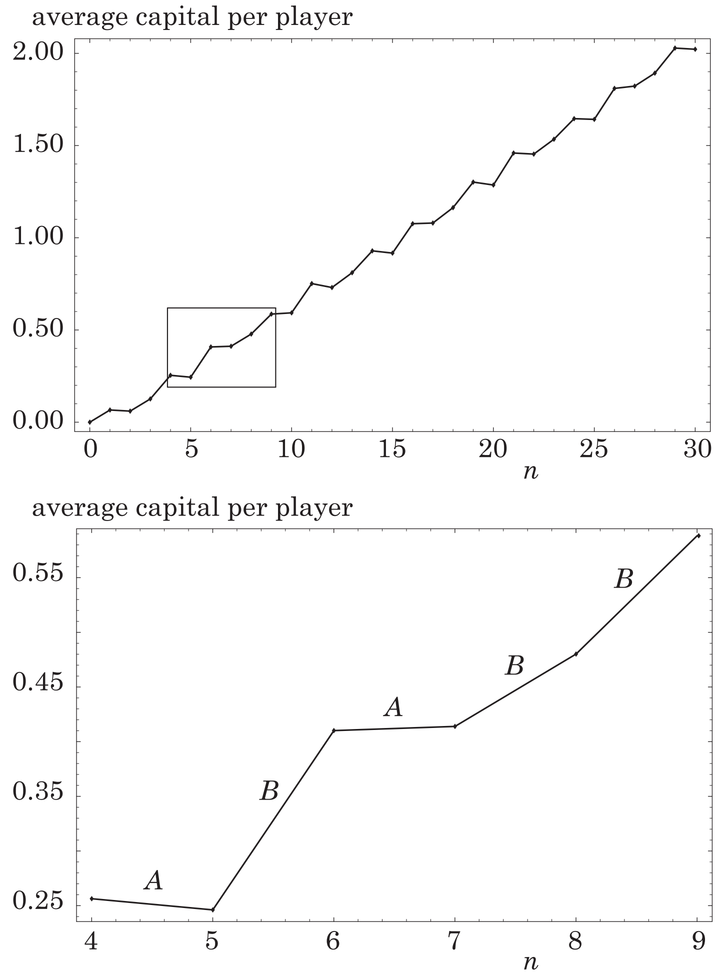

FIG. 7.6. Time evolution of the average capital (per player) of a collection of 10000 players, using the more intelligent greedy strategy (with the boundary line at $x_0 = 0.334$). It is clear that the gain received by the players is periodic in time: after five time steps, the same gain is obtained. This cycle can be identified by the $ABABB$ game sequence, as shown by the enlargement (lower part) of on period. Note that fluctuations in the gain are still significant for 10000 players.

8

PRIMARY PARRONDO PARADOX

8.1 Introduction

When constructing the original games, Parrondo introduced a discrete analogue of Brownian motion in a ratchet potential. To represent one period of the asymmetric sawtooth potential he introduced three states linked by transition rates that mimic the shape of the sawtooth, with transitions uphill being less likely than those downhill. This model has become the prototype for studying the Parrondo paradox and its variations and extensions. An alternative version of the Parrondo paradox has been formulated, which is no longer dependent on the capital of the player, but rather on the state of the player during the previous two games. In both instances it has been claimed that these models are the simplest possible formulations for the paradox [68, 78]. As we will show below, this is not the case: we will introduce a model requiring only two states or one memory step [79]. Furthermore we can choose ultra-simple dynamics involving so-called superstable fixed points. Both the intuitive and the technical discussion of this primary model is far more simple than the original Parrondo game. As a result, more complicated aspects or more involved questions are open to analytic investigation. For example, Parrondo games with strategy [72, 80] can be discussed in detail.

Another reason to study the primary model is the general interest in exactly solvable models. Based on the experience in statistical physics, one can expect that the exact analysis of a stochastic N-player model is usually out of the question for a general N value. Indeed, as was shown in the previous chapter for the original multi-player Parrondo paradox, results are only known in the limiting cases of a few (N small) or of an infinite number of players ($N \to \infty$) [80], or by perturbation analysis around the latter state (Gaussian limit) [72]. It has even been suggested that the problem of identifying the optimal strategy in the N-player game belongs to the class of NP-complete problems [59]. We will show below that the N-player version of the primary Parrondo paradox can be analyzed in full analytic detail for any value of N [81]. Furthermore, we will show that for this particular version of the Parrondo paradox, the problem of finding the optimal strategy is polynomial rather then exponential in the number of players.

8.2 Primary Parrondo paradox

As in the original Parrondo paradox, the primary model consists of an alternation between two games. In game A the capital of the player undergoes an unbiased random walk. With probability 1/4 the player wins or loses, and with probability 1/2 his capital does not change. The rules for game B depend on the capital of the player modulo 2. When the capital is even, the player has a probability 4/9 to win, 2/9 to lose and 1/3 to neither win or lose. When his capital is odd, the player has a probability 1/9 to win, 2/9 to lose and 2/3 to neither win or lose. To study the dynamics of the gain of the player, we introduce the probabilities $P_0(n)$ and $P_1(n)$ that the capital is odd or even respectively after the n-th game. In view of normalisation, $P_1(n) = 1 - P_0(n)$, we find the following simple equations of evolution:

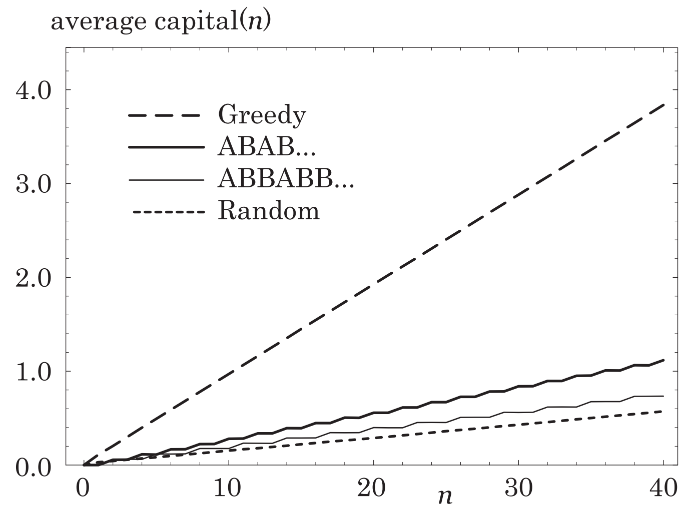

FIG. 8.1. Evolution of the average capital for different strategies.

$$\text{game } A : P_1(n+1) = \frac{1}{2}P_1(n) + \frac{1}{2}P_0(n) = \frac{1}{2}, \tag{8.1}$$

$$\text{game } B : P_1(n+1) = \frac{1}{3}P_1(n) + \frac{1}{3}P_0(n) = \frac{1}{3}. \tag{8.2}$$

Note the enormous simplification compared to the original Parrondo model. The linear maps given above involve a single scalar variable, and both are superstable. In other words, the fixed points $P_1^A = 1/2$ and $P_1^B = 1/3$ are reached in one iteration of the map. It is easy to verify that each game, played separately, is fair. The average gain G is identically zero in game A at any time n and this independent of $P_1(n)$. In game B, it is given by:

$$G_B(n) = \frac{2}{9}P_1(n) - \frac{1}{9}P_0(n) = \frac{1}{3}P_1(n) - \frac{1}{9}. \tag{8.3}$$

We conclude that game B may only be unfair at most once, namely the first time that it is played with initial condition $P_1(n) \neq 1/3$. For any subsequent play, $P_1(n) = 1/3$, and the game is fair. From this simple discussion, it is now also immediately clear that the alternating game, random or periodic, will not be fair. Whenever game A is chosen, the average gain is zero (since it is so identically). Whenever game B follows game B, the average gain is also zero, as explained before. However, whenever game B follows game A, i.e., the probability is evenly spread over the two states, $P_1(n) = 1/2$, game B is now on average a winning game, $G_B^{\rm st} = 1/18$, cf. (8.3). We conclude that the average gain will be 1/18 times the fraction of subsequent pairs of games which are of the type AB. This fraction is maximal and equal to 1/2 with resulting gain 1/36 for a periodic alternation ...$ABABABAB$... and equal to 1/4 with resulting gain 1/72 for a random alternation. In Fig. 8.1 we compare these theoretical predictions with numerical results for the average evolution of the capital of players for the pure games (see below) and for alternating or randomly selected games. We have also included the results for the sequence ...$ABBABBABB$... with average gain 1/54.

To make a connection with a history rather than a state dependent game B, we reformulate the latter game as follow. The B game is played with a "good" and a "bad" coin. At the start of the game, the good coin is used when the starting capital is even, otherwise one uses the bad coin. The important novel ingredient is that the coins have, apart from the usual head and tail, also a third state. For example, they are such that they land with a significant probability on their side. These probabilities are 1/3 and 2/3 for the good and the bad coin respectively. When this happens, the player neither wins nor loses and the same coin has to be used in the next toss. Otherwise the coins are switched. In view of the initial condition, this implies that the good coin is always used when the capital is even, in agreement with the previous description of the game. The good coin has a probability 4/9 to win, versus 2/9 to lose, while the bad coin is characterized by the probabilities 1/9 to win, and 2/9 to lose. The large expected gain, 2/9 per toss, for the good coin versus the small expected loss of 1/9 for the bad coin, is compensated by the fact that the bad coin will be used twice as frequently as the good coin, resulting in a fair game. Switching with any other game will obviously upset this balance, explaining the appearance of a systematic loss or gain. To transform the game into a history dependent setting, we note that the beginning capital is a matter of convention. Hence the coin used in the starting game is immaterial. Both the A and B games, or their alternation, can thus be formulated as a history dependent game with memory of one time step: switch coins if the previous toss was head or tail, otherwise use the same coin.

In Fig. 8.2, we have schematically represented a third realization of the scenario introduced here. A Brownian particle moves in either one of two different unbiased periodic potentials, each with two (pronounced) minima per period. For an appropriate choice of the barrier heights and of the time unit, the motion of the Brownian particle between the minima will correspond to game A and B respectively. While the motion in each potential taken separately is unbiased, it is clear that the switching from potential A, in which both minima are equally populated, to potential B, will generate a flux, resulting from the preferential decay over the small barrier to the right from the metastable minimum (see Fig. 8.2), and corroborating the statement that the resulting drift will be proportional to the fraction of AB pairs in the sequence of switches.

In the following sections, the use of strategy is introduced in the primary games. The reduction from three to two states and the superstability requirement enormously simplifies the analysis.

8.3 The primary games with strategy: single player

To get some perspective, we first turn to the case of a single player. Since the rules for both games A and B depend only on the player's capital modulo 2, the only relevant information is whether this capital is odd or even. The strategy is then specified by the probabilities s_0 and s_1 to choose game A when the capital is odd or even respectively. We will refer to such a strategy as pure or mixed depending on whether the choice is deterministic (s_0 and s_1 zero or one) or not. The dynamics for the probability $P_1(n)$ for an even capital and the average gain are now as follow:

$$\begin{aligned} P_1(n+1) &= (\frac{1-s_0}{3}+\frac{s_0}{2})P_0(n)+(\frac{1-s_1}{3}+\frac{s_1}{2})P_1(n) \\ &= \frac{2+s_0}{6}+(\frac{s_1-s_0}{6})P_1(n), \end{aligned} \tag{8.4}$$

and

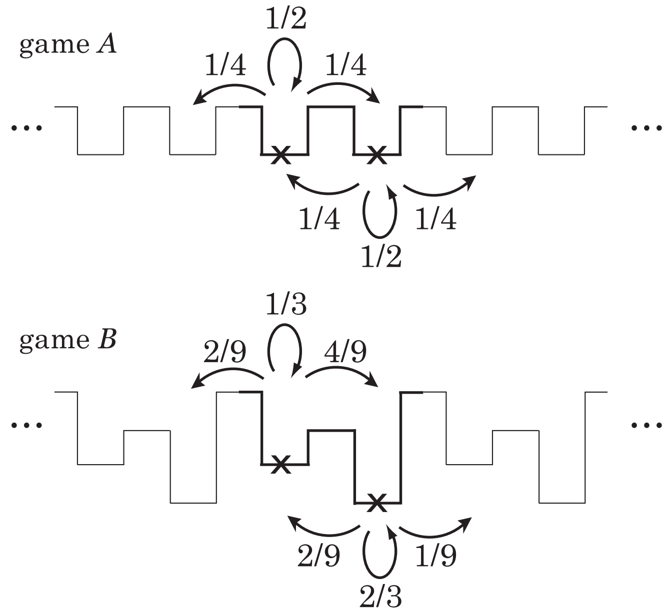

FIG. 8.2. Sketch of the two games and their respective transition rates between the two potential minima.

$$\begin{aligned} G(n) &= \frac{2}{9}(1-s_1)P_1(n) - \frac{1}{9}(1-s_0)P_0(n) \\ &= -\frac{1}{9}(1-s_0) + \frac{1}{9}(3-2s_1-s_0)P_1(n). \end{aligned} \tag{8.5}$$

The fixed point of (8.4) is $P_1^{st} = (2+s_0)/(6+s_0-s_1)$ and the corresponding steady state gain is:

$$G_1^{\mathrm{st}} = \frac{s_0(2-s_1)-s_1}{3(6+s_0-s_1)}. \tag{8.6}$$

Note that we have introduced, for comparison with the results in multi-player games, a subindex 1 referring to the number of players involved (one in the present case). A maximum gain, $G_1^{\mathrm{st}} = 2/21$, is obtained for the pure strategy $\{s_0, s_1\} = \{1, 0\}$. This strategy has a simple interpretation: it corresponds to the greedy strategy, i.e., the player chooses at each instant the game that gives him maximal average gain. When the capital of the player is even, the average gain when playing game B is positive, and so $s_1 = 0$. When his capital is odd, he selects game A ($s_0 = 1$). By comparing this result with the optimal result without strategy, corresponding to a pure alternation of the games with $G_1^{\mathrm{st}} = 1/36$, we see an increase of the gain by a factor close to 3 (see Fig. 8.1).

8.4 The primary games with strategy: multiple players

The collective version of the game is defined as before. A set of N players is allowed to choose, after each game, which game will be played next. Once this choice is made, all players will play the selected game, but independently of each other. Again we want to know which strategy should be followed by the players in order to maximize their gain. Since the statistics of the gains or losses only depend on the capital modulo 2 of each player, and all players are equivalent, the relevant information is contained in the number of players $i \in \{0, \ldots, N\}$ with an even capital. There are $N+1$ different such configurations. Hence the state of the players after the n-th game will be described by the probabilities $P_i(n)$ to find the players in these configurations i. We can now define the most general configuration-dependent strategy by introducing the probabilities s_i to choose game A (and $1 - s_i$ to choose game B) when being in state i. Introducing $w_A(j \to i)$ and $w_B(j \to i)$ as the transition probability from configuration j to i when playing game A or game B respectively, the (discrete) time evolution of $P_j(n)$ is given by the following master equation:

$$P_i(n+1) = \sum_{j=0}^{N} \left[s_j \, w_A(j \to i) + (1 - s_j) \, w_B(j \to i) \right] \, P_j(n). \tag{8.7}$$

The transition probabilities $w_A(j \to i)$ and $w_B(j \to i)$ are found as follow. As mentioned before, the probability for a player to have an even capital is $1/2$ after playing game A, and $1/3$ after game B. In view of the fact that the games are played independently, the probability to have i of the players in this state is given by a binomial distribution:

$$\begin{aligned} w_A(j \to i) \equiv w_A(i) &= \binom{N}{i} \left(\frac{1}{2}\right)^N, \\ w_B(j \to i) \equiv w_B(i) &= \binom{N}{i} \left(\frac{1}{3}\right)^i \left(\frac{2}{3}\right)^{N-i}. \end{aligned} \tag{8.8}$$

As a result of the special choice of the transition probabilities of the individual games, the transition rates for the collective game appearing in (8.7) factorize (such a process is called Kangaroo process in [7]). An immediate consequence is that the steady state solution $P_i^{st} = \lim_{n \to \infty} P_i(n)$ can be obtained explicitly:

$$P_i^{st} = w_A(i) \langle s \rangle + w_B(i)(1 - \langle s \rangle), \tag{8.9}$$

with $\langle s \rangle = \sum_{j=0}^{N} s_j \, P_j^{st}$ being the steady state (average) probability that the next game to be played is game A. Note that the normalization of the P_i^{st} follows immediately from the normalization of $w_A(i)$ and $w_B(i)$, cf. (8.9). The value of $\langle s \rangle$ follows from self-consistency: by multiplying (8.9) with s_i and summation over i, one finds:

$$\langle s \rangle = \frac{s_B}{1 - s_A + s_B}, \tag{8.10}$$

with

$$s_A = \sum_{i=0}^{N} s_i \, w_A(i) \; ; \; s_B = \sum_{i=0}^{N} s_i \, w_B(i), \tag{8.11}$$

the average conditional probability to choose game A when the previous game was A or B respectively. To complete the picture, we note that the expected gain after playing game A or game B when being in configuration i is respectively given by:

$$\begin{aligned} &\text{expected gain for game } A = 0, \\ &\text{expected gain for game } B = \tfrac{1}{3N}\left(i - \tfrac{N}{3}\right), \end{aligned} \tag{8.12}$$

where we have divided by the number of players (gain per player). From this result it follows that the greedy strategy for the N player games is given as:

$$\text{greedy strategy:} \begin{cases} \text{play game } A \text{ if } i \leq N/3 \\ \text{play game } B \text{ if } i > N/3 \end{cases} . \tag{8.13}$$

We conclude that the steady state average gain for the strategy games is given by:

$$\begin{aligned} G_N^{\text{st}}(\{s_i\}) &= \frac{1}{3N} \sum_{i=0}^{N} (i - \frac{N}{3})(1 - s_i) P_i^{st} \\ &= \frac{1}{3N} \sum_{i=0}^{N} (i - \frac{N}{3})(1 - s_i) \left[w_A(i) \langle s \rangle + w_B(i) \left(1 - \langle s \rangle\right) \right]. \end{aligned} \tag{8.14}$$

Equation (8.14) is the central result of this section: it expresses the average gain G_N^{st} as a function of the given strategy $\{s_i\}$. We quote the following exact results for $N = 2$ up to $N = 5$:

$$\begin{aligned} G_2^{\text{st}} &= \frac{s_0(8 - 2s_1 - 3s_2 - (2 + s_1)s_2)}{3(36 + 7s_0 - 2s_1 - 5s_2)}, \\ G_3^{\text{st}} &= \frac{s_0(32 - 4s_1 - 12s_2 - 7s_3) - s_2 s_3 - 6s_1(s_2 + s_3) + 4(4s_1 - 2s_2 + s_3)}{3(216 + 37s_0 + 15s_1 - 33s_2 - 19s_3)}, \\ G_4^{\text{st}} &= [s_0(128 - 8s_1 - 36s_2 - 42s_3 - 15s_4) + s_1(128 - 24s_2 - 48s_3 - 21s_4) \\ &\quad -s_4(s_3 + 8 + 9s_2) - 4s_3(8 + 3s_2)] \,/\, [3(1296 + 175s_0 + 188s_1 - 102s_2 \\ &\quad -196s_3 - 65s_4)], \\ G_5^{\text{st}} &= [16(16(3s_1 + s_2) - 5s_1 s_2 + s_0(32 - s_1 - 6s_2)) - 8(16 + 21s_0 + 30s_1 \\ &\quad +10s_2)s_3 - 2(48 + 60s_0 + 105s_1 + 60s_2 + 10s_3)s_4 - (16 + 31s_0 \\ &\quad +60s_1 + 42s_2 + 12s_3 + s_4)s_5] \,/\, [3(7776 + 781s_0 + 1345s_1 + 130s_2 \\ &\quad -1150s_3 - 895s_4 - 211s_5)]. \end{aligned}$$

For $N = 2$, $N = 3$ and $N = 4$, the greedy strategy is optimal:

$$\begin{array}{ll} \{s_0, s_1, s_2\} = \{1, 0, 0\} & G_2^{\text{st}} = 8/129, \\ \{s_0, s_1, s_2, s_3\} = \{1, 1, 0, 0\} & G_3^{\text{st}} = 11/201, \\ \{s_0, s_1, s_2, s_3, s_4\} = \{1, 1, 0, 0, 0\} & G_4^{\text{st}} = 248/4977. \end{array} \tag{8.15}$$

However, for $N = 5$, this is no longer the case. The greedy strategy:

$$\{s_0, s_1, s_2, s_3, s_4, s_5\} = \{1, 1, 0, 0, 0, 0\}, \tag{8.16}$$

with average gain of $G_5^{\text{st}} = 632/14853 \approx 0.04255$ is the second best. The strategy with optimal gain is:

$$\{s_0, s_1, s_2, s_3, s_4, s_5\} = \{1, 1, 1, 0, 0, 0\}, \tag{8.17}$$

and has an average gain $G_5^{\text{st}} = 28/627 \approx 0.04466$. It is easy to find a simple interpretation for the new optimal strategy, which can be readily generalized to any number of players. The new strategy is a "less" greedy strategy, defined as the pure strategy in which game A is chosen whenever the expected gain for playing game B is less than or equal to 1/3, i.e., $s_i = 1$ whenever $i \leq N/3 + 1$ and 0 otherwise.

Even though (8.14) is an exact and explicit result, the dependence on these variables is not so simple. In particular the search for the optimal strategy, leading to maximum gain, will require some further analysis.

Table 8.1 *Comparison between the optimal and greedy strategy for a small number of players. For $N = 1, 2, 3, 4, 6, 7$ and 9, both strategies coincide.*

N	Optimal strategy	Greedy strategy
1	$\{1,0\}$	$\{1,0\}$
2	$\{1,0,0\}$	$\{1,0,0\}$
3	$\{1,1,0,0\}$	$\{1,1,0,0\}$
4	$\{1,1,0,0,0\}$	$\{1,1,0,0,0\}$
5	$\{1,1,1,0,0,0\}$	$\{1,1,0,0,0,0\}$
6	$\{1,1,1,0,0,0,0\}$	$\{1,1,1,0,0,0,0\}$
7	$\{1,1,1,0,0,0,0,0\}$	$\{1,1,1,0,0,0,0,0\}$
8	$\{1,1,1,1,0,0,0,0,0\}$	$\{1,1,1,0,0,0,0,0,0\}$
9	$\{1,1,1,1,0,0,0,0,0,0\}$	$\{1,1,1,1,0,0,0,0,0,0\}$
10	$\{1,1,1,1,1,0,0,0,0,0,0\}$	$\{1,1,1,1,0,0,0,0,0,0,0\}$

8.5 The optimal strategy

The optimal strategy corresponds to the maximum of the function $G_N^{\rm st}(\{s_i\})$ reached in the $N+1$ dimensional hypercube with coordinates $s_i \in [0,1]$. Even for a moderate number of players, searching for such a maximum numerically is an enormous and not always reliable task. In the previous section, we obtained the optimal strategy for $N \leq 5$. In Table (8.1), we have completed the table up to $N = 10$. In all cases we find that the optimal strategy lies in the corner of the hypercube, with a first set of values for the s_i with lower index being identical to 1, followed by the remaining set s_i of higher index identically equal to 0. Motivated by this observation, we will now show that this is an exact and in fact general result, valid for any number of players N. First, we show that the value of $G_N^{\rm st}$ does not decrease when, at any point in the hypercube, we replace one of the coordinates, say s_k, by an appropriate corner value $s_k = 0$ or $s_k = 1$. The starting point is the evaluation of the partial derivatives of $G_N^{\rm st}$ with respect to s_k:

$$\frac{\partial G_N^{\rm st}}{\partial s_k} = \frac{P_k^{st}\left[\frac{N}{2} - k + \sum_{i=0}^{N}(k-i)s_i\left[w_A(i) - w_B(i)\right]\right]}{3N(1 - s_A + s_B)}. \tag{8.18}$$

Since $P_k^{st} > 0$, cf. (8.9), and $1 - s_A + s_B > 0$, see (8.11), the fact whether the derivative is positive, negative or zero, depends on the expression between square brackets in (8.18), namely:

$$g_k \equiv \frac{N}{2} - k + \sum_{i=0}^{N}(k-i)s_i\left[w_A(i) - w_B(i)\right]. \tag{8.19}$$

Furthermore, g_k does not depend on s_k. Hence, when searching for the maximum of $G_N^{\rm st}$ by varying s_k, we have only two possible situations. Either $g_k = 0$, implying $\partial G_N^{\rm st}/\partial s_k = 0$ for all values of s_k. The value of $G_N^{\rm st}$ does not depend on s_k and we can choose s_k either 0 or 1. In the other case, the maximum must be reached on the boundary, with either $s_k = 1$ when $g_k > 0$ or equivalently $\partial G_N^{\rm st}/\partial s_k > 0$ and $s_k = 0$ when $g_k < 0$ or equivalently $\partial G_N^{\rm st}/\partial_k < 0$. Since the argument given above can be applied, starting from any point in the hypercube, and repeated iteratively until we reach one of its corners, we conclude that the maximal value of $G_N^{\rm st}$ is reached in such a corner. Note that the same argument holds for locating the minimum of $G_N^{\rm st}$ (by choosing at each time the corner value which yield a minimum), which is also reached in a corner of the hypercube. To proceed to the next step of the proof, we rewrite the g_k as the following linear combination of g_0 and g_N:

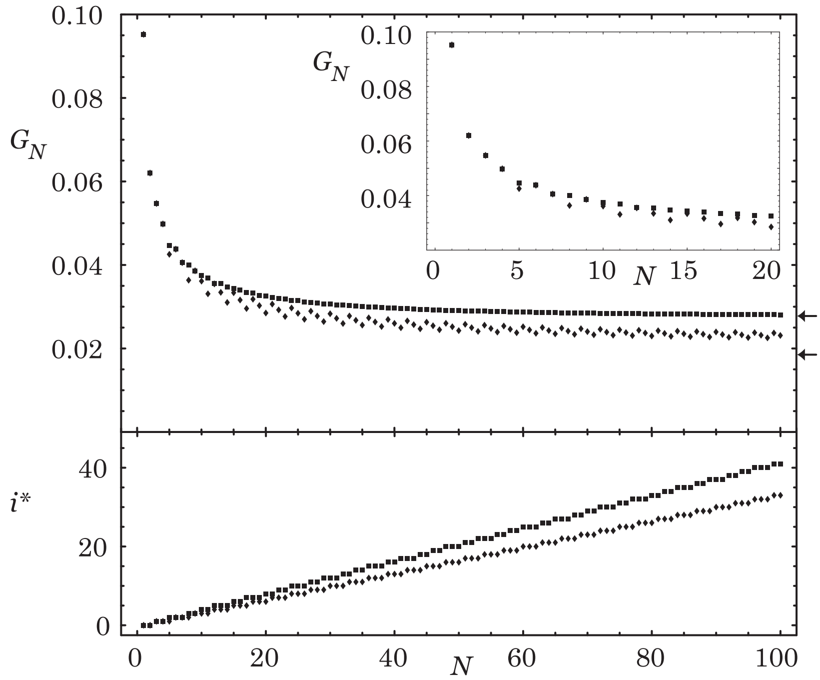

FIG. 8.3. Above: gain of the optimal (■) versus greedy strategy (♦) as a function of the number of players N. The arrows indicate the limiting value of the gain as $N \to \infty$ for the optimal strategy (upper arrow) and the greedy strategy (lower arrow). Inset: blow-up for a small number of players. Lower plot: threshold i^* value for both strategies.

$$g_k = \frac{N-k}{N} g_0 + \frac{k}{N} g_N = g_0 - \frac{k}{N}(g_0 - g_N). \tag{8.20}$$

This relation follows directly from the definition (8.19). In Appendix C, we show that $g_0 > 0$ and $g_N < 0$ for any strategy $\{s_i\}$. Hence, the g_k are strictly decreasing as a function of k. The optimal strategy is thus of the form:

$$\{s_i\}_{\text{opt}} = \{1, \dots, 1, 1, 0, 0, \dots, 0\}. \tag{8.21}$$

We give a proof ex absurdo: suppose that the optimal strategy violates this ordering, say $s_k = 0$, followed by $s_{k+1} = 1$. This would require $g_k \le 0$ with $g_{k+1} \ge 0$, in contradiction with the previous finding.

The result given above enormously simplifies the search for the optimal strategy. Not only does it limit our search to the corners of the $N+1$ dimensional space (of which there are 2^{N+1} in total), but we need only to check the $N+1$ corners whose coordinates have the special form (8.21). In other words the time to search increases linearly rather than exponentially in N. This is in contrast with the situation in the original Parrondo paradox where the search for the optimal strategy is thought to be an NP-complete problem [59]. Having established this fact, we proceed to a numerical search of the optimal strategy for larger values of N. The results are reproduced in Fig. 8.3, where we plot the value i^*, defined as the configuration such that $s_i = 1$ for $i \le i^*$, and $s_i = 0$ for $i > i^*$, as a function of N. The dependence of i^* on N appears to have a periodic behavior: $i^*(N)$ presents plateaus of size $2, 2, 3, 2, 3$ which are repeated, at least up to the value $N = 100$. This suggests that $i^*(N) \approx (5/12)N$

for N large, although we have not been able to prove this analytically. The optimal strategy can now be compared to the so-called greedy strategy. In this strategy game B is selected whenever the total expected gain of the players is positive. Otherwise one chooses game A with zero expected gain. From (8.12), we conclude that this strategy has the same form as the optimal strategy, cf. (8.21) but with the specific threshold value $i^* = \lfloor N/3 \rfloor$. The optimal strategy always outperforms the greedy one, except for $N = 1, 2, 3, 4, 6, 7, 9$, where they coincide, cf. Table 8.1 and Fig. 8.3. In the limit $N \to \infty$ the optimal strategy leads to a gain of $1/36 \approx 0.02777$, while the greedy strategy leads to a gain of $1/54 \approx 0.01851$ (see the arrows in Fig. 8.3).

8.6 Mean field analysis

To complete the picture for the primary games, we now proceed with a mean field analysis. As before, the state of the players in this limit is characterized by a continuous variable, namely the fraction $x(n) \in [0, 1]$ of players with even capital after n games. A strategy is defined as the probability $s(x(n))$ to choose game A, while being in the state $x(n)$. Game B is chosen with probability $1 - s(x(n))$. From (8.8) it follows that after playing game A or B, the probability to have i players with an even capital is given by a binomial distribution. For increasing N, the de Moivre-Laplace theorem states that the probability density for the random variable $x(n)$ is (approximately) given as:

$$f_A(x) = \sqrt{\frac{2N}{\pi}} e^{-2N(x-1/2)^2}, \tag{8.22}$$

$$f_B(x) = \frac{3}{2}\sqrt{\frac{N}{\pi}} e^{-9N(x-1/3)^2/4}. \tag{8.23}$$

The subindex refers to the game that is played. This approximation is to be understood in the following way: after a game is played (say game A), the probability for i to be in the interval $[\alpha, \beta]$, which is given as $\sum_{i=\alpha}^{\beta} w_A(i)$ is approximately given as $\int_{\alpha/N}^{\beta/N} f_A(x)dx$. The approximation becomes more precise as N increases.

In the limit $N \to \infty$, the probability densities (8.22) and (8.23) become δ-functions centered around $1/2$ (for game A) and $1/3$ (for game B). One concludes that upon selection of the corresponding game, $x(n)$ will be found in a narrow region around $1/2$ and $1/3$ respectively. The strategic element introduces randomness in the choice of game, which is most conveniently represented by a random variable, $\sigma(n)$, being equal to 1, when game A is selected -this happens with probability $s(x(n))$- and 0 for game B. If and only if $s(x)$ is continuous at $x = 1/2$ and $x = 1/3$, one can safely neglect any fluctuations around these points, and one is thus led to the following exact but random map for the evolution of the state variable $x(n)$:

$$x(n+1) = \frac{1}{2}\sigma(n) + \frac{1}{3}(1 - \sigma(n)). \tag{8.24}$$

Only if the requirement of continuity is fulfilled will the results for large N converge to the mean field results (note that the greedy strategy *is not* continuous at $x = 1/3$). It is clear that after the first play, $x(n)$ is either $1/3$ or $1/2$, and so one concludes that only the values $s(1/3)$ and $s(1/2)$ are relevant for the resulting average gain. One also recalls from the discussion with a single player that gain is only achieved when game A is followed by game B, with the average gain equal to $1/18$ times the fraction of such subsequent pairs AB. The probability for such a pair is the steady state probability for game A *times* the probability to follow the A with a B game, hence (see Appendix D):

$$G_{\infty}^{\mathrm{st}} = \frac{1}{18}\frac{s(1/3)(1-s(1/2))}{1-s(1/2)+s(1/3)}. \tag{8.25}$$

The maximum gain $G_{\infty}^{\mathrm{st}} = 1/36$ is obtained for all strategies for which $s(1/3) = 1$ and $s(1/2) = 0$. All such strategies lead to an alternation of the two games, i.e. to the game sequence $\ldots ABABABAB \ldots$. The fact that the maximal gain (per player) for an infinite number of players with strategy is identical to the optimal alternation of games for a single player without strategy is clearly a consequence of the self-averaging.

Next, we turn to the performance of th greedy strategy as $N \to \infty$. The strategy function $s(x)$ follows from (8.13):

$$s(x) = \begin{cases} 1 \text{ if } x \leq 1/3 \\ 0 \text{ if } x > 1/3 \end{cases}. \tag{8.26}$$

Blindly inserting the values $s(1/3) = 1$ and $s(1/2) = 0$ gives $G_{\infty}^{\mathrm{st}} = 1/36$, a result which is simply wrong. The flaw in the calculation is a result of the discontinuity at $x = 1/3$. This can be understood as follow. After playing game B, the state of the players is described by a binomial, cf. (8.8). In the limit $N \to \infty$, this distribution converges to a δ-function centered on the average $i = N/3$. But this value exactly coincides with the threshold for the greedy strategy, cf. (8.13). Hence, the Gaussian fluctuations around the average value $N/3$ cannot be ignored, and the probability to select game A or B is $1/2$ rather than 1 in this case. This probability $1/2$ is due to the fact that the Gaussian distribution is symmetrical around the average value, so that half of the fluctuations lead to values $i < N/3$, and the other half lead to values $i > N/3$. The correct result for the mean-field greedy strategy is therefore $G_{\infty}^{\mathrm{st}} = 1/54$, a result that is confirmed from simulations (see the lower arrow in Fig. 8.3). Note that for any other strategy, including the optimal one, with threshold strictly between $1/3$ and $1/2$, the problem does not occur, and the mean field result holds.

We have focused so far on the simplest possible Parrondo paradox. While the property of superstability makes the discussion extremely simple, it also removes some of the richness that more genuine dynamics can introduce. In Appendix E we present a mean field discussion of a more general model, keeping the simplification of involving only two states, but with games that are no longer superstable.

8.7 Discussion

The detailed analysis given above is presumably only possible for games that possess the property of superstability. For simplicity we have focused on a case with specific transition rates, but the results given above are representative for the general case represented in Fig. 8.4(a). Note that an extreme example was discussed briefly in [82], cf. Fig. 8.4(b). In game A the player wins with probability 1 when the capital is even, and neither wins or looses when his capital is odd. For game B the rules are the same, but with odd and even interchanged. This example exhibits the strongest possible Parrondo paradox, yet it does not produce the interesting collective features discussed here. Indeed, after having played once any one of the two games, the state (even or odd capital) of all players will be identical and will remain so forever. In this sense,

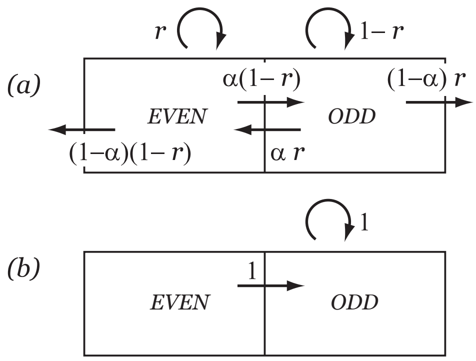

FIG. 8.4. (a) Schematic representation of the most general superstable and fair game with two states. The transitions are indicated by an arrow, with accompanying jump probabilities ($r \in [0, 1]$ and $\alpha \in [0, 1]$). (b) Special case with deterministic dynamics.

the multi-player features discussed here have a genuine probabilistic nature, while the Parrondo paradox does not.

APPENDIX A

GENERATION FUNCTION

For the calculation of the velocity v and diffusion coefficient D, we need to know the asymptotic behavior, i.e. $n \to \infty$, of both $\langle x(n) \rangle$ and $\langle x^2(n) \rangle$. This can be done as follow. First, expanding $F(k,z)$ around $k = 0$ gives:

$$F(k,z) = \sum_{m=0}^{\infty} \frac{\langle x^m(z) \rangle}{m!} (ik)^m \ , \tag{A.1}$$

where we define

$$\langle x^m(z) \rangle \equiv \sum_{n=0}^{\infty} \langle x^m(n) \rangle z^n. \tag{A.2}$$

For $F(k,z)$ given by (4.8), we find the following results for $\langle x(z) \rangle$ and $\langle x^2(z) \rangle$:

$$\langle x(z) \rangle = \frac{(2p-1)z}{(1-z)^2}, \tag{A.3}$$

$$\langle x^2(z) \rangle = \frac{z(1 + z(1-8pq))}{(1-z)^3}. \tag{A.4}$$

Inversion[2] of these power series can be done by using the following relations:

$$\begin{aligned} F_1(z) &= \sum_{n=0}^{\infty} z^n f_1(n) \\ F_2(z) &= \sum_{n=0}^{\infty} z^n f_2(n) \end{aligned} \tag{A.5}$$

$F_2(z)$	$f_2(n)$
$\frac{1}{(1-z)^k}$	$\frac{(n+k-1)!}{n!(k-1)!}$
$zF_1(z)$	$f_1(n-1)$ with $f_2(0) = 0$

The exact result (valid $\forall n$) for $\langle x(n) \rangle$ and $\langle x^2(n) \rangle$ is respectively:

$$\begin{aligned} \langle x(n) \rangle &= (2p-1)n, \\ \langle x^2(n) \rangle &= \frac{(n+1)n + (1-8pq)n(n-1)}{2}. \end{aligned} \tag{A.6}$$

After substitution of these results into (4.1-4.2) and taking the limit $n \to \infty$ gives the final results:

[2]By inversion we mean: obtaining an expression for the $f(n)$, given a power series $f(z) = \sum_{n=0}^{\infty} f(n) z^n$.

$$v = 2p - 1, \tag{A.7}$$
$$D = 2p(1-p). \tag{A.8}$$

When the expressions for $\langle x(z)\rangle$ and $\langle x^2(z)\rangle$ become more involved, as is the case for the random walk with negative mobility, a straightforward inversion becomes hard to do. However, since we only need the asymptotic behavior of the moments, we can make use of the so-called Tauberian Theorems. In the case of a power series, such as $f(z) = \sum_{n=0}^{\infty} f_n z^n$, they state that the asymptotic dependence of f_n for $n \to \infty$ is closely related to the singular behavior of $f(z)$. A useful theorem is the following [44]:

Let $f(z) = \sum_{n=0}^{\infty} f_n z^n$, with f_n a strictly positive and monotonic function of n. If $f(z)$ is singular in the limit $z \to 1$,

$$f(z) \sim \frac{L(\frac{1}{1-z})}{(1-z)^{\alpha}} \ , \tag{A.9}$$

with $L(x)$ a slowly varying function and $x^{\alpha}L(x)$ a positive monotonically increasing function of x for large x. Then, in the limit $n \to \infty$:

$$f_n \sim \frac{\alpha n^{\alpha-1}L(n) + n^{\alpha}L'(n)}{\Gamma(1+\alpha)} \ . \tag{A.10}$$

For the first moment $\langle x(n)\rangle$ one finds from (4.15) and (A.1):

$$\langle x(z)\rangle \sim \frac{v}{(1-z)^2} \ , \tag{A.11}$$

where v is the speed given by (4.16). Applying the theorem given above for $\alpha = 2$ and$L(x)$ a constant equal to v, we conclude that $\langle x(n)\rangle \sim nv$ for large n. The diffusion coefficient D can be obtained in a similar way, by considering $y(n) \equiv x(n) - \langle x(n)\rangle$ with $D = lim_{n\to\infty}\frac{\langle y^2(n)\rangle}{2n}$. Note that this requires the calculation to the next order in the asymptotic behavior of $\langle x(n)\rangle$, namely

$$\begin{aligned} \langle x(z)\rangle - \frac{v}{(1-z)^2} &\sim \frac{C-v}{1-z}, \\ C &= N\left[\frac{1-q^N(1+Np)}{(1-q^N)^2} - \frac{1-p^N(1+Nq)}{(1-p^N)^2}\right]. \end{aligned} \tag{A.12}$$

APPENDIX B

CALCULATION OF STATIONARY STATE

The time evolution of the probability $P_{[i,\sigma,I]}(t)$ is described by the following master equation:

$$\begin{aligned}
\partial_t P_{[1,+,I]}(t) &= -(k_{\leftarrow}^{+} + k_{\rightarrow}^{+})P_{[1,+,I]}(t) + k_{\rightarrow}^{+}P_{[3,+,I-1]}(t) + k_{\leftarrow}^{+}P_{[2,+,I]}(t) \\
&\quad +\gamma[P_{[1,0,I]}(t) - P_{[1,+,I]}(t)] \\
\partial_t P_{[2,+,I]}(t) &= -(k_{\leftarrow}^{+} + k_{\rightarrow}^{+})P_{[2,+,I]}(t) + k_{\rightarrow}^{+}P_{[1,+,I]}(t) + k_{\leftarrow}^{+}P_{[3,+,I]}(t) \\
\partial_t P_{[3,+,I]}(t) &= -(k_{\leftarrow}^{+} + k_{\rightarrow}^{+})P_{[3,+,I]}(t) + k_{\rightarrow}^{+}P_{[2,+,I]}(t) + k_{\leftarrow}^{+}P_{[1,+,I+1]}(t) \\
\partial_t P_{[1,0,I]}(t) &= -k_{\rightarrow}^{0}P_{[1,0,I]}(t) + k_{\leftarrow}^{0}P_{[2,0,I]}(t) + \gamma[P_{[1,+,I]}(t) - P_{[1,0,I]}(t)] \\
\partial_t P_{[2,0,I]}(t) &= -(k_{\leftarrow}^{0} + k_{\rightarrow}^{0})P_{[2,0,I]}(t) + k_{\rightarrow}^{0}P_{[1,0,I]}(t) + k_{\leftarrow}^{0}P_{[3,0,I]}(t) \\
\partial_t P_{[3,0,I]}(t) &= -k_{\leftarrow}^{0}P_{[3,0,I]}(t) + k_{\rightarrow}^{0}P_{[2,0,I]}(t) + \gamma[P_{[3,-,I]}(t) - P_{[3,0,I]}(t)] \\
\partial_t P_{[1,-,I]}(t) &= -(k_{\leftarrow}^{-} + k_{\rightarrow}^{-})P_{[1,-,I]}(t) + k_{\rightarrow}^{-}P_{[3,-,I-1]}(t) + k_{\leftarrow}^{-}P_{[2,-,I]}(t) \\
\partial_t P_{[2,-,I]}(t) &= -(k_{\leftarrow}^{-} + k_{\rightarrow}^{-})P_{[2,-,I]}(t) + k_{\rightarrow}^{-}P_{[1,-,I]}(t) + k_{\leftarrow}^{-}P_{[3,-,I]}(t) \\
\partial_t P_{[3,-,I]}(t) &= -(k_{\leftarrow}^{-} + k_{\rightarrow}^{-})P_{[3,-,I]}(t) + k_{\rightarrow}^{-}P_{[2,-,I]}(t) + k_{\leftarrow}^{-}P_{[1,+,I+1]}(t) \\
&\quad +\gamma[P_{[3,0,I]}(t) - P_{[3,-,I]}(t)].
\end{aligned} \tag{B.1}$$

Summing both sides of the master equation over I yields a closed set of nine coupled equations for the reduced probabilities $P_{[i,\sigma]}(t) = \sum_I P_{[i,\sigma,I]}(t)$. The latter quantities approach steady state values in the long time limit $t \to \infty$. In particular the total net probability flux between the horizontal layers must vanish, implying:

$$P_{[1,+]} = P_{[1,0]} \text{ and } P_{[3,0]} = P_{[3,-]}. \tag{B.2}$$

With these conditions, the set of nine equations decouple into three independent sets, one for each layer. Their unique solution is found by including the condition $\sum_i P_{[i,\sigma]} = P_\sigma$. The latter can be determined by using (B.2) and overall normalisation $\sum_\sigma P_\sigma = 1$. This procedure can also be repeated for more complicated spatially periodic structures including the calculation of both asymptotic velocity and diffusion coefficient, cf. [11].

For continuous space, we proceed in a similar way. The probability $P_{[x,\sigma,I]}(t)$ obeys the master equation:

$$\begin{aligned}
\partial_t P_{[x,+,I]}(t) &= -\partial_x J_{[x,+,I]}(t) + r_{[x,+,I]}(t), \\
\partial_t P_{[x,0,I]}(t) &= -\partial_x J_{[x,0,I]}(t) - r_{[x,+,I]}(t) - r_{[x,-,I]}(t), \\
\partial_t P_{[x,-,I]}(t) &= -\partial_x J_{[x,-,I]}(t) + r_{[x,-,I]}(t),
\end{aligned} \tag{B.3}$$

where $J_{[x,\sigma,I]}(t)$ is the probability current in state σ:

$$J_{[x,\sigma,I]}(t) = -[\partial_x V_\sigma(x) - F + k_B T \partial_x] P_{[x,\sigma,I]}(t), \tag{B.4}$$

and $r_{[x,\pm,I]}(t)$ is the net probability flux from state 0 to state $\pm$ at position $x + IL$, as a result of the localized transitions between the different states:

$$r_{[x,+,I]}(t) = \gamma\delta(x - x_0)\left[P_{[x_0,0,I]}(t) - P_{[x_0,+,I]}(t)\right] ,$$
$$r_{[x,-,I]}(t) = \gamma\delta(x - x_1)\left[P_{[x_1,0,I]}(t) - P_{[x_1,-,I]}(t)\right] . \tag{B.5}$$

As before, $P_{[x,\sigma]} = \lim_{t\to\infty} \sum_I P_{[x,\sigma,I]}(t)$ is found by summing both sides of the master equation over I, and taking the limit $t \to \infty$. The total net fluxes $r_{[x,\pm]} = \lim_{t\to\infty} \sum_I r_{[x,\pm,I]}(t)$ must vanish, so that:

$$P_{[x_0,0]} = P_{[x_0,+]} \text{ and } P_{[x_1,0]} = P_{[x_1,-]}. \tag{B.6}$$

The result for $P_{[x,\sigma]}$ reads:

$$P_{[x,\sigma]} = P_\sigma \frac{\Phi_\sigma(x)}{\int_0^L \Phi_\sigma(y)dy}, \tag{B.7}$$

where $\Phi_\sigma(x)$ and P_σ are given in (5.11) and (5.12) respectively. Finally, J_σ is obtained from

$$J_\sigma = -[\partial_x V_\sigma(x) - F + k_B T \partial_x] P_{[x,\sigma]} , \tag{B.8}$$

leading to the result given in (5.11).

APPENDIX C

EVALUATION OF g_0 AND g_N

In this appendix, we show that $g_0 > 0$ and $g_N < 0$ for any possible strategy $\{s_0, s_1, \ldots, s_N\}$. The expression of g_0 is:

$$g_0 = \frac{N}{2} - \sum_{i=0}^{N} i\, s_i \left[w_A(i) - w_B(i)\right]. \tag{C.1}$$

The minimal value of g_0 is obtained when the sum in the RHS is maximal. This maximum is obtained for the strategy $s_i = 1$ when $w_A(i) - w_B(i) > 0$ and $s_i = 0$ otherwise. From (8.8) we have $w_A(i) - w_B(i) > 0$ when $i > i_c = \lfloor N \log(4/3)/\log(2) \rfloor$. The minimal value for g_0 is then:

$$\begin{aligned}
(g_0)_{\min} &= \frac{N}{2} - \sum_{i=i_c+1}^{N} i \left[w_A(i) - w_B(i)\right] \\
&= \sum_{i=0}^{N} i\, w_A(i) - \sum_{i=i_c+1}^{N} i\, w_A(i) + \sum_{i=i_c+1}^{N} i\, w_B(i) \\
&= \sum_{i=0}^{i_c} i\, w_A(i) + \sum_{i=i_c+1}^{N} i\, w_B(i) > 0.
\end{aligned} \tag{C.2}$$

Here, we replaced $N/2$ by $\sum_{i=0}^{N} i\, w_A(i)$. By a similar argument, one finds that the maximal value of g_N is:

$$(g_N)_{\max} = \sum_{i=0}^{i_c} (i - N) w_A(i) + \sum_{i=i_c+1}^{N} (i - N) w_B(i) < 0. \tag{C.3}$$

APPENDIX D

FRACTION OF AB PAIRS

The fraction of AB pairs in a game sequence can be expressed as the product of the probability that any game is of type A, denoted as Prob(A), and the (conditional) probability that game B is played after game A, denoted as Prob(B after A):

$$\text{frac}(AB) = \text{Prob}(A) \times \text{Prob}(B \text{ after } A). \tag{D.1}$$

These probabilities can now be obtained in a self consistent way. For Prob(A) we have the following relation:

$$\text{Prob}(A) = \text{Prob}(A) \times \text{Prob}(A \text{ after } A) + \text{Prob}(B) \times \text{Prob}(A \text{ after } B). \tag{D.2}$$

In view of normalisation, $\text{Prob}(A) + \text{Prob}(B) = 1$, the solution to this equation reads:

$$\text{Prob}(A) = \frac{\text{Prob}(A \text{ after } B)}{1 - \text{Prob}(A \text{ after } A) + \text{Prob}(A \text{ after } B)}. \tag{D.3}$$

Together with the following observations:

$$\begin{aligned} \text{Prob}(A \text{ after } A) &= s(1/2), \\ \text{Prob}(B \text{ after } A) &= 1 - s(1/2), \\ \text{Prob}(A \text{ after } B) &= s(1/3), \end{aligned} \tag{D.4}$$

the final result for the fraction of AB-pairs reads:

$$\text{frac}(AB) = \frac{s(1/3)(1 - s(1/2))}{1 - s(1/2) + s(1/3)}. \tag{D.5}$$

APPENDIX E

MEAN-FIELD ANALYSIS OF NON SUPERSTABLE GAMES

In this appendix we present the mean field analysis of two non superstable games $\tilde{A}$ and $\tilde{B}$. In game $\tilde{A}$ the capital of the player undergoes again an unbiased random walk, but now the player wins or loses with probability 1/10, and with probability 4/5 his capital does not change. For game $\tilde{B}$, the player has a probability 8/15 to win, 4/15 to lose and 3/15 to neither win or lose, when the capital is even. When his capital is odd, the player has a probability 2/15 to win, 4/15 to lose and 9/15 to neither win or lose. The dynamics of $x(n)$ under the action of these games is:

$$\text{game } \tilde{A} : x(n+1) = \frac{1}{5} + \frac{3}{5}x(n), \tag{E.1}$$

$$\text{game } \tilde{B} : x(n+1) = \frac{6}{15} - \frac{3}{15}x(n). \tag{E.2}$$

The (attractive) fixed points are $x_{\tilde{A}} = 1/2$ and $x_{\tilde{B}} = 1/3$. A sketch of these two maps is given in Fig. E.1(a). The dynamics for the strategy game is then:

$$x(n+1) = \left(\frac{1}{5} + \frac{3}{5}x(n)\right)\sigma(n) + \left(\frac{6}{15} - \frac{3}{15}x(n)\right)(1-\sigma(n)), \tag{E.3}$$

with $\sigma(n)$ as before. Equation (E.3) is a random map. Such maps have been studied in great detail under the simplifying assumption that the randomness is not coupled to the dynamics, i.e., s is equal to a constant. In this case (E.3) is a random linear map, and the attractor becomes fractal, a feature that has been used extensively in fractal imaging [77]. To make a comparison with the previous results, we will consider another

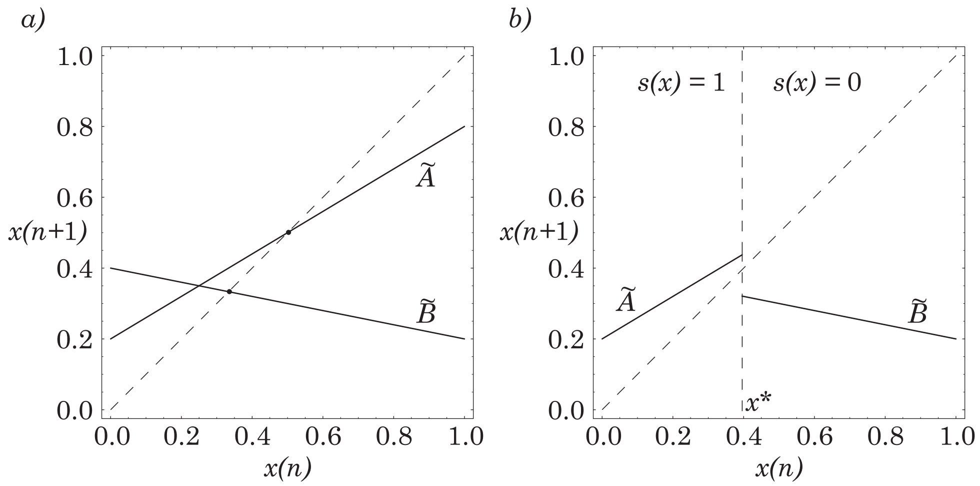

FIG. E.1. a) The linear maps from (E.1). The two dots represent the respective fixed points of the two maps. b) Piecewise linear map given by (E.3) for the strategy $s(x(n)) = 1$ if $x(n) \leq x^*$ and 0 otherwise.

limiting situation, namely that of a pure strategy, with $s(x(n)) = 1$ in a region of the state space $[0, 1]$. In this case (E.3) reduces to a piece-wise linear map. To illustrate the behavior, we focus on the following pure strategy, that can be seen as the natural generalization of greedy and "less" greedy scenarios, with the greediness determined by a continuous parameter x^*: when $x(n) \leq x^*$, one plays game $\tilde{A}$, otherwise one plays game $\tilde{B}$. Game $\tilde{B}$ is then played when the expected gain (after playing game $\tilde{B}$) is larger then $(6/15)x^* - 2/15$. A sketch of the corresponding piece-wise linear map is shown in Fig. E.1(b). Since the local Lyapounov exponent of the resulting piece-wise linear map is everywhere smaller then 1, except at the discontinuity $x = x^*$, and the latter point only has a finite number of pre-images, chaotic orbits are excluded. One also concludes that all the periodic orbits are necessarily stable. By noting that a $\tilde{B}$ game is necessarily followed by an $\tilde{A}$ game when $x^* \geq 1/3$, we can easily classify all the orbits as they appear as a function of x^*, and calculate their corresponding gain. The results are summarized below, cf. Fig. E.2 where we plot the average gain as a function of x^*:

$$
\begin{array}{lll}
0 \leq x^* < 1/3 & \ldots \tilde{B}\tilde{B}\ldots & G_\infty = 0, \\
9/28 \leq x^* < 11/28 & \ldots \tilde{A}\tilde{B}\ldots & G_\infty = 1/84, \\
26/67 \leq x^* < 29/67 & \ldots \tilde{A}\tilde{A}\tilde{B}\ldots & G_\infty = 8/603 \\
281/652 \leq x^* < 299/652 & \ldots \tilde{A}\tilde{A}\tilde{A}\tilde{B}\ldots & G_\infty = 19/3912 \\
\ldots & \ldots & \ldots \\
\frac{5(5/3)^i-(7/3)}{2(5(5/3)^i+1)} \leq x^* < \frac{5(5/3)^i-1}{2(5(5/3)^i+1)} & \ldots \underbrace{\tilde{A}\tilde{A}\ldots\tilde{A}}_{i \text{ times}}\tilde{B}\ldots & G_\infty = \frac{(5/3)^i-1}{3(i+1)(5(5/3)^i+1)}, \\
\ldots & \ldots & \ldots \\
1/2 \leq x^* & \ldots \tilde{A}\tilde{A}\ldots & G_\infty = 0.
\end{array}
$$

Compared to superstable dynamics, we note a number of interesting new features. First we can have coexistence of several orbits, implying that the attractor, and hence the corresponding gain, will depend on the initial condition. Second, the gain will undergo abrupt transitions when the parameter x^* controlling the strategy, is shifted leading to the appearance and/or disappearance of cycles. Third, concomitant hysteresis phenomena will be observed. Finally, we note that the optimal gain is not achieved by a simple alternation of the games but rather by the more complicated period 3 cycle $\ldots\tilde{A}\tilde{A}\tilde{B}\tilde{A}\tilde{A}\tilde{B}\ldots$.

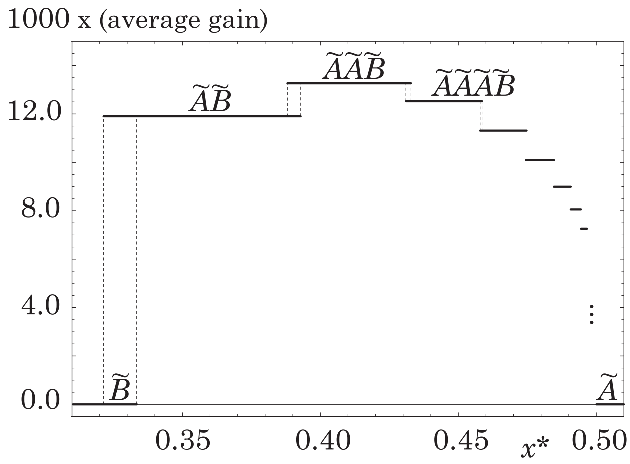

FIG. E.2. Average gain as a function of x^*.

REFERENCES

[1] A. Kudrolli, *Size separation in vibrated granular matter*, Rep. Prog. Phys., **67**, 209, (2004).

[2] K. Liffman, K. Muniandy, M. Rhodes, D. Gutteridge and G. Metcalfe, *A segregation mechanism in a vertically shaken bed*, Granular Matter, **3**, 205, (2001).

[3] P. Reimann, *Brownian motors: noisy transport far from equilibrium*, Phys. Rep., **361**, 57, (2002).

[4] J. Howard, *Molecular motors: structural adaption to cellular functions*, Nature, **389**, 561, (1997).

[5] R. Landauer, *Inadequacy of entropy an entropy derivatives in characterising the steady state*, Phys. Rev. A, **12**, 636, (1975).

[6] M. Büttiker, *Transport as a consequence of state-dependent diffusion*, Z. Phys. B, **68**, 161, (1987).

[7] N.G. Van Kampen, *Stochastic processes in physics and chemistry.* North Holland, Amsterdam, (1981).

[8] L. Onsager, *Reciprocal relations in irreversible processes I*, Phys. Rev., **37**, 405, (1931).

[9] R. Eichhorn, P. Reimann and P. Hänggi, *Brownian motion exhibiting absolute negative mobility*, Phys. Rev. Lett., **88**, 190601, (2002).

[10] B. Derrida, *Velocity and diffusion constant of a periodic one-dimensional hopping model*, J. Stat. Phys., **31**, 433, (1983).

[11] I. Claes and C. Van den Broeck, *Dispersion of particles in periodic media*, J. Stat. Phys., **70**, 1215, (1993).

[12] R. Eichhorn, P. Reimann and P. Hänggi, *Paradoxical motion of a single Brownian particle: absolute negative mobility*, Phys. Rev. E, **66**, 066132, (2002).

[13] R. Eichhorn, P. Reimann and P. Hänggi, *Absolute negative mobility and current reversals of a meandering Brownian particle*, Physica A, **325**, 101, (2003).

[14] R. Eichhorn and P. Reimann, *Meandering Brownian donkeys*, Act. Phys. Pol., **35**, 1407, (2004).

[15] D. Helbing, *Traffic and related self-driven many-particle systems*, Rev. Mod. Phys., **73**, 1067, (2001).

[16] D. Helbing, I. Farkas and T. Vicsek, *Simulating dynamical features of escape panic*, Nature, **407**, 487, (2000).

[17] A. Engel and C. Van den Broeck, *Statistical mechanics of learning.* Cambridge University Press, Cambridge, (2001).

[18] M. Mezard, G. Parisi, and M.A. Virasoro, *Spin glass theory and beyond.* World Scientific, Singapore, (1987).

[19] S.A. Kaufman, *The origins of order.* Oxford University Press, New York, (1993).

[20] J.-P. Bouchaud and M. Potters, *Theory of financial risks.* Cambridge University Press, Cambridge, (2000).

[21] R.N. Mantegna and H.E. Stanley, *An introduction to econophysics.* Cambridge University Press, Cambridge, (2000).

[22] C. Tanford, *Simple model can explain self-inhibition of red cell anion exchange,*

Biophys. J., **47**, 15, (1985).

[23] B. Cleuren and C. Van den Broeck, *Ising model for a Brownian donkey*, Europhys. Lett., **54**, 1, (2001).

[24] C. Van den Broeck, B. Cleuren, R. Kawai and M. Kambon, *A trio of Brownian donkeys*, Int. J. Mod. Phys. C, **13**, 1195, (2002).

[25] B. Cleuren and C. Van den Broeck, *Random walks with absolute negative mobility*, Phys. Rev. E, **65**, 030101(R), (2002).

[26] B. Cleuren and C. Van den Broeck, *Brownian motion with absolute negative mobility*, Phys. Rev. E, **67**, 055101(R), (2003).

[27] P. Hänggi and R. Bartussek, *Brownian rectifiers: how to convert Brownian motio into directed transport*, In J. Parisi, S.C. Müller and W. Zimmermann, editors, *Lect. Notes Phys*, volume **476**, page 294, Berlin, (1996). Springer Verlag.

[28] F. Jülicher, A. Ajdari and J. Prost, *Modelling molecular motors*, Rev. Mod. Phys., **69**, 1269, (1997).

[29] R.D. Astumian, *Thermodynamics and kinetics of a brownian motor*, SCI, **276**, 917, (1997).

[30] C. Van den Broeck, P. Reimann, R. Kawai and P. Hänggi, *Coupled Brownian motors*, In D. Reguera, J.M.G. Vilar and J.M. Rubi, editors, *Statistical Mechanics of Biocomplexity*, page 93, Berlin, (1999). Springer Verlag.

[31] R. Landauer, *Motion out of noisy states*, J. Stat. Phys., **53**, 233, (1988).

[32] J. Marro and R. Dickman, *Nonequilibrium phase transitions in lattice models.* Cambridge University Press, Cambridge, (1999).

[33] V. Privman, *Nonequilibrium statistical mechanics in one dimension.* Cambridge University Press, Cambridge, (1997).

[34] P. Reimann, R. Kawai, C. Van den Broeck and P. Hänggi, *Coupled Brownian motors: anomalous hysteresis and zero-bias negative conductance*, Europhys. Lett., **45**, 545, (1999).

[35] P. Reimann, C. Van den Broeck and R. Kawai, *Nonequilibrium noise in coupled phase oscillators*, Phys. Rev. E, **60**, 6402, (1999).

[36] C. Van den Broeck, I. Bena, P. Reimann and J. Lehmann, *Coupled Brownian motors on a tilted washboard*, Ann. Phys., **9**, 713, (2000).

[37] J. Buceta, J.M.R. Parrondo, C. Van den Broeck and J. de la Rubia, *Negative resistance and anomalous hysteresis in a collective molecular motor*, Phys. Rev. E, **61**, 6287, (2000).

[38] P.E. Kloeden and E. Platen, *Numerical solution of stochastic differential equations.* Springer-Verlag Berlin, Heidelberg, (1992).

[39] H. Callen, *Thermodynamics and an introduction to thermostatistics.* Wiley, New York, (1985).

[40] M.N. Barber and B.W. Ninham, *Random walks: theory and selected applications.* Gordon and Breach, New York, (1970).

[41] H.C. Berg, *Random walks in biology.* Princeton University Press, Princeton, (1983).

[42] E.W. Montroll and M.F. Shlesinger, *The wonderful world of random walks in nonequilibrium phenomena II*, In J.L. Lebowitz and E.W. Montroll, editors, *From Statistics to Hydrodynamics*, Amsterdam, (1984). North-Holland.

[43] J.W. Haus and K.W. Kehr, *Diffusion in regular and disordered lattices*, Phys. Rep., **150**, 263, (1983).

[44] G.H. Weiss, *Aspects and applications of the random walk.* North Holland, Amsterdam, (1994).
[45] R.M. Mazo, *Brownian motion: fluctuations, dynamics, and applications.* Clarendon Press, Oxford, (2002).
[46] I. Claes and C. Van den Broeck, *Random walk with persistence*, J. Stat. Phys., **49**, 383, (1987).
[47] D.J. Griffiths, *Introduction to electrodynamics.* Prentice Hall, Upper Saddle River, (1989).
[48] C. Kettner, P. Reimann, P. Hänggi and F. Müler, *Drift ratchet*, Phys. Rev. E, **61**, 312, (2000).
[49] D. Braess, *Über ein Paradoxon aus der Verkehrsplanung*, Unternehmens-forschung, **12**, 258, (1969).
[50] J.E. Cohen, *The counterintuitive in conflict and cooperation*, Am. Sci., **76**, 577, (1988).
[51] T. Alarcon, A. Perez-Madrid and J.M. Rubi, *Energy transduction in periodically driven non-Hermitian systems* , Phys. Rev. Lett., **85**, 3995, (2000).
[52] N.W. Ashcroft and N.D. Mermin, *Solid state physics.* Holt, Rinehart and Winston, New York, (1976).
[53] G.P. Harmer and D. Abbott, *Parrondo's paradox*, Statistical Science, **14**, 206, (1999).
[54] G.P. Harmer and D. Abbott, *Parrondo's paradox: losing strategies cooperate to win*, Nature, **402**, 846, (1999).
[55] G.P. Harmer, D. Abbott, P.G. Taylor and J.M.R. Parrondo, *Parrondo's paradoxical games and the discrete Brownian ratchet*, In D. Abbott and L. Kish, editors, *Proceedings of the 2nd International Conference on Unsolved Problems of Noise*, volume **511**, page 189, New York, (2000). American Insitute of Physics.
[56] J.M.R. Parrondo and L. Dinis, *Brownian motion and gambling: from ratchets to paradoxical games*, Contemp. Phys., **45**, 147, (2004).
[57] E. van Damme, *Stability and perfection of Nash equilibria.* Springer-Verlag, Berlin, (1991).
[58] F.J. Cao, L. Dinis and J.M.R. Parrondo, *Feedback control in a collective flashing ratchet*, Phys. Rev. Lett. (in press), (2004).
[59] E. Behrends. The mathematical background of Parrondo's paradox. unpublished, (2003).
[60] J.M.R. Parrondo. How to cheat a bad mathematician. unpublished, (1996).
[61] D. Velleman and S. Wagon, *Parrondo's Paradox*, Mathematica in Education and Research, **9**, 85, (2000).
[62] G.P. Harmer and D. Abbott, *A Review of Parrondo's Paradox*, Fluct. Noise Lett., **2**, R71, (2002).
[63] G.P. Harmer, D. Abbott, P.G. Taylor and J.M.R. Parrondo, *Brownian ratchets and Parrondo's games*, Chaos, **11**, 705, (2001).
[64] P.C.W. Davies, *Physics and life*, In J. Chela-Flores, T. Owen and F. Raulin, editors, *Proceedings of the Sixth Trieste Conference on Chemical Evolution*, page 13, Dordrecht, (2001). Kluwer Academic.
[65] S. Maslov and Y. Zhang, *Optimal investment strategy for risky assets*, Int. J. Th. Appl. Finance, **1**, 377, (1998).
[66] S. Blakeslee, *Paradox in game theory: losing strategy that wins*, New York Times,

(2000).

[67] P. Arena, S. Fazzino, L. Fortuna and P. Maniscalco, *Game theory and non-linear dynamics: the Parrondo paradox case study*, Chaos, Solitons and Fractals, **17**, 545, (2003).

[68] J.M.R. Parrondo, G.P. Harmer and D. Abbott, *New paradoxical games based on Brownian ratchets*, Phys. Rev. Lett., **85**, 5226, (2000).

[69] R.J. Kay and N.F. Johnson, *Winning combinations of history-dependent games*, Phys. Rev. E, **67**, 056128, (2003).

[70] R. Toral, *Cooperative Parrondo's games*, Fluct. Noise Lett., **1**, L7, (2001).

[71] R. Toral, *Capital redistribution brings wealth by Parrondo's paradox*, Fluct. Noise Lett., **2**, L305, (2002).

[72] L. Dinis and J.M.R. Parrondo, *Optimal strategies in collective Parrondo games*, Europhys. Lett., **63**, 319, (2003).

[73] L. Dinis and J.M.R. Parrondo, *Inefficiency of voting in Parrondo games*, Physica A, **343**, 701, (2004).

[74] J. von Neumann and O. Morgenstern, *Theory of games and economic behavior*. Princeton University Press, Princeton, (1944).

[75] `http://www.prisoners-dilemma.com/competition.html`.

[76] `http://www.unifr.ch/econophysics/minority/`.

[77] M.F. Barnsley, *Fractals everywhere*. Academic Press, Boston, (1988).

[78] Y. Lee, A. Allison, D. Abbott and H.E. Stanley, *Minimal Brownian ratchet: an exactly solvable model*, Phys. Rev. Lett., **91**, 220601, (2003).

[79] B. Cleuren and C. Van den Broeck, *Primary Parrondo paradox*, Europhys. Lett., **67**, 151, (2004).

[80] B. Cleuren and C. Van den Broeck, *Parrondo games with strategy*, In Z. Gingl, J.M. Sancho, L. Schimansky-Geier and J. Kertesz, editors, *Proc. of SPIE*, volume **5471**, page 109, Bellingham, (2004). SPIE.

[81] B. Cleuren and C. Van den Broeck, *Optimizing strategies in the primary Parrondo paradox*, Phys. Rev. E (accepted for publication).

[82] G.C. Berresford and A.M. Rockett, *Parrondo's paradox*, Int. J. Math. Math. Sci., **62**, 3957–4444, (2003).

CURRICULUM

Education

Licentiaat natuurkunde UIA 1999

List of publications

- W. Malfliet and B. Cleuren, *Analytical solution of a reaction-diffusion problem in chemical physics*, Ukr. J. of Phys., **45**, 459, (2000).

- B. Cleuren and C. Van den Broeck, *Ising model for a Brownian donkey*, Europhys. Lett., **54**, 1, (2001).

- B. Cleuren and C. Van den Broeck, *Random walks with absolute negative mobility*, Phys. Rev. E, **65**, 030101(R), (2002).

- B. Cleuren and C. Van den Broeck, *Directed transport by pumping of excited states*, Phys. Rev. E, **66**, 012101, (2002).

- C. Van den Broeck, B. Cleuren, R. Kawai and M. Kambon, *A trio of Brownian donkeys*, Int. J. Mod. Phys. C, **13**, 1195, (2002).

- B. Cleuren and C. Van den Broeck, *Brownian motion with absolute negative mobility*, Phys. Rev. E, **67**, 055101(R), (2003).

- B. Cleuren and C. Van den Broeck, *Parrondo games with strategy*, In Z. Gingl, J.M. Sancho, L. Schimansky-Geier and J. Kertesz, editors, *Proc. of SPIE*, volume **5471**, page 109, Bellingham, (2004). SPIE.

- B. Cleuren and C. Van den Broeck, *Primary Parrondo paradox*, Europhys. Lett., **67**, 151, (2004).

- B. Cleuren and C. Van den Broeck, *Optimizing strategies in the primary Parrondo paradox*, Phys. Rev. E (accepted for publication).

- R. Eichhorn and B. Cleuren, *Current reversals in the response behavior of a Brownian particle*, Fluct. Noise Lett. (accepted for publication).

List of international presentations

- *Brownian Donkeys and Donkey Games*, International Meeting on Game Theory and Applications, Ishia, 11-14 July 2001

- *Brownian Donkeys*, CECAM workshop: Brownian Motors: The Physics and Biology of Microscopic Machines, ENS Lyon, 13-15 May 2002

- *Primary Parrondo Paradox*, CECAM Workshop: Taming Stochasticity, ENS Lyon, 31 March - 2 April 2004

- *Primary Parrondo Paradox*, ESF Workshop: Control in Games and Ratchets, Toledo, 28 April - 1 May 2004